AD-A150 114 HIGH TIME RESOLUTION THERMOSPHERIC TEMPERATURE AND WIND STUDIES IN THE ARCTIC(U) ALASKA UNIV FAIRBANKS GEOPHYSICAL INST G G SIVJEE 30 SEP 84 4 1/2

UNCLASSIFIED AFOSR-TR-84-1255 AFOSR-80-0240 F/G 4/1 NL

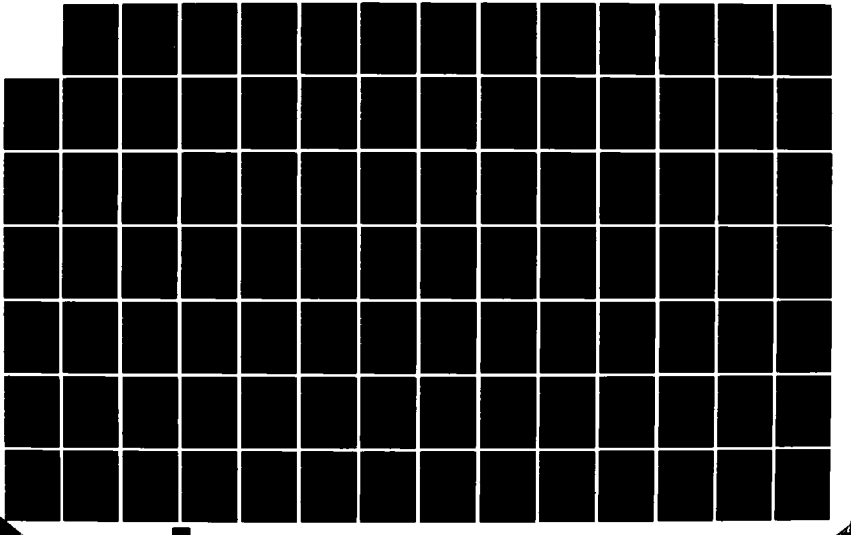

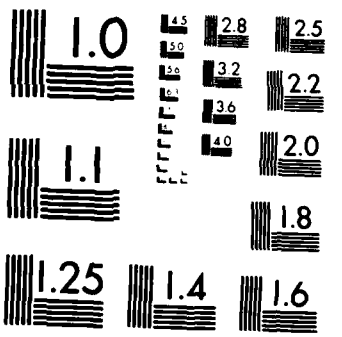

AFOSR-TR- 84-1255

AD-A150 114

GEOPHYSICAL INSTITUTE
UNIVERSITY OF ALASKA
Fairbanks, Alaska 99701

FINAL REPORT

Report Period Covered:	August 1, 1980 - September 30, 1984
Grant Number:	AFOSR-80-0240
Grant Title:	High Time Resolution Thermospheric Temperature and Wind Studies in the Arctic
Principal Investigator:	G. G. Sivjee
Participating Scientists:	G. Hernandez G. Romick
Junior Research Personnel:	R. Sica
Program Manager:	Lt. Col. Gerald J. Dittberner

Prepared for

Air Force Office of Scientific Research
Building 410
Bolling AFB, D.C. 20332

"This report is intended only for the internal management use of the contractor and the Air Force"

UNCLASSIFIED

SECURITY CLASSIFICATION OF THIS PAGE (When Data Entered)

REPORT DOCUMENTATION PAGE	READ INSTRUCTIONS BEFORE COMPLETING FORM
1. REPORT NUMBER: #4 AFOSR-TR- 84-1255	2. GOVT ACCESSION NO.: AD-A150 114
	3. RECIPIENT'S CATALOG NUMBER:
4. TITLE (and Subtitle): High Time Resolution Thermospheric Temperature and Wind Studies in the Arctic	5. TYPE OF REPORT & PERIOD COVERED: Final Report 8-1-80 - 9-30-84
	6. PERFORMING ORG. REPORT NUMBER:
7. AUTHOR(s): G. G. Sivjee	8. CONTRACT OR GRANT NUMBER(s): AFOSR-80-0240
9. PERFORMING ORGANIZATION NAME AND ADDRESS: Geophysical Institute, University of Alaska, Fairbanks, AK 99701	10. PROGRAM ELEMENT, PROJECT, TASK AREA & WORK UNIT NUMBERS: 61102F 2310/AD
11. CONTROLLING OFFICE NAME AND ADDRESS: Air Force Office of Scientific Research/NC, Building 410, Bolling AFB, DC 20332 - 6448	12. REPORT DATE:
	13. NUMBER OF PAGES: 109
14. MONITORING AGENCY NAME & ADDRESS (if different from Controlling Office): Air Force Office of Scientific Research/NC, Building 410, Bolling AFB, DC 20332 - 6448	15. SECURITY CLASS. (of this report): Unclassified
	15a. DECLASSIFICATION/DOWNGRADING SCHEDULE:

16. DISTRIBUTION STATEMENT (of this Report)

Distribution unlimited

17. DISTRIBUTION STATEMENT (of the abstract entered in Block 20, if different from Report)

18. SUPPLEMENTARY NOTES

None

19. KEY WORDS (Continue on reverse side if necessary and identify by block number)

t.v., low light level, interferometer, Fabry-Perot, aurora, image processing, thermospheric dynamics

20. ABSTRACT (Continue on reverse side if necessary and identify by block number)

See following page

DD FORM 1 JAN 73 1473

UNCLASSIFIED

SECURITY CLASSIFICATION OF THIS PAGE (When Data Entered)

This research program was initiated to develop state-ofthe art instrumentation to study the dynamics of the polar thermosphere with high time resolution. The technique involves the measurement of Doppler profiles as well as wavelength shifts in various optical emissions to study the upper and lower thermosphere. Initially, a low light level television system (image orthicon) was coupled to a 150 mm aperture Fabry-Perot index-ofrefraction scanning system. Acquisition of aurorally associated fringes in fractions of a second were obtained, however, lack of electronic stability in these older T.V. systems precluded the routine analysis of the data. A subsequent attempt to use a solid state intensified CID, T.V. camera indicated promise, but the lack of sensitivity limited high time resolution data to very bright events. Rather than continue this direction, emphasis was switched to obtaining high quality temperature and wind measurements in the index-of-refraction scanning mode simultaneously in the upper and lower thermosphere. This was coupled with the installation and operation of a new piezo-electric rapid scanning system to assist in the investigation of thermospheric neutral (6300 OI) and ion (7320 OII), and D-Region (OH) dynamics.

The results of the analyses of much of these data have been reported in various scientific meetings and published in the scientific literature. Other studies are still in progress. The initial results show the presence of gradients and divergences in the winds in both the high and low thermosphere in response to magnetic activity. From 44 nights of data collected prior to spring 1983, The dynamical behavior has been investigated both on individual nights and as a statistical average. In general on individual nights westward drifting auroral forms accompany the westward evening zonal wind. The arrival of the westward electrojet heralds the change from westward to eastward zonal flow, with time delays from less than 15 minutes to over 2 hours. Increasing electrojet strength results in higher zonal wind speeds.

Around magnetic midnight as the aurora moves east, the equatorward meridional wind decreases in velocity. Vertical winds are commonly observed and can be quite large and variable, particularly during periods associated with pulsating aurora. Statistically the general flow pattern is poleward and westward in the evening changing to southward and eastward in the morning. With increasing geomagnetic activity the change in direction occurs earlier in magnetic local time and the meridional wind pattern shifts equatorward along with the auroral oval. Consequently the low geomagnetic activity average wind pattern in the north is similar to the moderate activity average in the south. The average thermospheric temperature is governed by the geomagnetic activity and by the previous days 10.7 cm solar flux. The increase in temperature with solar flux is about the same as with auroral activity (225°K). The piezoelectric system provided a number of additional nights (40) of λ6300 OI wind data during the spring and fall of 1984 with much better time resolution than any heretofore obtained. Those data are being analyzed in continuing studies with various thermospheric models of atmospheric dynamics.

ABSTRACT

This research program was initiated to develop state-ofthe art instrumentation to study the dynamics of the polar thermosphere with high time resolution. The technique involves the measurement of Doppler profiles as well as wavelength shifts in various optical emissions to study the upper and lower thermosphere. Initially, a low light level television system (image orthicon) was coupled to a 150 mm aperture Fabry-Perot index-of-refraction scanning system. Acquisition of aurorally associated fringes in fractions of a second were obtained, however, lack of electronic stability in these older T.V. systems precluded the routine analysis of the data. A subsequent attempt to use a solid state intensified CID, T.V. camera indicated promise, but the lack of sensitivity limited high time resolution data to very bright events. Rather than continue this direction, emphasis was switched to obtaining high quality temperature and wind measurements in the index-of-refraction scanning mode simultaneously in the upper and lower thermosphere. This was coupled with the installation and operation of a new piezo-electric rapid scanning system to assist in the investigation of thermospheric neutral (6300 OI) and ion (7320 OII), and D-Region (OH) dynamics.

The results of the analyses of much of these data have been reported in various scientific meetings and published in the scientific literature. Other studies are still in progress. The initial results show the presence of gradients and divergences in the winds in both the high and low thermosphere in response to magnetic activity. From 44 nights of data collected prior to spring 1983, The dynamical behavior has been investigated both on individual nights and as a statistical average. In general, on individual nights westward drifting auroral forms accompany the westward evening zonal

wind. The arrival of the westward electrojet heralds the change from westward to eastward zonal flow, with time delays from less than 15 minutes to over 2 hours. Increasing electrojet strength results in higher zonal wind speeds.

Around magnetic midnight as the aurora moves east, the equatorward meridional wind decreases in velocity. Vertical winds are commonly observed and can be quite large and variable, particularly during periods associated with pulsating aurora. Statistically the general flow pattern is poleward and westward in the evening changing to southward and eastward in the morning. With increasing geomagnetic activity the change in direction occurs earlier in magnetic local time and the meridional wind pattern shifts equatorward along with the auroral oval. Consequently the low geomagnetic activity average wind pattern in the north is similar to the moderate activity average in the south. The average thermospheric temperature is governed by the geomagnetic activity and by the previous days 10.7 cm solar flux. The increase in temperature with solar flux is about the same as with auroral activity (225°K). The piezoelectric system provided a number of additional nights (40) of λ6300 OI wind data during the spring and fall of 1984 with much better time resolution than any heretofore obtained. Those data are being analyzed in continuing studies with various thermospheric models of atmospheric dynamics.

1. INTRODUCTION

The basic scientific objectives of this project were to detect and quantify the dynamical changes that occur in the neutral temperature and wind of the polar thermosphere. Initially the proposal sought to accomplish this task by the use of an innovative imaging Fabry-Perot interferometer system. This initial technique required the coupling of an image intensified television system to an existing 6" Fabry-Perot interferometer system in a cooperative program between the Geophysical Institute of the University of Alaska and the Aeronomy Laboratory of NOAA in Boulder, Colorado.

Throughout 1981 and 1982 extensive tests of various television systems were made to determine relative sensitivities, electronic stability and ease of data analysis. The T.V. systems evaluated were a C.I.D. (charge injection device) solid state system, the image orthicon and the intensified image orthicon. Although the C.I.D. system did not have as high a sensitivity as the intensified image orthicon, the inherent stability, simplicity of operation and compact design appeared to hold promise. Tests of a two stage intensified C.I.D. system were arranged and unfortunately proved disappointing. However, it was recognized that some increase in sensitivity could be achieved if cooling of the device was possible in order to take advantage of extended integration times. Integration of 16 to 32 seconds would allow for the detection of intensities of the 557.7 n meter OI emission of 600 Rayleighs without any loss in image resolution. The initial tests of a C.I.D. system cooled to 0°C seemed to confirm our ideas, but unfortunately during these tests the epoxy bond that cemented the intensifer to the C.I.D. chip cracked, requiring the unit to be shipped back to the factory for repair. When this unit was returned it never seemed to have the required resoltuion nor sensitivity needed to adequately detect the weak emissions of

interest in times significantly shorter than available with some of the new piezoelectric scanning systems currently in operation within the field.

Consequently, it was decided to change our approach and to discontinue further efforts in this area for the time being due primarily to the lack of sensitivity and electronically stable imaging devices.

In addition to using the Fabry-Perot interferometer as an imaging system, it was also used in the index-of-refraction scanning mode. Scientifically interesting data was acquired in this operational mode on both the 630 n meter OI and the 557.7 n meter OI emissions with time resolution in each look direction of about eight minutes. During this same period we operated another 6" Fabry-Perot index-of-refraction scanning system on the 630 n meter OI emission so that at times simultaneous upper and lower thermospheric data are available with time resolution of about 10 minutes in each look direction, about 50 minutes for a complete sky survey. In 1983 Dr. G. Hernandez initiated the construction of a new piezoelectric scanning system which upon completion was to be installed in Alaska to continue the basic purposes of this project, since the intrinsic scan speed of this system was eight seconds. Much higher time resolution could be obtained depending on the emission intensity and the total number of scans needed to be co-added for adequate signal-to-noise to produce high quality temperature and wind values. The piezoelectric system was tested at the Fritz Peak Observatory of NOAA in Boulder, Colorado during the fall of 1983 and was installed in Alaska in January 1984. This sytem operated until the end of March, 1984 over many clear nights and after minor repairs during the summer of 1984 it was started in August and had accumulated another dozen nights of observations by the end of September, 1984. On night with significant auroral activity this new system acquires 630 n meter

OI data with a one minute integration period in each look direction, about five minutes for each sky survey. This is the highest time resolution neutral dynamics data available which provides both wind and temprature information on the upper thermosphere.

Much of the upper thermospheric data obtained prior to the spring of 1984 is incorporated in the Ph.d dissertation of R. Sica. This information has been analyzed on the basis of 44 individual nights in terms of the relationship to geomagnetic activity and the average data and its relation to solar flux and geomagnetic activity. These data will be discussed later in this report and will be the basis of a number of scientific articles.

In addition, during this project the interferometers were operated in conjunction with the Chatanika Incoherent Scatter radar prior to its departure from this area. One study in progress is concentrated on March 5, 1981, the date of a major geomagnetic disturbance and bright red aurora seen in Colorado and in Australia. On this particular event, simultaneous data exists from interferometers operating in Alaska, Fritz Peak, Colorado and near Melborne, Australia. These data are also being compiled in association with the NCAR TGCM (Thermospheric Global Circulation Model) as one of the first attempts to compare multi-station observations to a thermospheric model.

This report will review the basic instrumentation, the data that has been obtained during this program, its reduction, analysis and interpretation, with some indication of our anticipation for future studies.

2. REVIEW OF INSTRUMENTATION USED IN THIS PROGRAM

The initial instrumentation system proposed for this project coupled a low light level television system using an intensified image orthicon tube with a 6" aperture index-of-refraction scanning Fabry-Perot interferometer.

The interference fringes from the interferometer were amplified by the image intensifier and re-imaged on the photocathode of the T.V. camera. The T.V. image is displayed on a monitor and is digitized and stored in a digital image processor. Those picture elements (pixels) that compose the fringe are transformed by way of the interface to the minicomputer where each fringe is broken into a number of circular annuli and pixels are added within each annulus. The temperature and winds are calculated from the resultant doppler broadened and shifted line profiles. The original T.V. frames are recorded ona video tape recorder for later analysis. Details of this system were given in detail in the first scientific report submitted in 1981. Figures 2.1 and 2.2 show block diagrams of the system in both the imaging and index-of-refraction scanning configuraitons. Figure 2.3 shows an example of the T.V. fringe data and the computer analysis. From Figure 2.3 the shading and non-linear characteristics of the image associated with the image orthicon systems are easily seen. Any routine type of analysis requires extremely stable systems because the shift in the position of the fringe is a measure of the wind speed. It was just this realization and difficulty with these older T.V. systems that initiated our interest in the modern solid state T.V. systems. A detailed discussion of our attempts to use an intensified C.I.D. (charge injection device) system is in the first and second scientific reports. Basically it was found that their electronic stability was acceptable, however neither the single stage or double stage intensifier devices that were tested had sufficient sensitivity to record images substantially faster than modern piezoelectric scanning systems.

In 1983 Dr. Hernandez obtained funding through AFOSR to construct a new piezoelectric scanning Fabry-Perot similar to the ones in operation at the NOAA Fritz Peak Observatory, Hernandez and Mills, 1973. This system

was assembled in January 1984 at the Geophysical Institute in Alaska. This system operates with an eight second scan over two full fringes. The electronics is designed to accumulate scans to some preset number of integral counts under the profile or number of scans. This number is set by analysis requirements for a signal-to-noise that allows errors of less than 30 meters per sec. in wind speed and 25 K in temperature. In this operational mode data has been acquired in the 630 n meter OI emission in less than one minute and within five minutes for a complete sky survey during auroral activity. In conditions of no auroral activity the time for a good fringe increases to approximately ten minutes.

3. REVIEW OF DATA ACQUIRED IN THIS PROGRAM

The analyzable data acquired in this program pertains to upper thermospheric measurements using the 630 n meter OI emission on two index-of-refraction scanning Fabry-Perot instruments and one piezoelectric scanning system. In addition, there is some data from one of the index-of-refraction scanning systems on data from the lower thermosphere using the 557.7 n meter OI emission. Table 3.1 lists all of the data obtained with the various instruments. Details of the analysis of some of these data and future studies are presented in the next section.

4. REVIEW OF ANALYSES OF DATA AND PUBLISHED MATERIAL

In the course of taking the data from the index-of-refraction scanning systems, it was realized that slow constant time scans in the auroral region did not optimize the signal-to-noise at low signal levels and wasted time resolution at high signal levels. Consequently, a new data taking technique was devised which accumulated data at each position in the scan to yield a constant signal-to-noise ratio, Hernandez et al., 1984. Much of the data discussed later was obtained using this technique.

TABLE 3.1

AVAILABLE DATA AT 6300A

Index-of-Refraction Scanning Fabry-Perot Interferometer	1984 Piezoelectric Scanning Fabry-Perot Interferometer
March 5, 1981	January 1-25, 1984
March 30, 1981	January 26, 1984
April 6, 1981	January 28, 1984
February 23, 1982	February 3, 1984
February 24, 1982	February 7, 1984
February 25, 1982	February 10, 1984
February 26, 1982	February 12, 1984
February 28, 1982	February 13, 1984
March 27, 1982	February 21, 1984
March 28, 1982	February 22, 1984
March 29, 1982	February 24, 1984
April 22, 1982	February 28, 1984
November 18, 1982	February 29, 1984
November 19, 1982	March 1, 1984
December 18, 1982	March 2, 1984
December 20, 1982	March 3, 1984
December 21, 1982	March 5, 1984
December 22, 1982	March 6, 1984
February 6, 1983	March 9, 1984
February 14, 1983	March 10, 1984
February 15, 1983	March 11, 1984
February 16, 1983	March 12, 1984
February 17, 1983	March 13, 1984
March 6, 1983	March 24, 1984
March 7, 1983	March 26, 1984
March 8, 1983	March 27, 1984
March 9, 1983	March 28, 1984
March 12, 1983	March 29, 1984
March 14, 1983	April 1, 1984
March 17, 1983	April 2, 1984
March 18, 1983	August 28, 1984
March 19, 1983	August 29, 1984
March 20, 1983	August 31, 1984
March 21, 1983	September 1, 1984
April 4, 1983	September 2, 1984
April 6, 1983	September 3, 1984
April 7, 1983	September 4, 1984
April 8, 1983	September 22, 1984
April 19, 1983	September 23, 1984
April 20, 1983	September 24, 1984
April 22, 1983	September 25, 1984
April 25, 1983	September 27, 1984
	September 28, 1984
	September 29, 1984

1984 Piezoelectric Scanning
Fabry-Perot Interferometer

October 1, 1984
October 5, 1984
October 6, 1984
October 7, 1984
October 9, 1984

In the course of developing the piezoelectric system initial test on the possibility of observing the molecular OH emissions were carried out successfully at Fritz Peak with the operating systems there (Hernandez and Smith, 1984).

During this project, many discussions of various aspects of these data have been presented at national and international scientific meetings by scientists associated with this project and their colleagues (Romick et al., 1981; Sica et al., 1982a, b; Romick et al., 1982; Hallinan et al., 1982; Hernandez et al., 1983; Smith et al., 1983; Hernandez et al., 1984; Wickwar et al., 1984).

Much of the analysis of the data is contained in the Ph.d. dissertation of R. Sica, 1984. Two main topics within the dissertation will be the topic of future publications and exemplify the type of analyses and quality of data obtained within this project and will be discussed in detail as major findings of this project.

4.10 AVERAGES

This section discusses the averages of wind and temperature measurements from College, Alaska. Section 4.20 will discuss the behavior of individual nights in relation to auroral morphology. Additional discussion and further details of auroral zone thermospheric dynamics and the College Fabry-Perot interferometer are available in the dissertations (Sica, 1984).

Measurements of wind, temperature, and intensity from the Fabry-Perot interferometer are displayed in a component format. The symbols N (north), S (south), E (east), W (west), and Z (zenith) refer to the direction of observation. The vertical bar through the letter is plus and minus the standard deviation of the measurement. For wind, above the zero line is northward, eastward, and upward, below the zero line is southward, westward, and downward. All spatial directions are in magnetic coordinates, while time is typically magnetic local time (MLT), though occasionally universal time (UT) is employed. In local time (solar and magnetic), zonal observations are shifted ahead (back) to the east (west), from the local station time i.e., to the point of observation. The station field-of-view from College is shown in Figure 4.1. For College at winter solstice 0:00MLT ≈ 11:30UT ≈ 1:30LT, where solar local time (LT) for this data set was Alaska Standard Time.

The apparent importance of ion drag in the auroral zone suggests that the wind averages may be best studied at various levels of geomagnetic activity. A commonly employed indicator of global geomagnetic activity is the Ap index. This is related to the sum

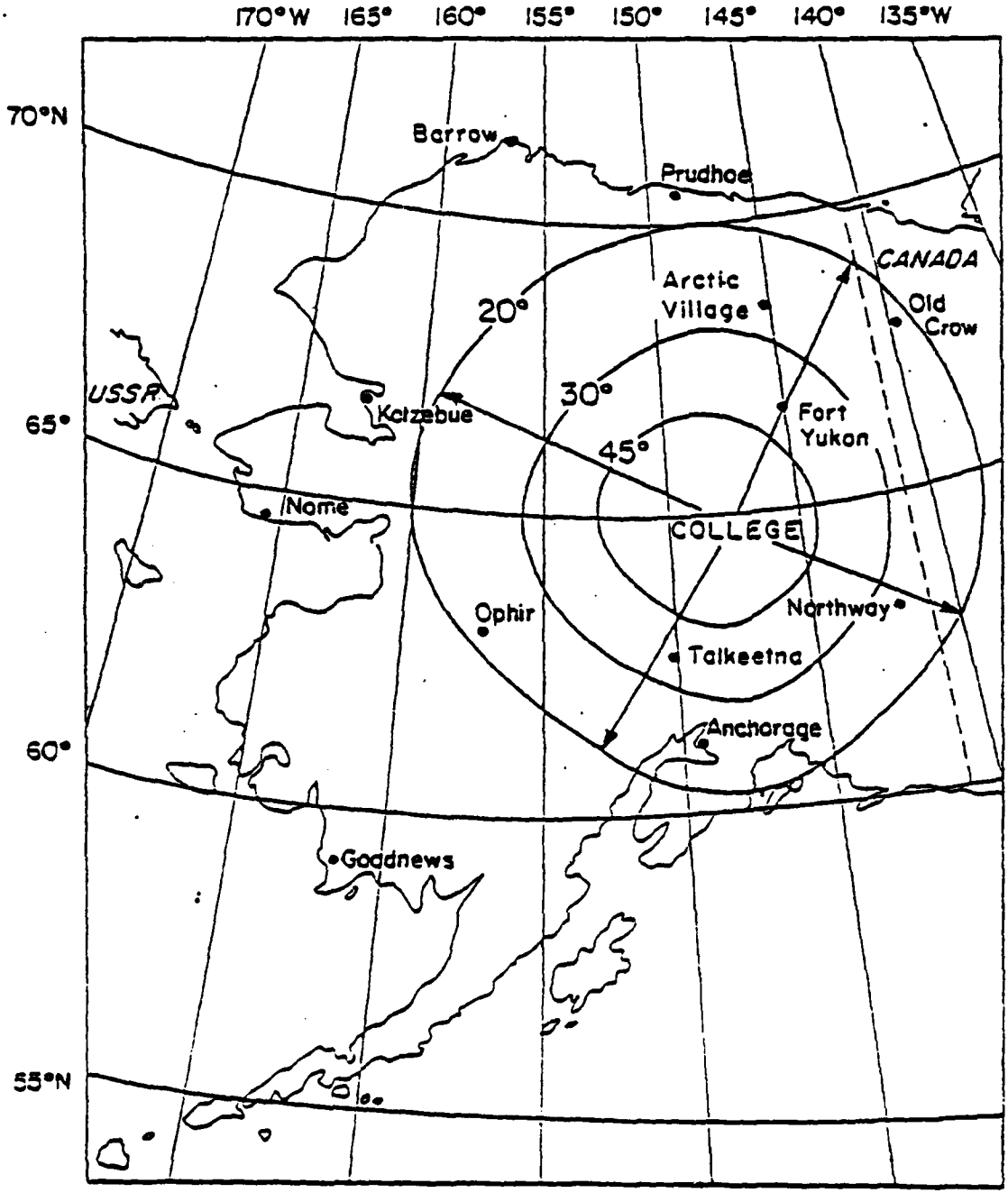

Figure 4.1 The field-of-view from College of an emission layer at 300km for 45°, 30° and 20° elevation angles, in geomagnetic coordinates.

of the Kp index for the twenty-four hour universal day. Unlike the Kp index, the Ap scale is linear, and is also a better indicator of true global magnetic activity (Mayaud, 1980). The distribution by Ap of the forty-four nights included in this study is shown in Figure 4.2, and the relevant geophysical parameters for each night are listed in Table 4.1. Low activity (quiet) is defined as $0 < Ap < 11$, moderate $12 < Ap < 39$, and high activity (active) $Ap > 40$. Ten nights had low activity, twenty-five moderate and nine high activity.

Weighted averages of wind measurements acquired during one-half hour intervals were performed. The weighting is the individual measurements' variance (Bevington, 1969). The averages are restricted to include only the times when 25% or more of the nights in a subset are present. The variance of the average is determined by two methods. The first is to compute the variance for a Gaussian parent distribution

$$\sigma_\mu^2 = (\sum_i w_i)^{-1}$$

where μ is the mean, σ_i^2 the variance of an individual measurement and $w_i = \sigma_i^2$. If the data in the bin are fluctuating near the mean, this will properly represent the variance.

The root mean square error was also computed. This is given by

$$\sigma_\mu^2 = (\sum_i x_i^2 w_i) (\sum_i w_i)^{-1} - \mu^2$$

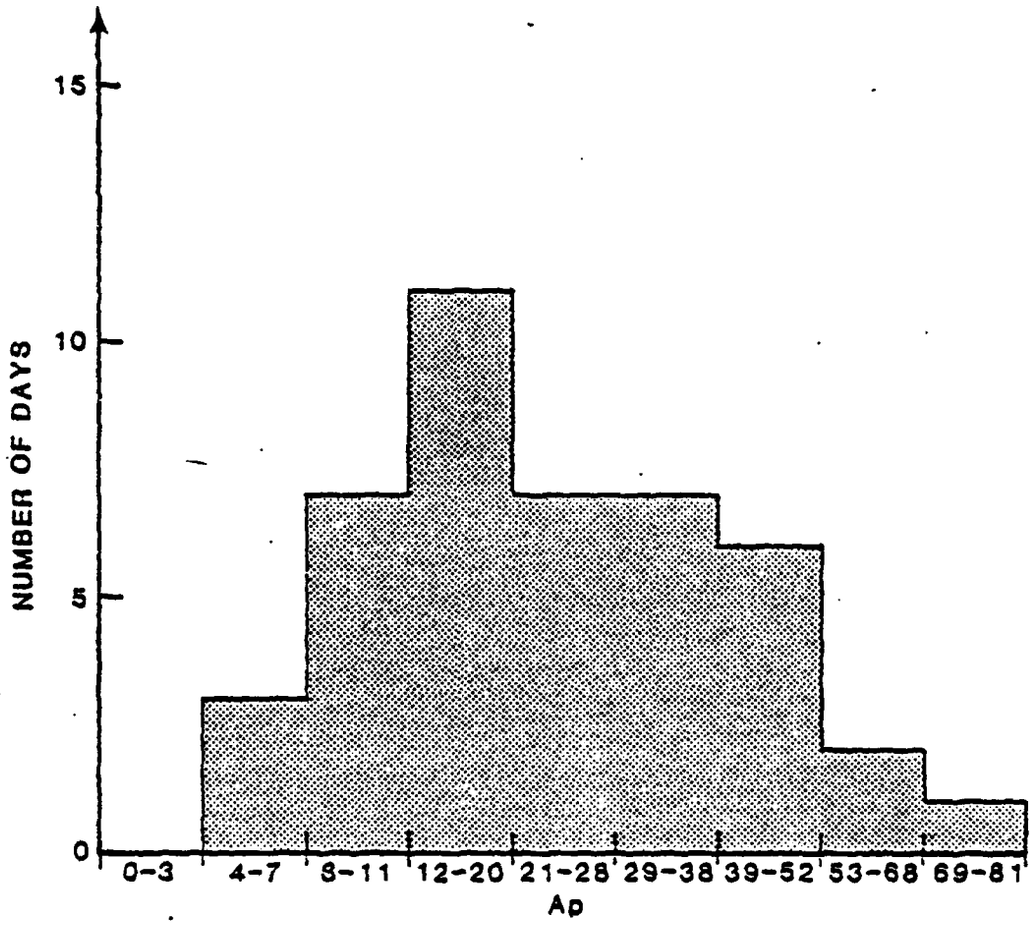

Figure 4.2 The number of nights at various Ap levels, for the data in Table 2.

TABLE 4.1

The Previous Day's 10.7 cm Solar Flux and the Ap Index on Each Night Used in this Study

Universal Day	Previous Day's Solar Flux ($\times 10^4$ J)	Ap
March 5, 1981	245.6	81
March 30, 1981	212.4	16
April 6, 1981	226.2	10
February 23, 1982	163.7	29
February 24, 1982	173.1	24
February 25, 1982	185.9	42
February 26, 1982	184.1	43
February 28, 1982	222.1	10
March 27, 1982	192.8	9
March 28, 1982	195.4	6
March 29, 1982	200.6	13
April 22, 1982	145.2	18
November 18, 1982	158.0	12
November 19, 1982	170.2	10
December 17, 1982	213.2	62
December 18, 1982	200.5	41
December 20, 1982	176.8	46
December 21, 1982	159.2	37
December 22, 1982	149.4	42
February 6, 1983	154.3	47
February 14, 1983	95.5	28
February 15, 1983	91.7	25
February 16, 1983	88.5	30
February 17, 1983	89.7	16
March 6, 1983	146.6	12
March 7, 1983	139.3	7
March 8, 1983	132.3	6
March 9, 1983	128.1	8
March 12, 1983	103.0	53
March 13, 1983	99.5	24
March 14, 1983	95.8	26
March 17, 1983	107.8	11
March 18, 1983	114.5	20
March 19, 1983	117.7	28
March 20, 1983	118.3	32
March 21, 1983	120.7	12
April 4, 1983	101.4	16

TABLE 4.1 (cont.)

April 6, 1983	98.7	35
April 7, 1983	99.5	34
April 8, 1983	102.2	25
April 19, 1983	120.7	9
April 20, 1983	125.0	13
April 22, 1983	133.3	17
April 25, 1983	142.7	32

where x_i is the ith data value. This is a better representation of the variance when the measurements are not fluctuating about a Gaussian mean, or when the sample amount is insufficient to be Gaussian. The variance of the average is taken as the larger of the two calculated variances. The averages are then smoothed using a three point moving triangular window (Bloomfield, 1976).

4.11. THE GROSS STRUCTURE OF THE WIND AVERAGES

The average results will first be discussed in a vector format, which allows general patterns to be easily discerned. It does not explicitly show the uncertainties in measurements and smoothes gradients in the observed flow. The following section will present the results in a component format.

With these caveats, the averages for quiet conditions are shown in Figure 4.3a. The vectors are displayed in geomagnetic coordinates with midnight at the bottom of the dial. The measurements begin after 19:30MLT, when the wind is directed to the northwest at 50m/sec. By 21:15MLT it has turned westward, increasing to 75m/sec. The vector slowly rotates to the south between 22:15 to 0:15MLT with a magnitude of 100m/sec. A small eastward component is present in the morning, as the flow remains at 125m/sec until 2:45MLT.

Figure 4.3b displays the vectors for moderate activity. The vector at 17:45MLT has a magnitude of 150m/sec and is directed to the northwest. The magnitude remains fairly constant, but the direction changes to westward by 20:15MLT. The wind then gradually turns to the south, though now at about 100m/sec. By 23:15MLT the southward flow increases to a magnitude of 150 m/sec. An eastward

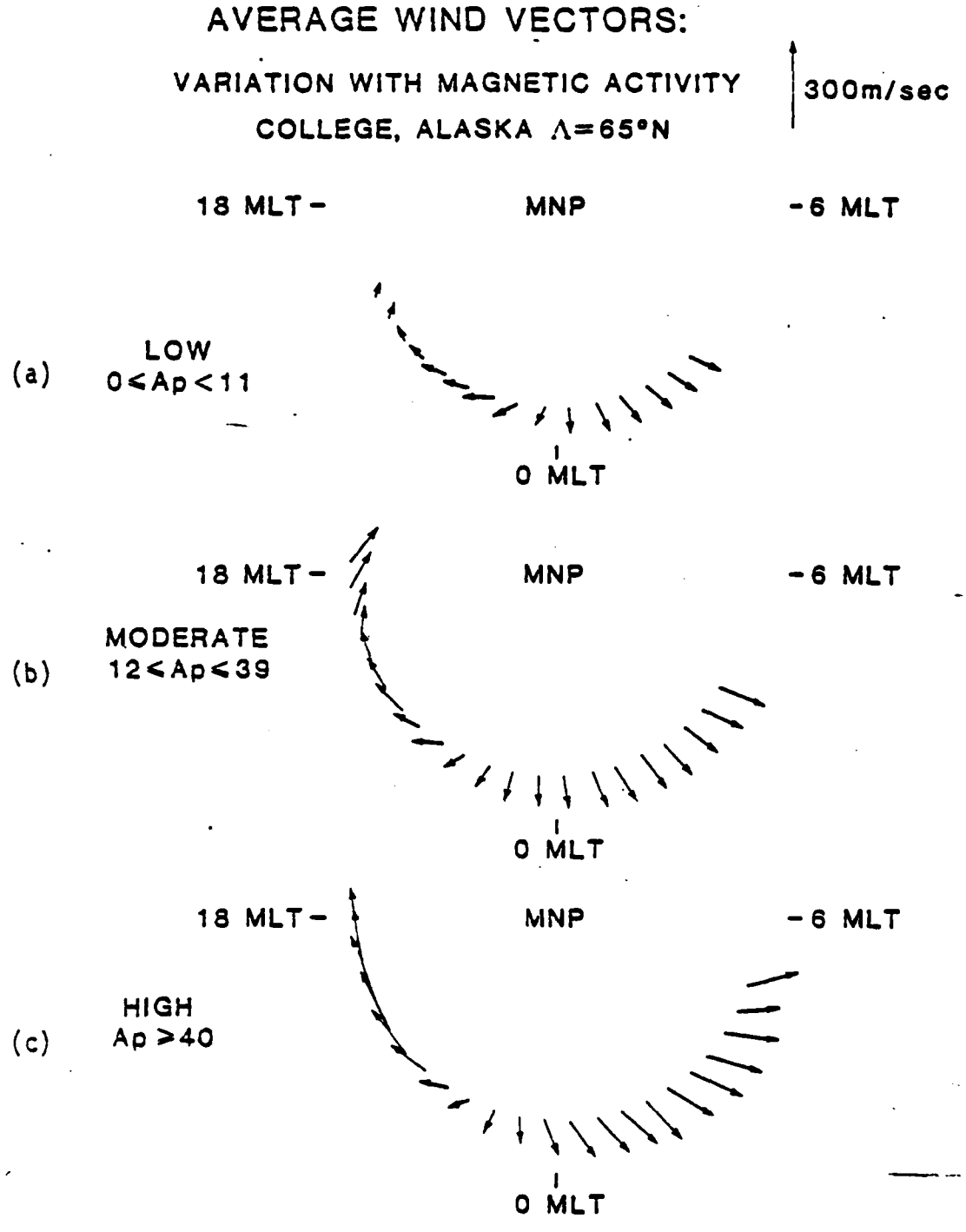

Figure 4.3 The average wind vectors at College for a: low, b: moderate, and c: high geomagnetic activity. The location of the magnetic north pole is identified as MNP.

component develops after 0:45MLT as the morning wind increases to 180m/sec by 3:45MLT.

The active case has a strong westward component of 325m/sec at 19:15MLT, the beginning of the wind averages (Figure 4.3a). The magnitude of the vector decreases to 190m/sec in the following two hours. The wind turns to the south while decelerating to 85m/sec at 22:15MLT. The vector rotates to the southeast around 23:00MLT, after which the flow is to the southeast until the averages end at 4:45MLT. The magnitude increases to a maximum of 220m/sec at 2:45MLT, decreasing to 200m/sec by 4:45MLT.

The early evening flow to the northwest seen in the quiet and moderate cases is due both to the Coriolis effect in the meridional direction and to ion drag in the zonal direction. The vector turns from the northwest to the south an hour earlier in the moderate case. This is not seen in the averages during active periods, though it probably occurs at an earlier time, before measurements exist. This change in the wind pattern with magnetic activity is similar to the behavior of the auroral oval. As magnetic activity increases, the oval expands and auroral phenomena occur earlier in magnetic local time (Akasofu, 1968).

The duration of equatorward flow is longest for the moderate case, as Joule heating enhances the southward flow over the polar cap (Roble et al., 1982). During moderate conditions the auroral oval which is the region of maximum Joule heating (Banks, 1977) expands over College. The flow becomes southward with a smaller magnitude about 1 1/2 hours later during quiet conditions when the Joule heating rate is smaller.

The wind for the active case shows enhanced zonal flow due to increased ion drag. The wind magnitude is larger but the amount of Joule heating on the average may not be, since the auroral oval has expanded equatorward of College. Though Joule heating may be more intense for a shorter period, the relative ion-neutral velocity more quickly approaches zero. The meridional component is about the same as in the moderate case. Increased activity is also associated with stronger electrojets due to the higher electron density raising the ionospheric conductivity and from enhanced magnetospheric convection increasing the ionosphere electric fields. These conditions also result in large ion drift velocities, which increase the momentum due to ion drag.

Finally, observational evidence suggests that even for quiet conditions, ion drag is important in the auroral zone during solar maximum. Magnetospheric convection always exists to some extent. Auroral activity may occur to the north of the station beyond the field-of-view in the evening, but usually during solar maximum, College will lie within the auroral oval during some phase of the diurnal cycle. The invariant latitude of College can be thought to vary with changing magnetic activity with the auroral oval held fixed. The auroral oval is not, of course, static, but a dynamic feature of the polar atmosphere; this is merely a simple way to visualize the difference. Comparison between Fabry-Perot interferometer observations from College and the NCAR Thermospheric General Circulation Model (TGCM) supports this result of the station sampling different regions of the convection pattern with varying polar cap potential (Roble 1983). In the NCAR model two convection

models are used with a range of cross-tail potentials, Sojka et al. (1979) (symmetric) and Heelis et al. (1982) (asymmetric) (Figure 4.4). The best fit of the model zonal wind to the observed zonal wind for an individual night is found by adjusting the station's latitude in the model; examples are shown in Figure 4.5. Data were obtained from two Fabry-Perot interferometers at College in the period from 1981 to 1984. The "S" fits use the Sojka et al. (1979) convection pattern; the "H" results employ the Heelis et al. (1982) model. The "latitude" of College varies from 52.5° to 77.5°. This result, which will be shown to hold for the meridional wind, is important for correctly interpreting the data. The assumption in the NCAR TGCM of a steady-state convection pattern is unrealistic, as the real cross-tail potential exhibits significant dynamic behavior. Historically, the aurora has been treated as a perturbation on mid-latitude models. The data here clearly show that during solar maximum, the presence of the auroral oval defines the "steady-state" behavior of the thermosphere. The farther north or south of College the oval is displaced, the larger the deviation from this steady-state.

4.12 THE RELATIONSHIP OF WIND VELOCITY TO GEOMAGNETIC ACTIVITY

A study of the wind in component form as a function of geomagnetic activity will amplify some of the above arguments. The average meridional wind viewed to the north for quiet, moderate and active conditions is shown in Figure 4.6a and the corresponding observations to the south are shown in Figure 4.6b. The magnitude of the wind remains almost constant with increasing magnetic activity, contrary to the result of Wallis (1974). The measurements to

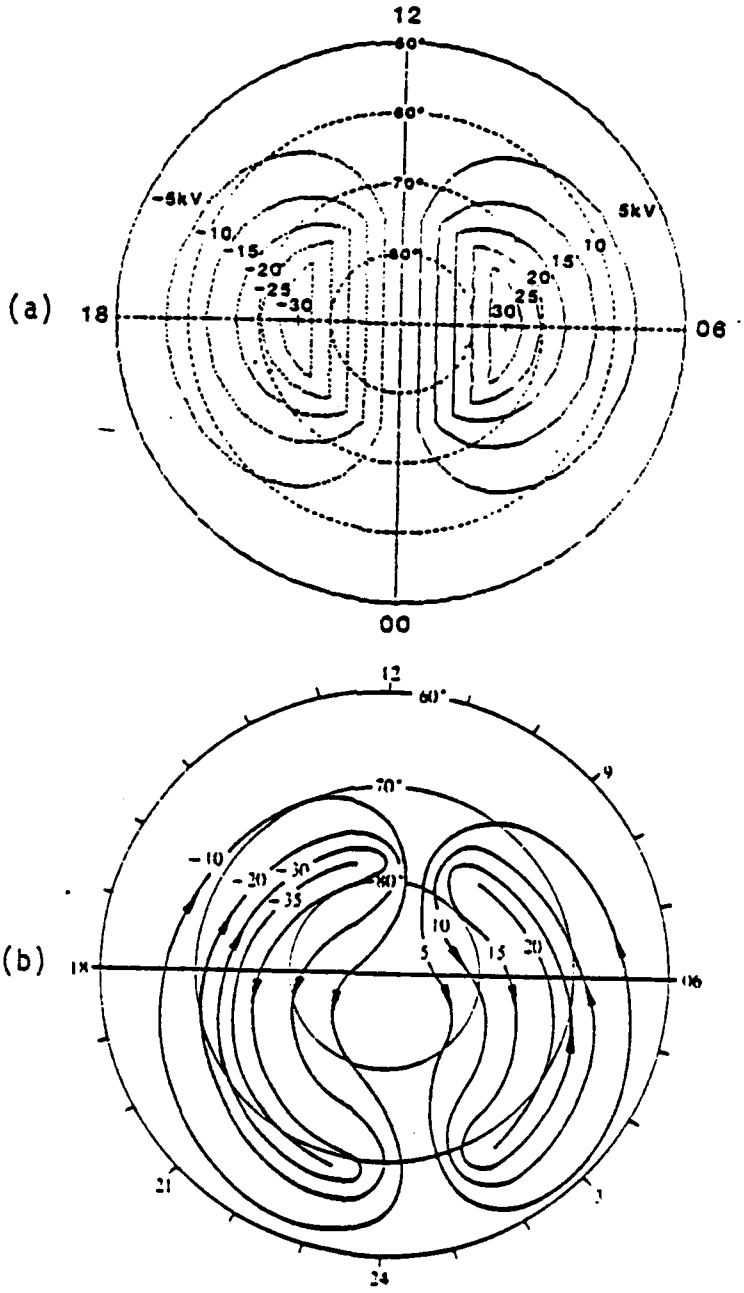

Figure 4.4 a: Equipotential contours for a symmetric Volland-Sojka convection pattern (picture courtesy of R. Williams). b: Plasma flow trajectories and equipotential contours for an asymmetric convection pattern (from Heelis et al., 1982).

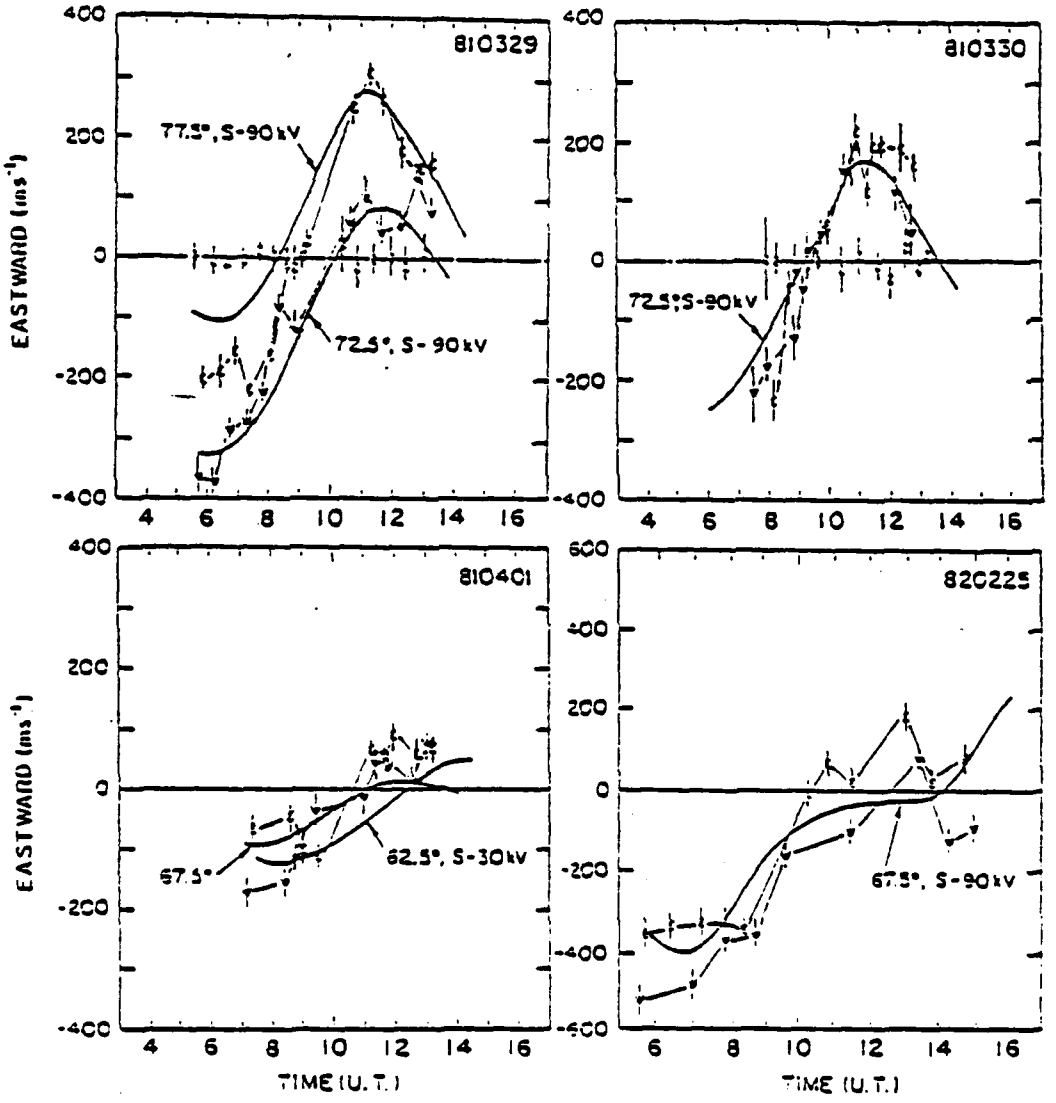

Figure 4.5 Wind measurements acquired at College and fitted with the NCAR TGCM using two convection models, as described in the text. The "S" fits use the Sojka et al. (1979) convection pattern, the "H" results employ the Heelis et al. (1982) model.

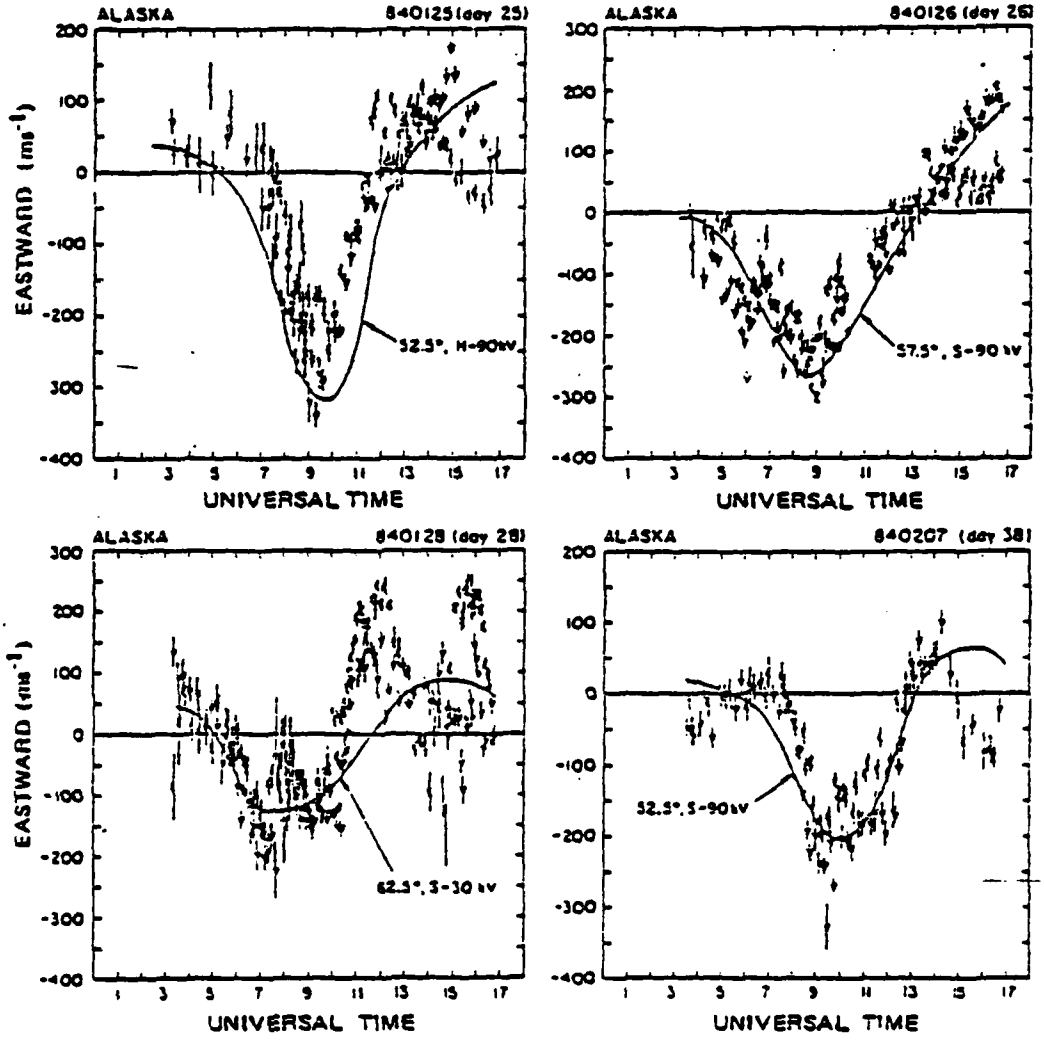

Figure 4.5 (Con't)

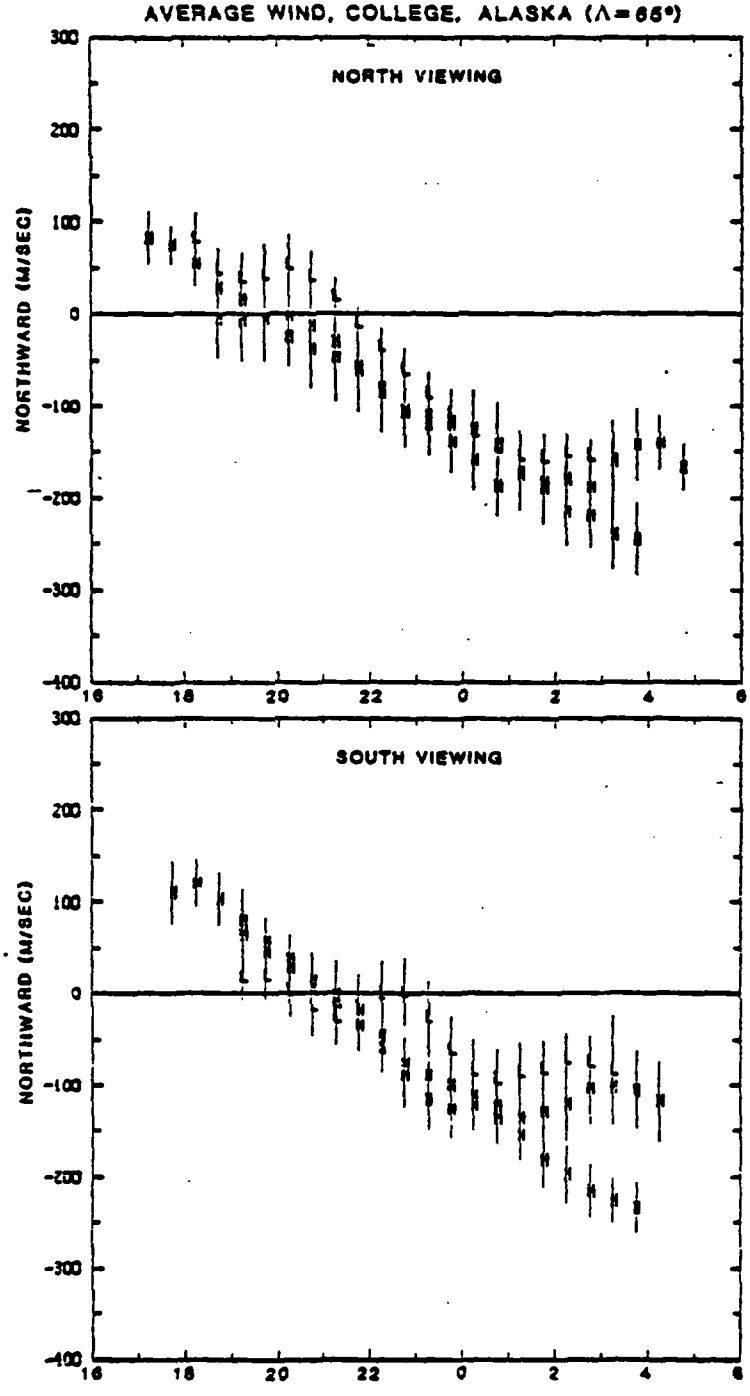

(a)

(b)

Figure 4.6 Diurnal variation of the average wind for different degrees of geomagnetic activity in component form viewed, a: in the north, b: in the south, c: in the east, and d: in the west for the low (L), moderate (M), and high (H) cases.

(c)

(d)

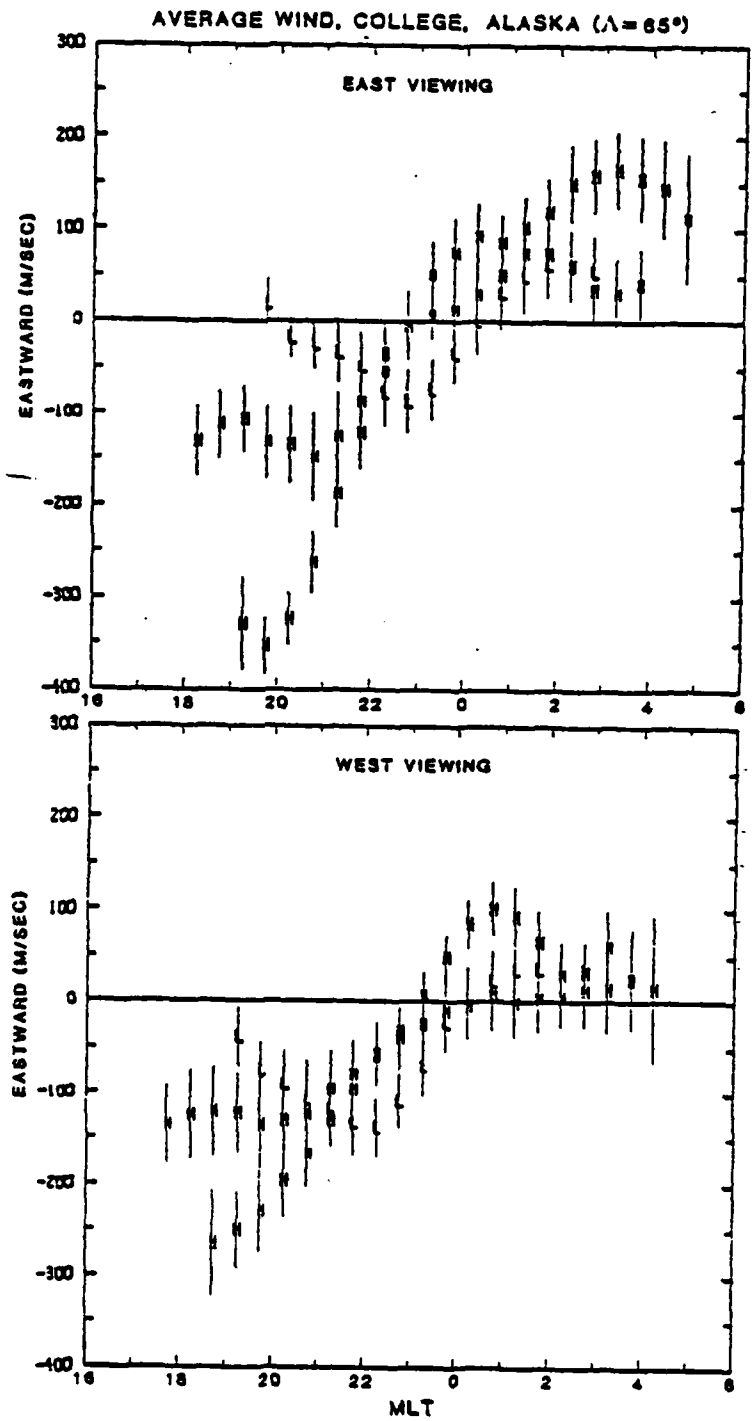

Figure 4.6 (Con't)

the north show that for quiet and active cases the wind is constant and southward after 1:00MLT, while in the moderate case the magnitude of the wind continues to increase. The wind viewed to the south for quiet and moderate cases is constant in magnitude after 1:00MLT, while for active conditions it continues to increase an additional 100m/sec. Relative to the moderate case in the north, the low activity meridional measurements in the north change from poleward to equatorward about two hours later.

The apparent movement of the station relative to the auroral oval can also be seen in this presentation. The moderate wind viewed to the north has the same shape and magnitude as the high activity average viewed in the south. Similarly, the low activity average in the north is essentially the same as the moderate activity wind viewed to the south. As the geomagnetic activity increases, the wind component which was viewed to the north during lower geomagnetic activity, is now observed to the south of the station.

The zonal averages are displayed for measurements to the east and west in Figure 4.6c and d. The increase in magnitude with magnetic activity is obvious. The wind direction changes from westward to eastward about one and one half hours earlier in the active average compared to the quiet average. Ion drag is clearly the dominant forcing term for the zonal wind during active conditions. The evening westward wind is probably greater than the morning eastward wind on the average, because of the enhanced electron density to the west in the evening following the decay of the F region, a daily feature. Increases in density due to auroral

activity often occur, but are not distributed as regularly in magnetic local time.

4.13. THE FINE STRUCTURE OF THE WIND AVERAGES

The final level of analysis for the wind averages is the behavior of the meridional and zonal components, when the viewing directions are compared. The low activity meridional, zonal and zenith components are shown in Figure 4.7. The evening meridional flow is uniform, (i.e., no convergences, divergences or gradients). The wind increases equatorward in the morning faster in the north than in the south and is about 60m/sec larger in the north by morning. This is consistent with magnetospheric-icnospheric heating in the north. The zonal wind is larger measured in the west in the evening. The apparent deceleration over the station is probably due to the Coriolis effect diverting the air poleward, since the pressure bulge in the quiet case is to the north of College. The morning zonal wind is uniform in magnetic local time.

The apparent deceleration in the low activity averge zonal wind may alternatively be explained by displaying the same average in universal time (Figure 4.8). Between 6:00 to 9:30UT, the westward increase in the wind is uniform, as is computed by global models that employ a steady-state convection pattern (Roble et al., 1982). Since substorms occur on the average later in magnetic local time during quiet geomagnetic periods, the assumption of steady-state convection may be valid, without local effects.

For each activity level, the mean zenith wind for that average and its variance were computed. These are 1.10±10.7m/sec (low), .660±7.33m/sec (moderate) and -1.75±15.5m/sec (high). As previous-

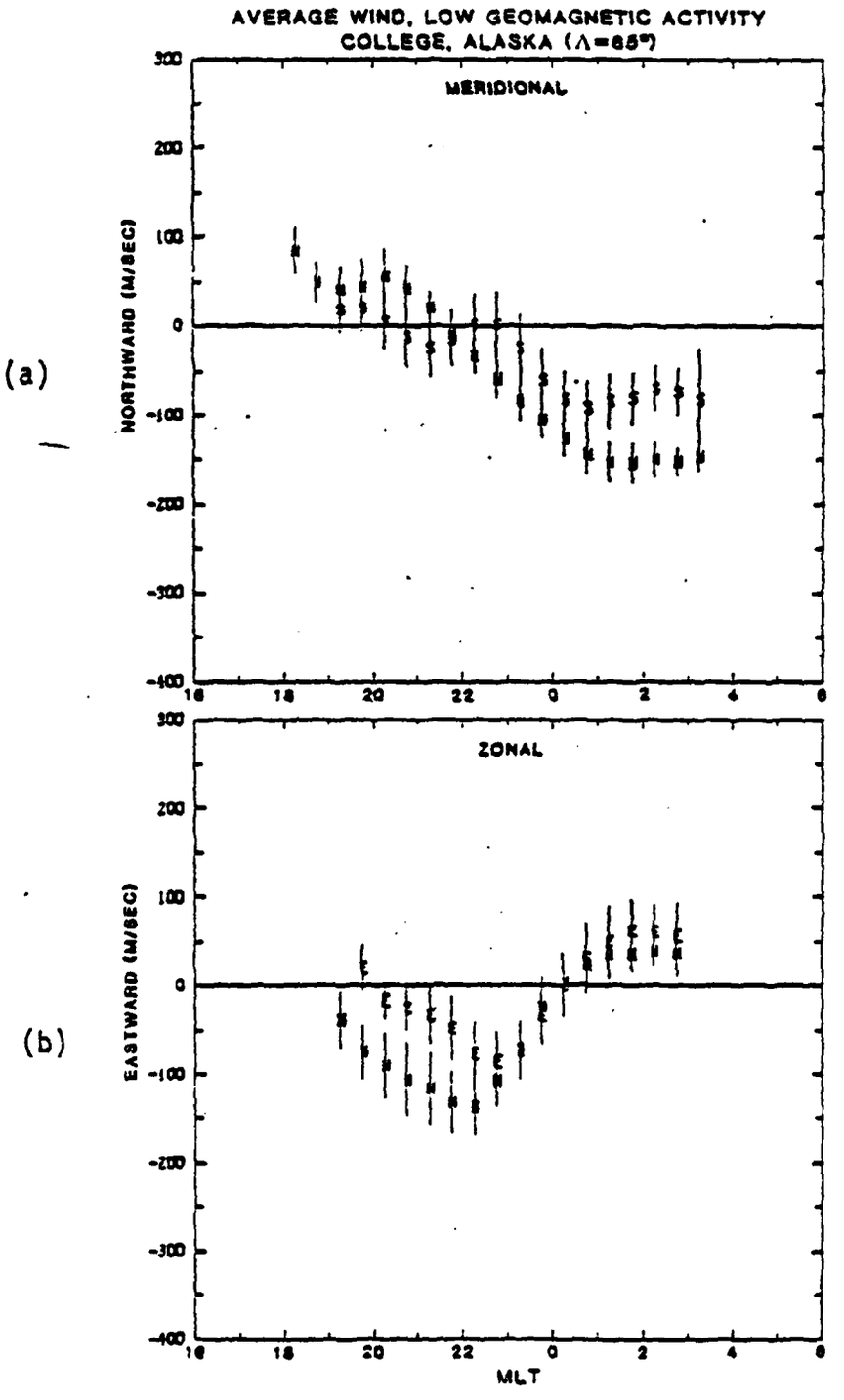

Figure 4.7 Diurnal variation of the average wind components for low geomagnetic activity in, a: the meridional direction, b: the zonal direction, and c: the zenith.

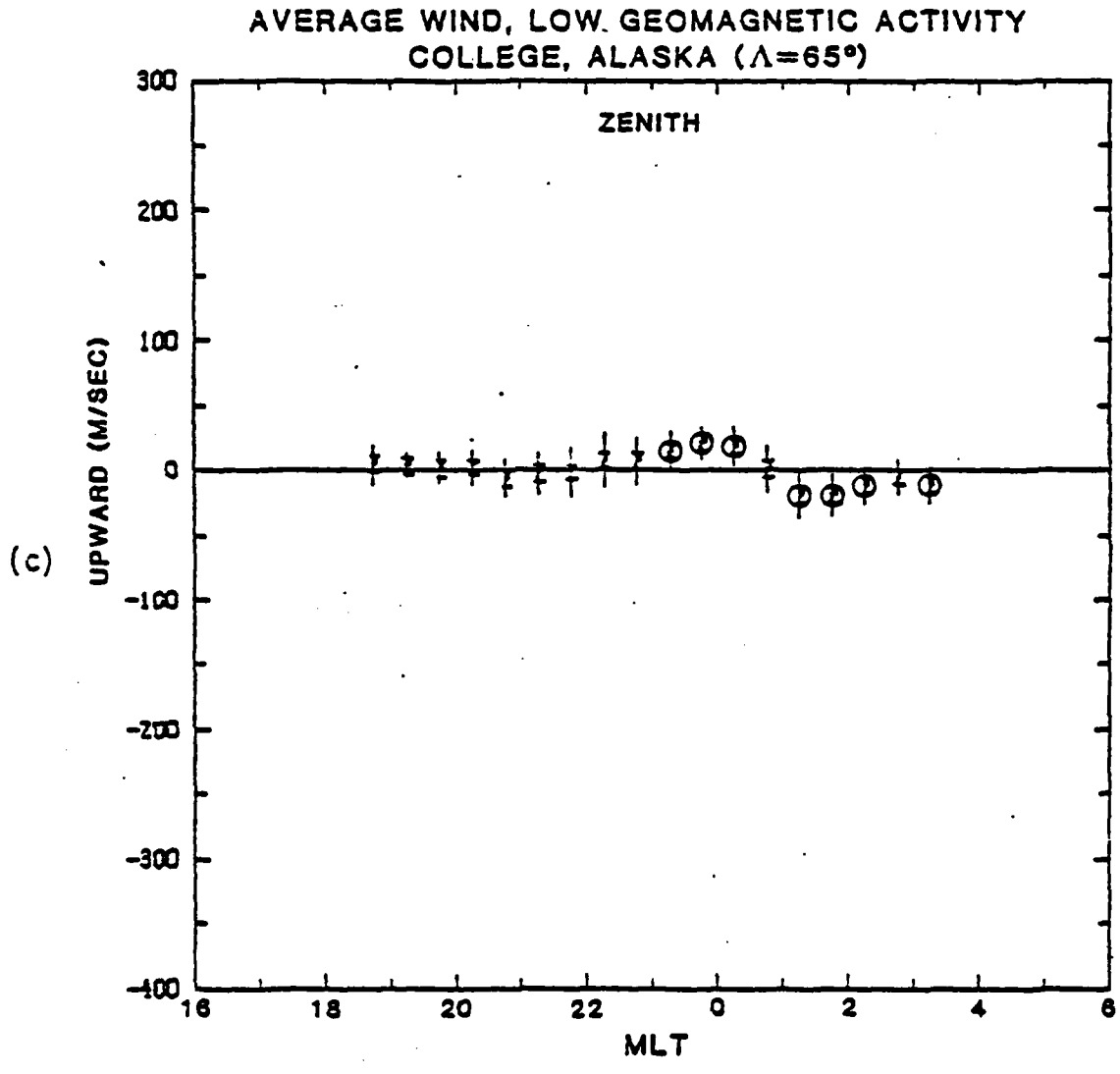

(c)

Figure 4.7 (Con't)

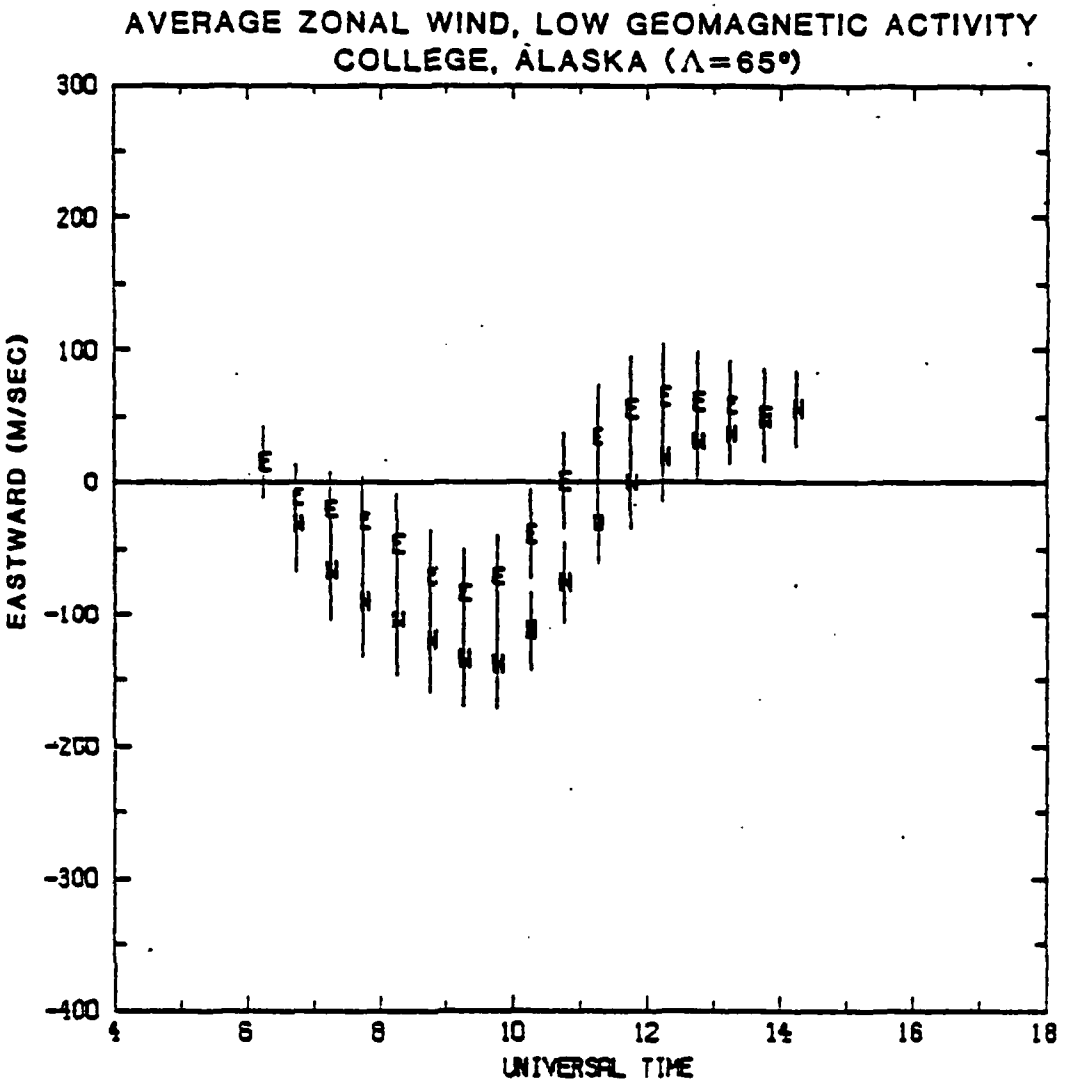

Figure 4.8 The low geomagnetic activity zonal components of the wind in universal time.

ly stated, the weighted average of an individual night was adopted as zero wind. The means of the averages show that zero was well within the stability of the instrument for winds (about 10m/sec). Using these averages, individual one-half hour measurements were compared to the mean value using Student's t test (Parratt, 1961). This gives a quantitative measure of the difference from the mean which is a more sensitive test than comparing the overlap of standard deviations.

Figure 4.7c displays the zenith wind for the quiet case. The circled measurements are different from the mean to the 95% confidence level. A small, upward, zenith wind exists from 23:15 to 0:15MLT, then becomes downward from 0:45MLT to 2:15MLT. Convergence and divergence in the wind flow can cause a zenith wind, but these are not observed in this case. The Coriolis effect yields a vertical component that is typically small compared to the vertical viscosity. A model of the thermospheric response to an auroral substorm has been presented by Richmond and Matsushita (1975). The measured vertical wind is consistent with their result, and will be discussed in more detail at the end of this section.

The moderate geomagnetic activity average shows a small gradient in the evening poleward flow, with the wind component viewed to the south larger (Figure 4.9a). The Coriolis effect more efficiently deflects the flow to the north, away from the polar cap boundary. After 20:00MLT the wind becomes uniform until 2:00MLT. Thereafter the poleward component of the wind, viewed in the north, continues to increase, while to the south the wind speed remains constant. The zonal wind is uniform in the evening, but slightly larger

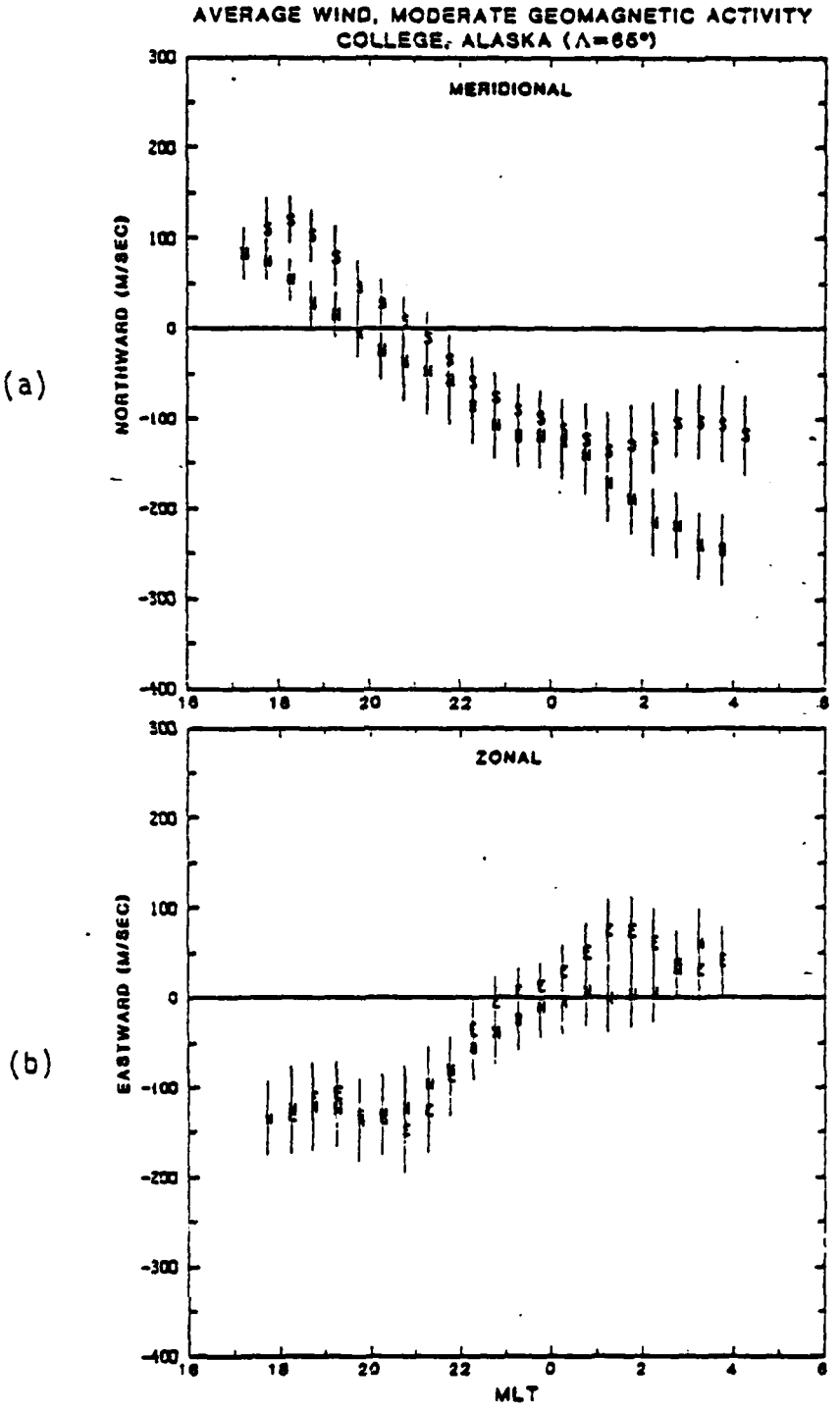

Figure 4.9 Average wind components for moderate geomagnetic activity in a: the meridional direction, b: the zonal direction, and c: the zenith.

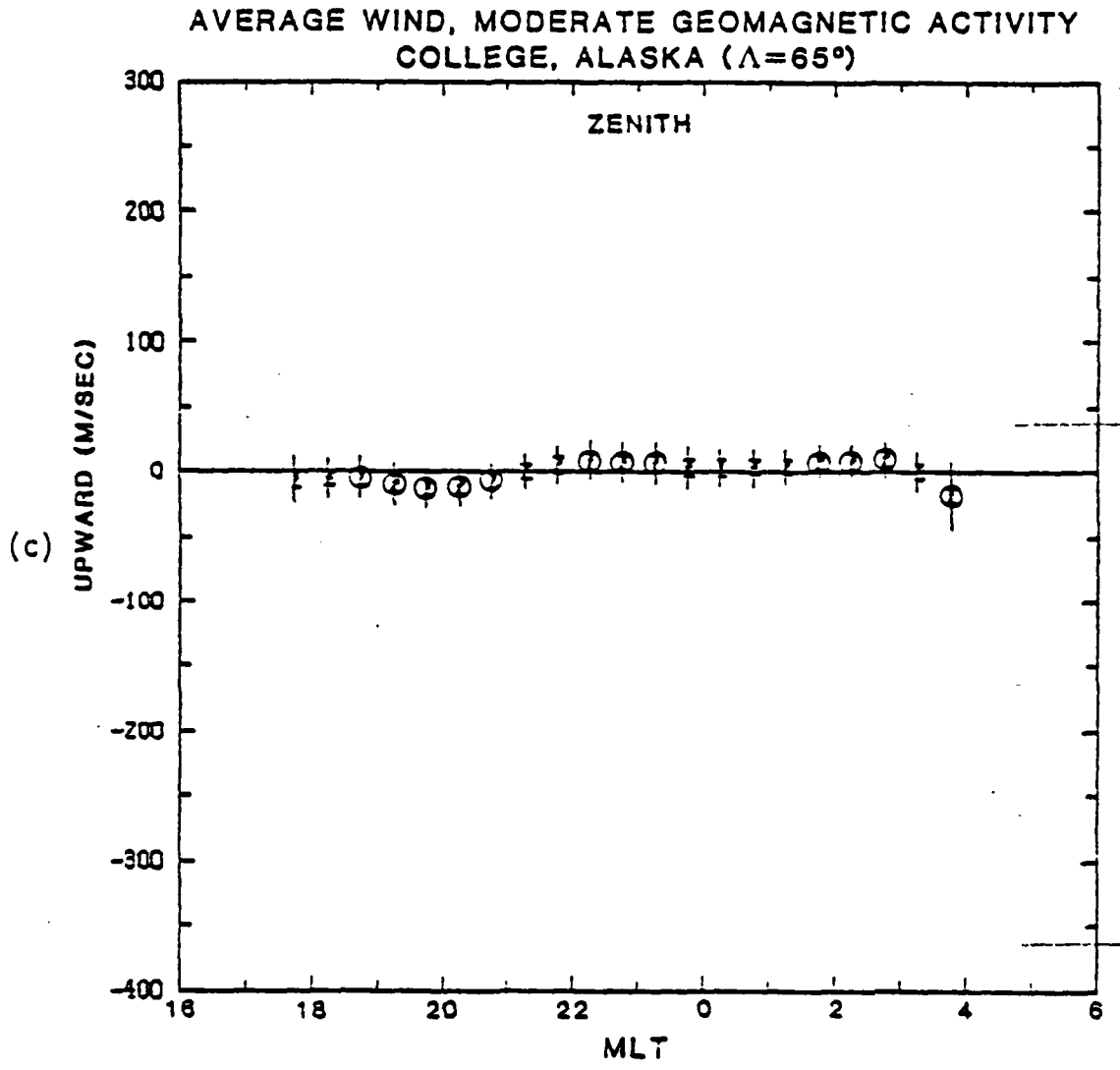

Figure 4.9 (Con't)

viewed to the east in the morning (Figure 4.9b). Enhanced ion drag may have initiated the morning eastward wind of 75m/sec in the east. The zenith wind is significantly different from the mean though the speed is low, less than 18m/sec (Figure 4.9c).

The high geomagnetic activity average meridional wind, viewed to the north at 19:00MLT, is consistent with a pressure bulge north of the station, where the wind is zero (Figure 4.10a). The meridional wind becomes uniform and increases equatorward until 2:00MLT, thereafter it decreases to zero. The zonal wind is larger to the east in the evening and morning (Figure 4.10b). In the morning this is probably due to acceleration of the neutral wind by ion drag. It is not immediately clear why the westward wind viewed to the east should be larger than the wind viewed in the west in the evening. Since the meridional wind is small in the evening, the same air parcel viewed to the west probably is seen again in the east. The air parcel may enter a region of higher ionospheric conductivity and hence enhanced ion drag as it moves eastward. The westward traveling surge associated with an auroral substorm can provide the increased conductivity.

Alternatively, the difference in evening zonal velocity in the two viewing directions may be a universal time effect (Figure 4.11). The evening gradient is no longer present, though a gradient appears in the region of the westward-to-eastward crossover. The apparent evening gradient in magnetic local time may be due to a universal time effect of the convection pattern during high activity, when the magnetospheric convection electric field can increase rapidly (Sojka et al, 1979). Suddenly increasing the global magnetospheric

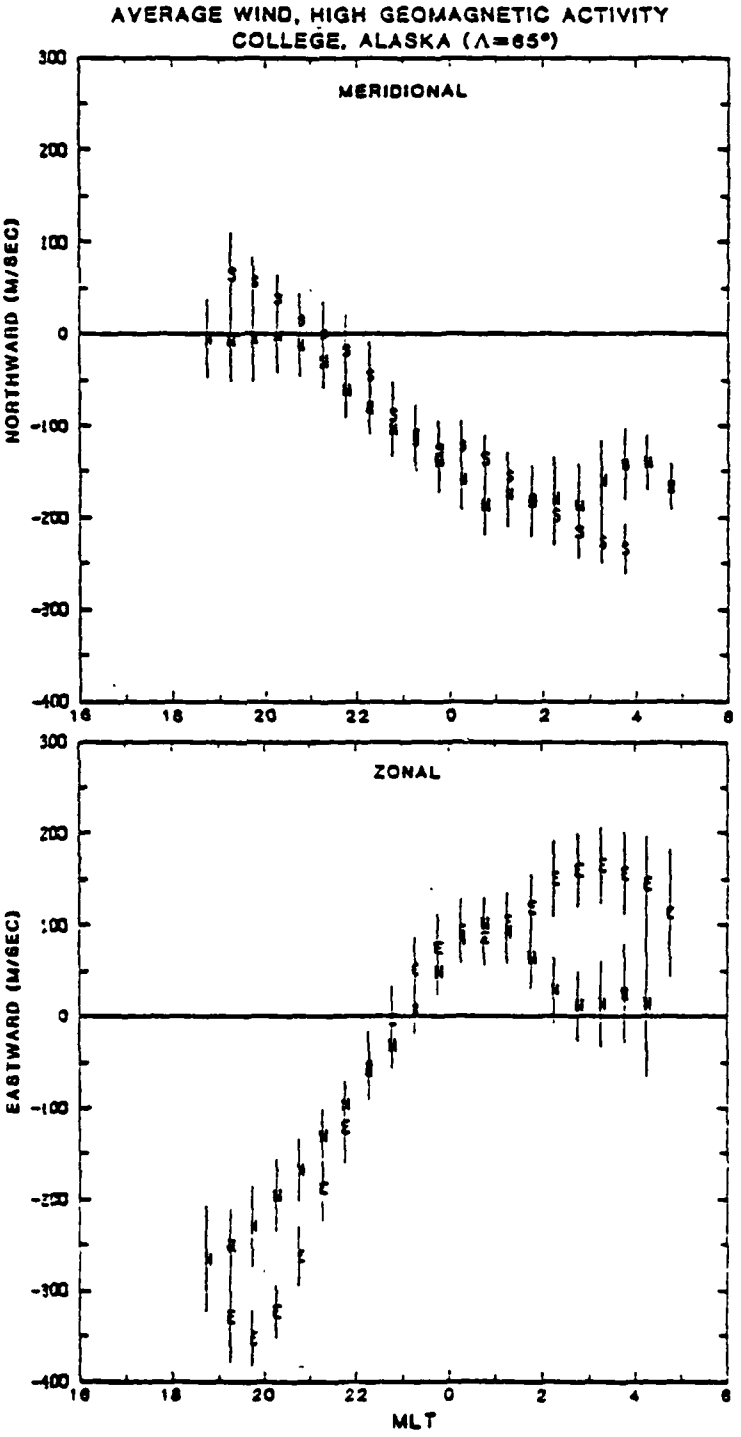

(a)

(b)

Figure 4.10 Average wind components for high geomagnetic activity in a: the meridional direction, b: the zonal direction, and c: the zenith.

(c)

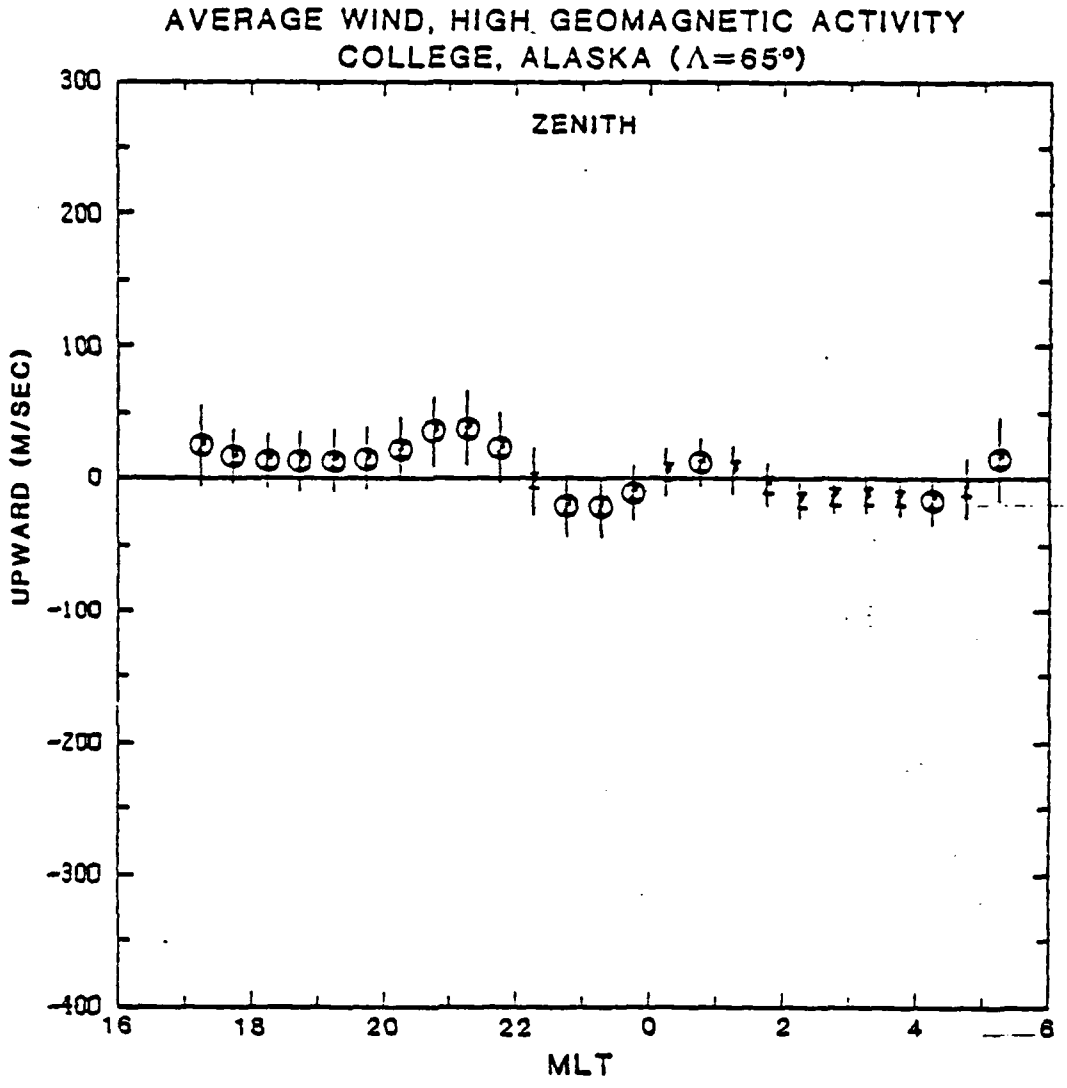

Figure 4.10 (Con't)

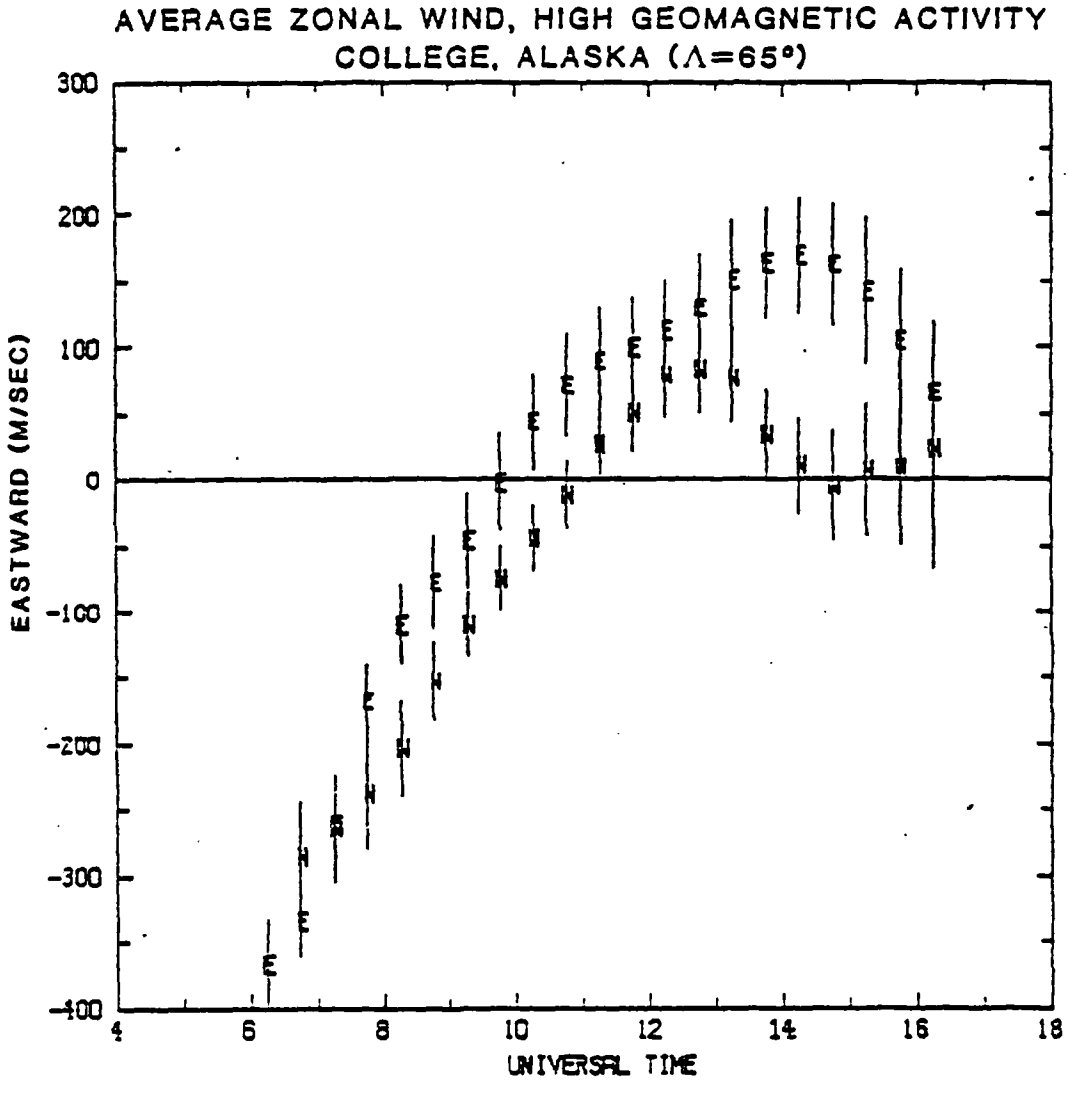

Figure 4.11 The high geomagnetic activity zonal wind components in universal time.

convection in this manner would affect a large area of the atmosphere simultaneously, in contrast to an auroral substorm which is a local effect. The enhanced convection (and increased power from the solar wind-magnetospheric interaction) can then lead to local substorm activity which becomes important after 21:00MLT.

The zenith wind is significantly more disturbed in the high activity averages (Figure 4.10c). It is upward from 17:15 to 21:45MLT, then turns downward briefly. This could be caused by the poleward auroral zone and equatorward polar cap flow regions interacting over the station, providing forcing for a vertical wind.

A longitudinally independent model of substorm effects on the thermosphere has been studied by Richmond and Matsushita (1975). For a power input of 10^{12}W at 70° latitude, a large meridional disturbance is produced that propagates poleward and equatorward. An upward vertical wind of 50m/sec lasting about one hour is obtained. During high geomagnetic activity auroral breakups often occur earlier in magnetic local time than for quiet conditions. Thus the average high activity vertical wind occurs earlier in magnetic local time than the low activity average. Even averaging over many nights, the vertical wind is a consistent feature. Current global circulation models do not predict such large vertical wind.

The moderate geomagnetic activity averages do not show as much structure as the low and high activity cases. The large number of moderate activity nights include many auroral substorms with varying onset times. The low and high activity cases, however, show more structure.

VII. THE AVERAGE TEMPERATURE

Averages of the observed kinetic temperature of the neutral gas were calculated, using the same statistical criteria as for the wind averages. Within the error of the measurements, average temperatures in the individual viewing directions show little variation when compared with one another. Therefore, the measurements from all viewing directions were averaged to increase the number of events in each sample. The physical reason for this smoothness is that energy advection between "hot" spots of particle and Joule heating tends to smooth out temperature variations around the sky when many nights are averaged. Since the profile of the 6300A emission height broadens during the periods of maximum particle heating, the temperature may appear to remain constant. After the precipitation has stopped, advection can smooth out the regions of enhanced temperature. The small variations in the average temperatures with viewing direction may also be due to vertical heat conduction. This would require a large gradient in the temperature height profile.

The primary heat source in the thermosphere is the absorption of solar UV radiation. The UV solar flux is not routinely monitored. However, the solar flux at 10.7cm is obtained daily by the National Research Council in Ottawa, Canada. During solar maximum, the values of the 10.7cm flux correlate reasonably well with satellite UV spectrometer measurements in the wavelength region of the Schumann-Runge continuum of molecular oxygen (Torr et al., 1980). The 10.7cm solar flux (abbreviated by Sa) normally varies from about 75 to 250 x 10^4 Jansky (1J = 10^{-26}Wm^{-2} Hz^{-1}).

Three averages were computed, low ($Sa^{-1}<130x10^4$ J), moderate ($130x10^4$ J$<Sa^{-1}<190x10^4$ J) and high ($Sa^{-1} > 190x10^4$ J) 10.7cm solar flux from the day previous to the measurements, where Sa^{-1} refers to the previous day's solar flux. These averages were performed to determine the importance of UV heating in the auroral zone thermosphere. A one day time lag is used as a nominal period for solar wind particles to interact with the earth's magnetosphere. There were nineteen low 10.7 cm solar flux days, sixteen moderate, and nine high.

The resulting average in universal time is shown in Figure 4.12. The solid horizontal line through each set of measurements is the mean. As with the zenith wind averages, the circled values differ from the mean according to Student's t test at the 95% confidence level. The averages are: for low Sa^{-1}, 953±18°K, moderate Sa^{-1}, 1060 ± 40°K, and high Sa^{-1}, 1176±30°K. This temperature increase with the previous day's 10.7cm solar flux has been experimentally verified by long-term ground-based Fabry-Perot interferometer measurements at mid-latitude by Hernandez (1982a).

The individual low activity temperature average points are not statistically different from their mean for the low solar activity case. For moderate solar flux conditions, the temperature decreases in the early evening, reaches a minimum around 12:30UT, and then recovers. Higher particle energies have been measured in the post-midnight auroral oval in the diffuse aurora by Wallis and Budzinski (1981). This temperature decrease could be due to the emission region extending to lower altitudes when the diffuse aurora is over College, causing an apparent decrease in temperature.

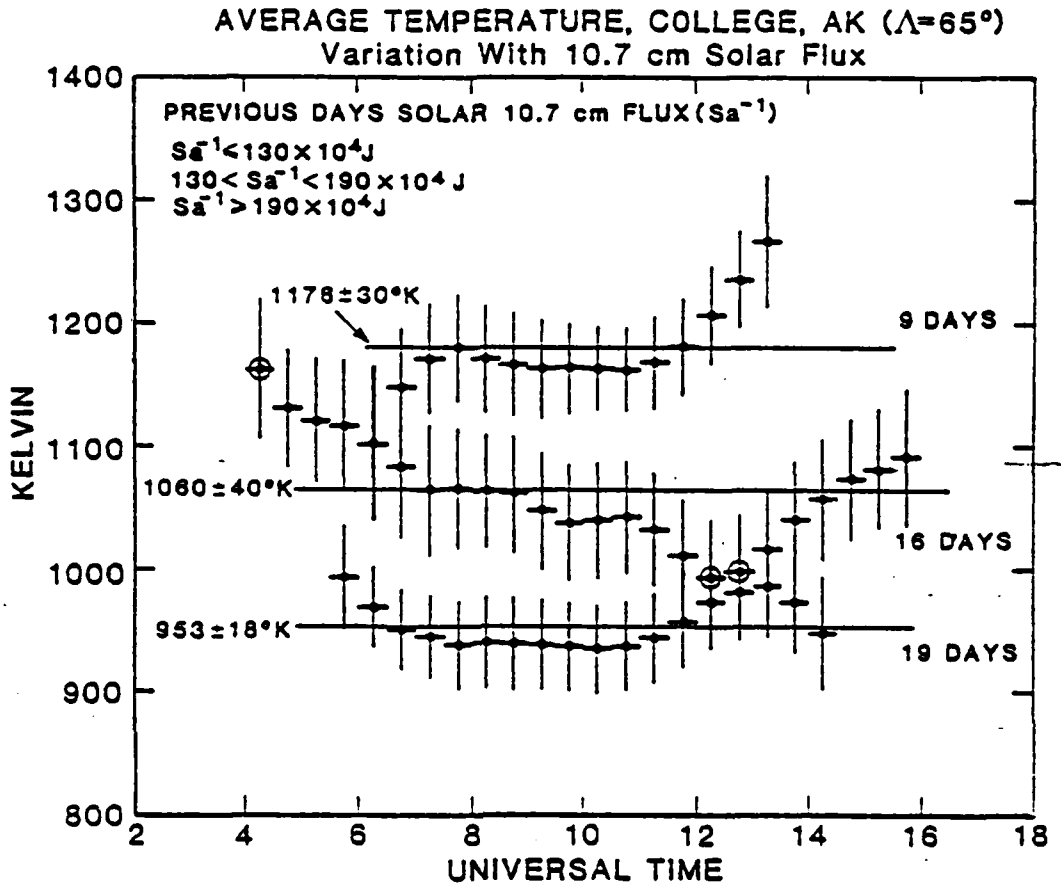

Figure 4.12 Average temperature for low ($Sa^{-1} < 130 \times 10^4$ J), moderate ($130 \times 10^4 < Sa^{-1} < 190 \times 10^4$ J), and high ($Sa^{-1} > 190 \times 10^4$ J) previous day's 10.7 cm solar flux. The data point at 6:15UT (with the thick error bar) represents two data points, one for the moderate average and the initial point for the active average. The circled points are different from the mean at the 95% confidence level as determined from Student's t test. The two circled points after 12:00UT are associated with the moderate case.

The high solar flux case has higher temperatures in the morning than the evening. These high solar flux conditions are typical of magnetic storm periods. Two of the nights in this group featured type-A red aurora. Large temperature enhancements accompany the increase in soft particle flux associated with type-A red aurorae.

To investigate the geomagnetic effects of atmospheric heating, the moderate solar flux case was subdivided by the Ap index as for the wind averages. Neither the low nor high solar flux cases have enough measurements to warrant additional subdivisions. The results, displayed in Figure 4.13, show that no individual average point is significantly different from the group mean as calculated from Student's t test. The group averages are for quiet geomagnetic conditions 925±23°K (three days), moderate 1002±28°K (eight days), and active 1170±66°K (5 days).

The average for the quiet days shows an approximately constant temperature with respect to the group mean. As the magnetic activity increases, the eight moderate geomagnetic activity nights exhibit an apparent temperature decrease at 12:30UT as in the moderate solar flux case, but in this average they are not statistically different from the mean. The high activity case has a large decrease in temperature in the evening, which may be a height effect. The height range of the emission profile increases with the occurrence of auroral substorms at lower altitudes. Thus the measurements have a larger contribution from a cooler region of the atmosphere. However, overall, as geomagnetic activity increases, the average temperature increases due to magnetospheric-ionospheric heating. The change in average temperature for the moderate Sa^{-1}

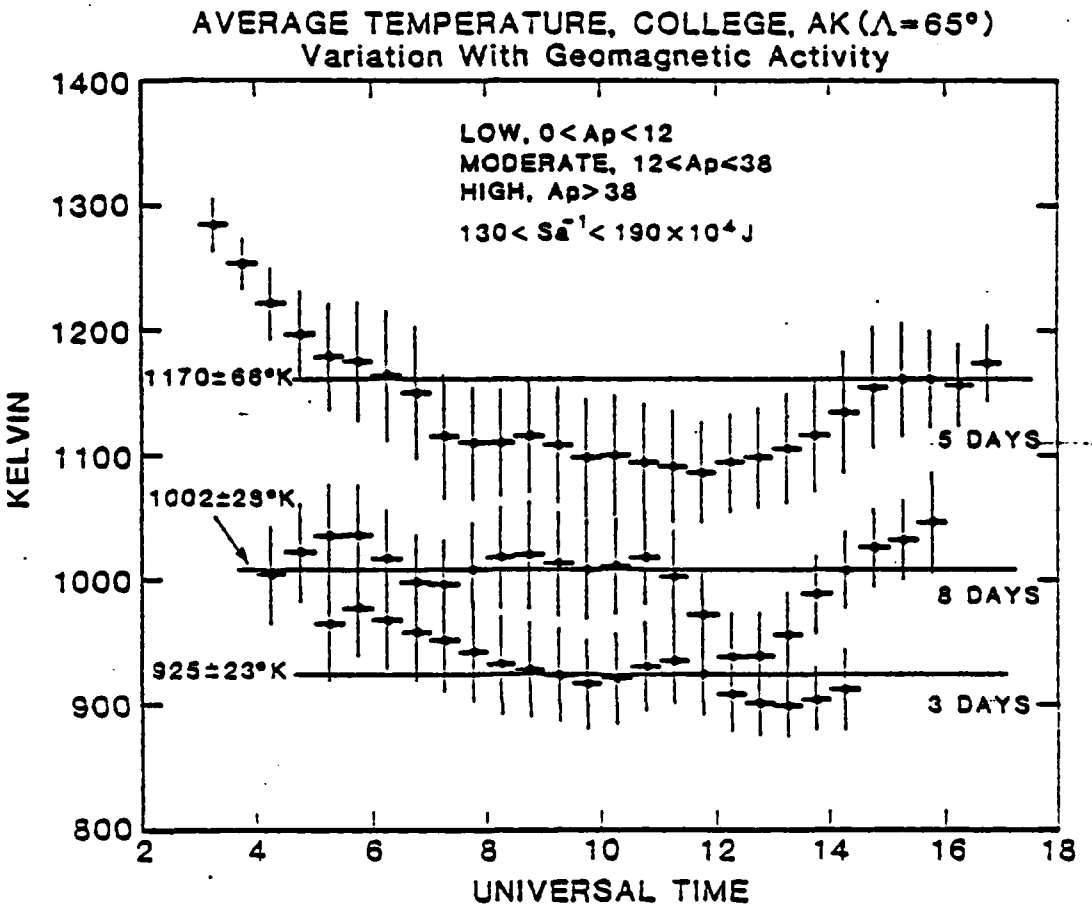

Figure 4.13 Average temperature at low, moderate and high geomagnetic activity levels for moderate previous day's 10.7 cm solar flux.

case from low to high Ap (about 250°K) is on the same order as the change between low and high Sa^{-1} (about 225°K). Clearly, geomagnetic activity can cause a large change in the atmospheric temperature in the auroral zone during solar maximum, as much as solar UV in the winter, which in turn affects the neutral atmospheric composition and the dynamics.

4.15. COMPARISONS OF THE OBSERVED AVERAGES WITH THE NCAR TGCM

The measurements presented in the previous sections can be used to test the predictions of the NCAR thermospheric global circulation model, albeit with measurements from only one station. A run of the NCAR TGCM was performed for the geophysical conditions of December, 1981, Figure 4.14. The general shape of the experimental and model results is similar, but there are large differences in the zero crossing time, about one hour in the meridional direction and over three hours in the zonal direction. The wind crossover time could be adjusted by shifting the convection pattern and altering the size of the polar cap potential. The model slightly overestimates the morning meridional and zonal wind velocities.

The NCAR TGCM with the more symmetric convection pattern represents the average data quite well, suggesting that the important physical properties of the auroral zone thermosphere are well represented. In Section 4.2 it is shown that the NCAR model, with its steady-state convection pattern and large grid cell size, cannot explain deviations from the average behavior due to local auroral substorms.

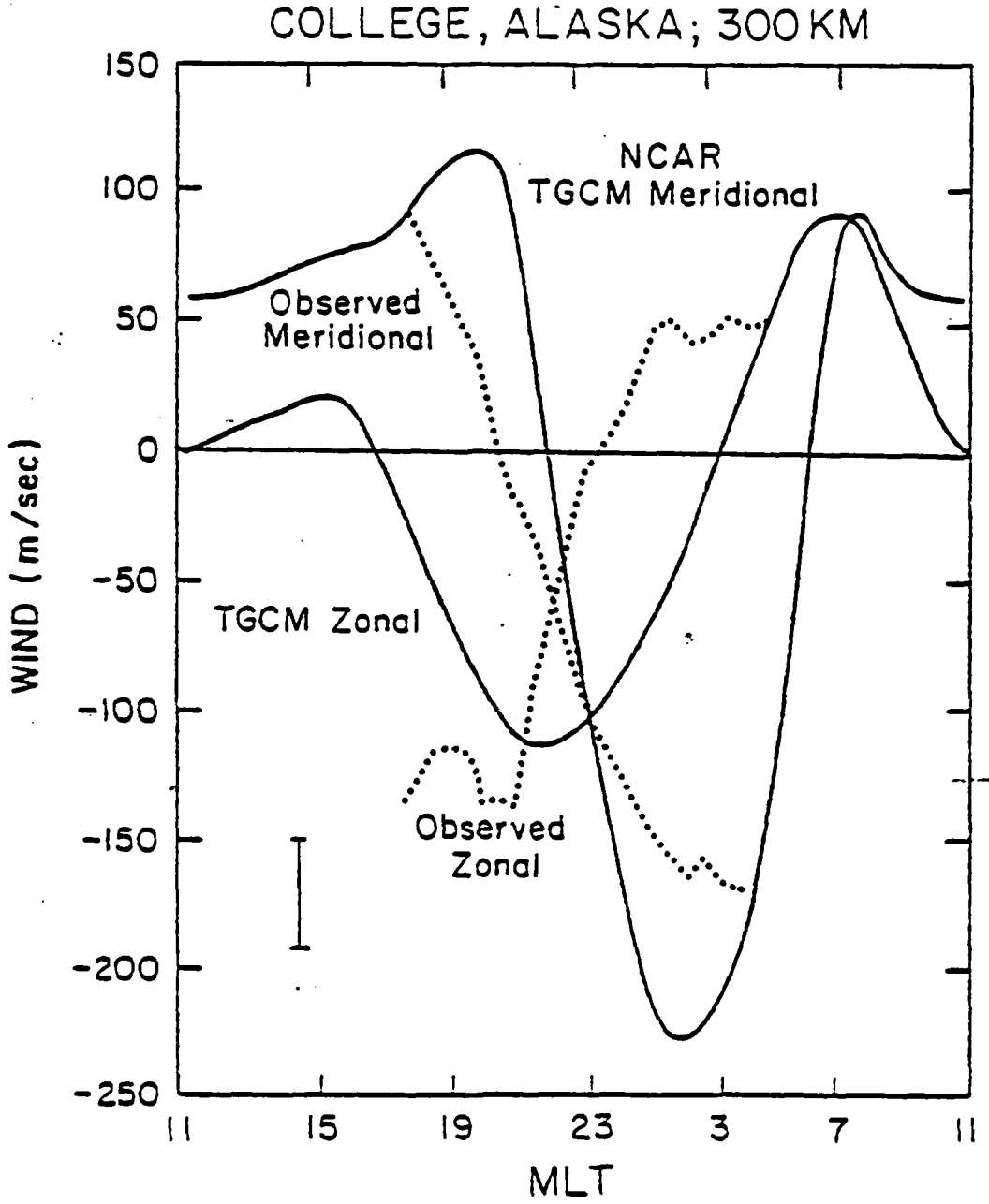

Figure 4.14 The meridional and zonal wind prediction for College by the NCAR TGCM for the geophysical conditions of December, 1981. Also plotted is the moderate geomagnetic activity average from College. The nominal error bar for the College averages is shown in the lower left corner. NCAR TGCM results have been made available by T. Killeen and R. Roble.

4.16. DISCUSSION OF AVERAGE DATA RESULTS

The average wind patterns for low, moderate and high geomagnetic activity are alike. The average wind is poleward and westward in the evening, then changes to equatorward around magnetic midnight. However, as the geomagnetic activity increases and the auroral oval expands, the wind speed increases and the equatorward shift occurs at an earlier magnetic local time. On individual nights, the wind behaves similarly to the average wind for corresponding geomagnetic activity if the auroral oval is situated over the station to order the wind flow.

The apparent latitudinal motion of the station relative to the auroral oval is also important in interpreting the relation of the wind components to the pattern predicted by global models, which currently employ only steady-state convection and a fixed ionosphere. A comparison between meridional averages at different geomagnetic activity levels shows that the component viewed to the south during moderate and active conditions is similar to the wind component viewed to the north at low and moderate geomagnetic activity. The measured zonal wind on individual nights agreed with the NCAR TGCM when the latitude of the station was adjusted relative to an assumed convection pattern.

The meridional and zonal wind components are each primarily influenced by different forces. The average meridional evening wind direction is poleward in the auroral zone and equatorward in the polar cap due to the Coriolis effect. The regions of opposite flow form a pressure ridge that is occasionally observed from College during active conditions. The predominant meridional

momentum source in the middle of the night is the anti-sunward pressure gradient resulting from solar heating on the dayside. The Joule and auroral particle heat sources contribute to a temperature increase in the polar cap. This heating also enhances the anti-sunward pressure gradient. The averages show no increase of meridional wind velocities with increasing magnetic activity.

However, the zonal winds show large increases in velocity with increased geomagnetic activity. This is consistent with ion drag being the most important momentum source for the zonal wind. Ion drag forcing is determined by the strength of the flow produced by magnetospheric convection. When displayed in magnetic coordinates, the zonal wind average is uniform within the region sampled from College around midnight and in the morning. However, in the evening the zonal wind averages during low and high activity are uniform in universal time. This is probably due to large scale magnetospheric convection dominating the ionospheric plasma drift. The average westward evening component of the zonal wind is larger than the morning eastward component. On the average, the coupling of the ion motion to the neutrals by collisions is higher in the afternoon and evening, due to a higher electron density in the post sunset ionosphere. The evening westward component is not always larger on active individual nights when high electron densities and electric fields can occur to drive a strong eastward morning flow. An additional cause for a difference between the evening and morning zonal velocities is the speed of the drifting ions. Asymmetric convection patterns such as the Heelis et al. (1982) model can have higher plasma drifts in either the dawn or the dusk cell.

Thus, the higher ion speeds can also cause larger neutral velocities. When local substorms occur, magnetic local time effects can dominate the observed zonal wind and temperature pattern. The zonal wind on individual nights can be understood in terms of the position and direction of the auroral electrojet and oval

Vertical winds are a persistent feature observed at College, and they are seen in the averages as well as the individual nights. They are often large, occasionally greater than 200 m/sec. The vertical winds are often associated with disturbances generated by substorm activity, as predicted by the model of Richmond and Matsushita (1975). The low and high geomagnetic activity average cases showed vertical winds consistent with this model, as did some individual nights. Often the largest and most rapidly changing vertical wind is measured during pulsating aurora.

The presence of the auroral oval defines the steady-state of the thermosphere over College during solar maximum. Based on the results of the forty-four nights studied, when the auroral oval contracts well poleward of College, the thermosphere begins to relax to a mid-latitude flow. This relaxation ends when the auroral oval arrives over College, accompanied by enhanced magnetospheric convection and increased particle precipitation.

The average temperature observed on a night increases with increasing previous day's solar flux. The average temperature for low activity was 953±18°K, moderate 1060±40°K and high 1176±30°K. For moderate previous day's solar flux the average temperature is 925±23°K, 1002±28°K and 1170±66°K for low, moderate, and high levels, respectively. The change in temperature from low to high

geomagnetic activity at a constant solar flux is about the same as the temperature change from low to high solar flux. As observed from College, the auroral effect on the thermospheric temperature is as large as the heating due to solar UV radiation during solar maximum.

Comparison with the NCAR TGCM for College showed reasonable agreement for moderate activity levels using a symmetric convection pattern. However the crossover time, when the wind components change sign, was different by one hour in the meridional direction and over three hours in the zonal direction. This is most likely a result of magnetospheric convection used in the model. Varying the convection pattern was shown to improve the fit between the model and the observations.

4.200 INDIVIDUAL NIGHTS

Individual nights show departure from the average pattern due to local auroral activity.

In the following discussion, reference will be made to crossover time, the time at which a wind measurement in a given direction changes sign (i.e., direction). Though the crossover time is very helpful in understanding the effect of local auroral substorms on the dynamics of the thermosphere, there are experimental and geophysical uncertainties present. Since an absolute zero-shift reference does not exist for the wind measurement, there is an uncertainty in establishing the zero wind on a given evening. Furthermore, since measurements in a given viewing direction can be separated by more than one-half hour, the changes between points will not necessarily be smooth, an additional uncertainty in defining a crossover time. Finally, on some nights, geophysical variation in the wind can cause measurements in a given direction to cross zero several times.

In an effort to separate changes in the emission height profile from actual heating or cooling of the neutral gas, ratios of the 6300A/4287A emission for two nights were determined. Ratio data were obtained from a five channel tilting-filter meridian scanning photometer at Poker Flat, Alaska (Romick, 1976). The intensity, corrected for extinction, is averaged over four degrees elevation angle at the College magnetic zenith for each wavelength (6300A, 4278A, 5577A, and 4861A (Hβ)) as a function of time. The

data were smoothed using a running average (Bloomfield, 1976). The ratio is an indicator of the spectral hardness of the incident electrons. As the incident particle energy increases, the ratio decreases. Correspondingly, the emission height profile of 6300A broadens, possibly yielding a lower temperature.

4.21. THE RELATIONSHIP OF THE AURORAL ELECTROJETS TO THE NEUTRAL CIRCULATION

The ionospheric conductivity couples the ionospheric current system to the neutral gas. The horizontal momentum due to ion drag is given by

$$P_{ID} = (\sigma_p B^2/\rho)\ \{(u_I-u) + \sin^2 I(v_I-v)\} + (\sigma_H B^2 \sin I/\rho)\ \{(v_I-v) + (u_I-u)\} \qquad (1)$$

(Killeen and Roble, 1983). Here σ_p and σ_H are the Pedersen and Hall conductivities, u_I (v_I) and u(v) are the zonal (meridional) ion and neutral bulk velocities, positive eastward and northward, ρ is the neutral gas density and B the magnetic field.

The ionospheric current can be related to the conductivity via Ohm's law

$$\underset{\sim}{J} = \underset{\approx}{\sigma} \cdot \underset{\sim}{E}$$

where $\underset{\approx}{\sigma}$ is the conductivity tensor and $\underset{\sim}{E}$ the ionospheric electric field. Since the neutral atmosphere is in motion,

$$\underset{\sim}{E} = \underset{\sim}{E}_{\perp} + \underset{\sim}{v} \times \underset{\sim}{B}$$

where $\underset{\sim}{E}$ is an invariant in the rest frame of the neutrals. The electric field $E_\perp$ is the applied ionospheric electric field and $\underset{\sim}{v}$ the neutral velocity, both height dependent. The conductivity depends on the electron density and the electron and ion collision and gyrofrequencies (Bostrøm, 1973). Below 100km the collision frequencies of both the ions and electrons are much larger than their gyrofrequencies. Above 100km the electrons tend to move with the $\underset{\sim}{E}\underset{\sim}{x}\underset{\sim}{B}/B^2$ drift velocity because the gyrofrequency is larger than the collision frequency. Ion motion, however, is still dominated by collisions with the neutrals, and a current develops. The Hall component, perpendicular to the electric field, is given by

$$\underset{\sim}{J}_H = -\sigma_H(\underset{\sim}{E} \times \underset{\sim}{B})B^{-1}$$

where in the F region

$$\sigma_H = \nu_{in}^2 \, (\nu_{in}^2 + \omega_{ci}^2)^{-1} \, en_e \, B^{-1} \, .$$

Here ν_{in} is the ion-neutral collision frequency, ω_{ci} the ion gyrofrequency, e the electron charge and n_e the electron density (Bostrøm, 1973). Without ion-neutral collisions the ions and electrons would both drift with $\underset{\sim}{E}\underset{\sim}{x}\underset{\sim}{B}/B^2$ and there would be no perpendicular current, as in the exosphere. Note the current is in the opposite direction of the relative drift. The Pedersen component parallel to the electric field is

$$\underset{\sim}{J}_p = \sigma_p \underset{\sim}{E}$$

with conductivity

$$\sigma_p = \nu_{in}\omega_{ci} \ (\nu_{in}^2 + \omega_{ci}^2)^{-1} \ en_e B^{-1} \ .$$

The addition to the momentum equation 4.2 due to vertical ion drag will be neglected. The parallel conductivity, $\sigma_\parallel$, decreases at lower altitudes due to collisions because

$$\sigma_\parallel = [(m_e \ \nu_{en})^{-1} + (m_i \ \nu_{in})^{-1}] \ e^2 n_e .$$

It then approaches the conductivity of a completely ionized gas at higher altitudes, about six orders of magnitude higher than the perpendicular conductivities (Bostrøm, 1973). Therefore, the parallel electric field is very small, and consequently little $\underset{\sim}{E}\times\underset{\sim}{B}/B^2$ drift will occur in the vertical direction.

At 65° an eastward current exists in the evening, with a stronger westward current displacing it after magnetic midnight. The region of current (or electric field) reversal near midnight is the Harang discontinuity. In this region the Pedersen current is dominant, as the electric field vector swings from poleward to equatorward. Increasing magnetic activity causes the pattern to expand equatorward, increases the intensity of the current, and shifts the Harang discontinuity to an earlier magnetic local time. The field-aligned currents are typically into the ionosphere in the evening eastward electrojet region and away from the ionosphere in the morning westward electrojet (Iijima and Potemra, 1976). An estimate of the horizontal current flow can be made from groun-dbased magnetometers. The horizontal component of the geomagnetic field (H component) decreases during auroral substorms. In the evening it typically

increases above a quiet time zero. These negative and positive deviations are interpreted as westward and eastward flowing currents. Great effort has been devoted to the study of the high-latitude ionospheric current system from magnetometer data. Meridian and zonal chains of magnetometers allow mapping of the currents (Hughes and Rostoker, 1979, Akasofu et al., 1983).

Data from twelve International Magnetospheric Study (IMS) magnetometer stations were obtained. Fifteen-minute average vectors of the horizontal disturbance field are obtained from available stations for individual nights with Fabry-Perot interferometer measurements. The most quiet magnetic day for each month, the Q1 day, is averaged for the station baseline and subtracted from the data. The vectors are plotted as a function of magnetic local time (Cole, 1963).

The horizontal disturbance vectors are related to the ion flow direction. The disturbance vector rotated by 90° to a first approximation is the horizontal current over the station (hence a westward current for a negative disturbance vector). The ions flow in the opposite direction of the current.

This is because the magnetometers measure primarily the Hall current. The maximum current flow is near 130km where the electrons move with essentially the $\underset{\sim}{E}\times\underset{\sim}{B}/B^2$ drift, while the ion-neutral collision frequency is large enough that the ions are almost stationary. Previously it was shown that the ion drag momentum equations 1 is a function of the Hall and Pedersen conductivities. Thus, the magnetometers can give insight into the direction of the ion flow but not the actual ion velocities or

ionospheric conductivity (without additional assumptions). The response of the neutrals to the currents is not instantaneous. Estimates of the time scale for the response of the neutrals to enhanced ion flow have been made by Fedder and Banks (1972). The response time of the zonal neutral wind to a 20mV/m electric field was calculated to be about one hour in the F region. This time varies from about one half hour to two hours depending on the strength and temporal evolution of the applied electric field.

The latitudinal and longitudinal separation of the IMS stations also shows the spatial and temporal morphology of the auroral electrojets. In the study of individual nights this will be important in the interpretation of the wind.

4.22. THE EMISSION HEIGHT PROFILE OF THE AURORAL RED LINE

The wind and temperature data are obtained by measurement of the total light in the instrument's field-of-view from the ground to the top of the atmosphere. For nighttime measurements, the amount of 6300A emitted below 125km and above 500km is negligible. Below 125km, $O(^1D)$ does not radiate due to collisions of the oxygen atoms with the surrounding gas (quenching). The $O(^1D)$ state is metastable, with a radiative lifetime of about 150sec. Above 500km, the density of OI atoms is typically small and though the emission is not quenched, the production of the $O(^1D)$ state is minimal.

There are three primary sources of $O(^1D)$ in aurora. Historically, the first is electron impact of the atomic oxygen ground state

$$e^* + O(^3P) \rightarrow e + O(^1D)$$

where the star denotes a secondary electron. More important is dissociative recombination of O_2^+ ions

$$O_2^+ + e \rightarrow O(^3P) + O(^1D).$$

The third is the chemical reaction

$$N(^2D) + O_2 \rightarrow NO\ (X^2\pi,\ v \leq 8) + O(^1D),$$

an important source of the auroral red line (Rusch et al., 1978). The reaction yields nitric oxide in vibrational levels (v) less than or equal to 8 (Kennealy et al., 1978). The sum of the production rate of these, plus other minor contributions due to ion-atom interchange, cascading from the $O(^1S)$ state and electron impact dissociation of O_2, give the total production rate, $\eta(O^1D)$.

Quenching of $O(^1D)$, primarily by N_2, limits the emission of the 6300A photons. The emission rate of 6300A in the steady-state is

$$\eta(6300A) = \eta(O(^1D))\ A_{6300}\ [A_{1D} + kn(N_2)]^{-1} \text{ photons cm}^{-3}\ \text{sec}^{-1}.$$

The Einstein coefficients are $A_{6300} = 5.15 \times 10^{-3}$ sec^{-1} and $A_{1D} = 6.81 \times 10^{-3}$ sec^{-1}. The rate coefficient for the quenching reaction

$$O(^1D) + N_2(X^1\Sigma_g^+) \rightarrow O(^3P) + N_2^{\emptyset}\ (X^1\Sigma_g^+)$$

is $k = 2.3 \times 10^{-11}$ cm^3 sec^{-1}, where the ø denotes a vibrationally excited state (Link et al., 1981). The amount of 6300A light produced is thus a function of the N_2 density.

Model emission profiles for airglow and auroral conditions for 6300A light are shown in Figure 4.15. It is generated by a time-dependent, one-dimensional, numerical model. The model and the detailed

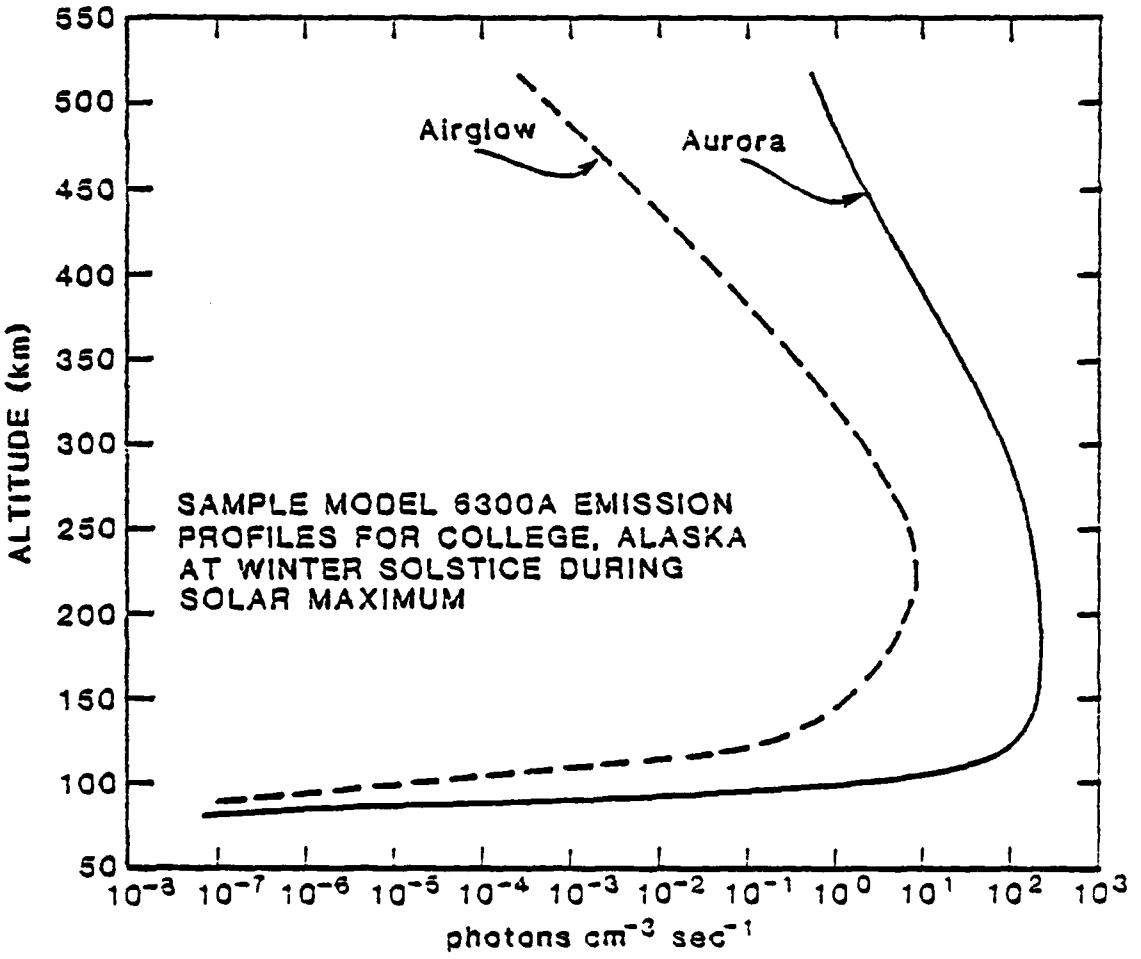

Figure 4.15 Comparison of a model 6300A emission he'ght profile without and with auroral electron precipitation (courtesy of M. Rees). Details of the model are given in the text.

chemistry included has been described by Roble and Rees (1977). For this run at 65° latitude, the input particle spectrum is a Maxwellian peaked at 2keV, and the exospheric temperature is 1100°K corresponding to solar maximum conditions at winter solstice.

The difference between the airglow and auroral emission profiles is quite pronounced. The maximum of the airglow profile is two orders of magnitude smaller than in the aurora. Furthermore, the auroral emission profile is much broader in height. The altitudes of one-half of the maximum emission are 180 and 275km in the airglow, while in the aurora the height variation is between 125 to 290km. Hence, the Fabry-Perot interferometer measurements are typically made over a larger height range in aurora. Also, the auroral emission is larger at lower altitudes, where the temperature height profile has a steep gradient and a variation of wind direction with heigh is observed (Edwards et al., 1955; Heppner and Miller, 1982).

4.23. COUPLING OF THE E AND F REGIONS

The individual nights show some interesting correlations between the E region (the lower thermosphere) where the maximum energy is deposited in typical (type-B, c, and f) aurora, and the F region (the middle and upper thermosphere), the location of the 6300A radiation.

The flow chart in Figure 4.16 illustrates the physics of the coupling between the two regions. The energy delivered from the solar wind enters the magnetosphere and ultimately regulates both the magnetospheric convection and the auroral particle precipitation. These, in turn, generate the ionospheric electric field and

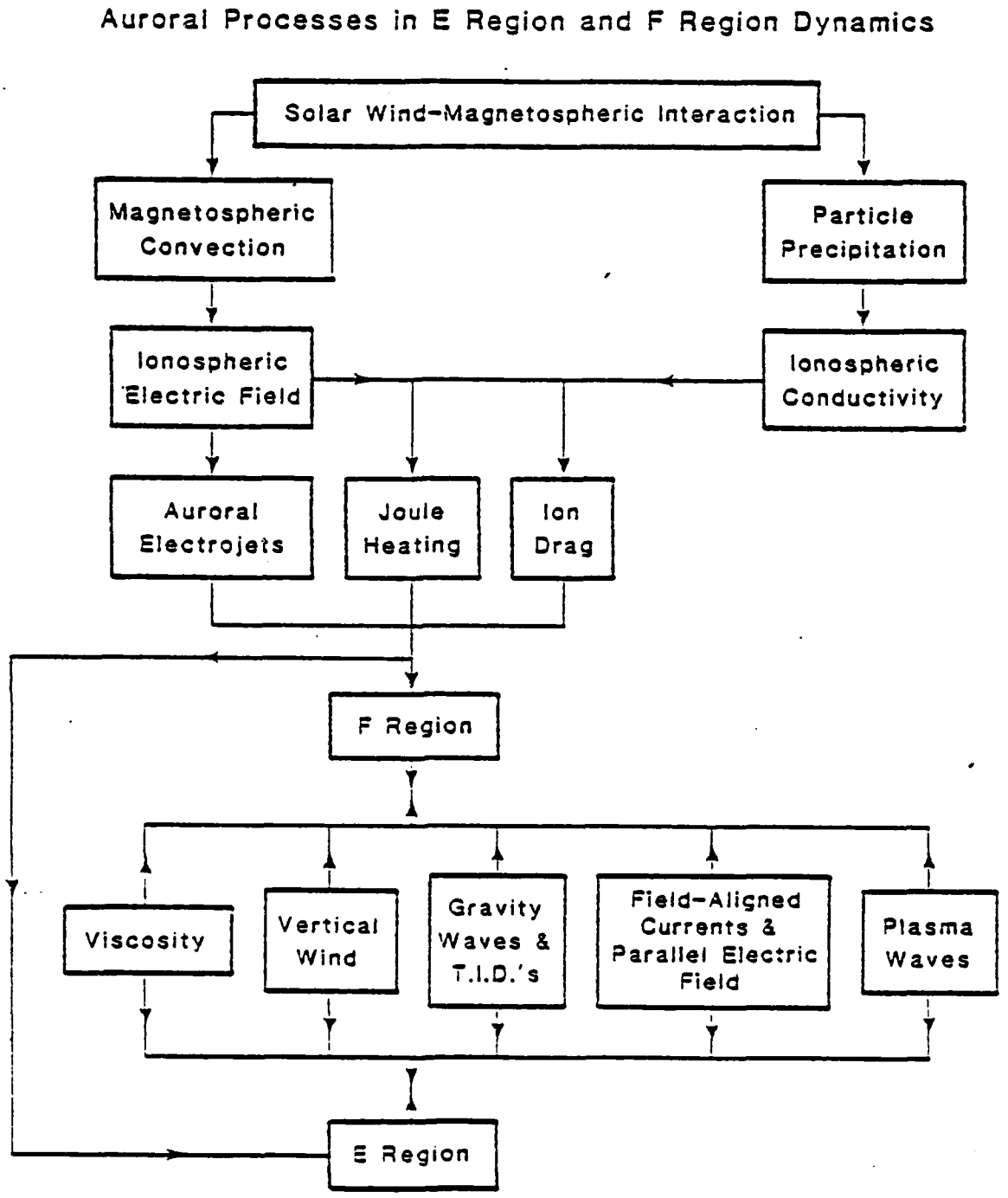

Figure 4.16 A flowchart of auroral processes in the E and F regions.

enhanced electron density. Joule heating and ion drag operate in the E and F regions.

In addition to local forcing and heating, coupling forces also exist. The first branch is the viscosity force, which acts between the two regions. The next branch is the vertical wind, which can exist simultaneously at both levels. An example of this in the data acquired at College is displayed in Figure 4.17. Vertical wind in the E region was obtained from the line profile of the OI 17924K (5577A) emission, observed with the NOAA Fabry-Perot interferometer at College. Initially, the E region vertical wind is downward, while the F region wind is zero. As the E region wind goes to zero, an upward wind develops in the F region. Between 11:30 and 13:30UT the zenith winds are zero, but after 14:00UT a downward wind develops in both the E and F regions. The F region vertical wind is generally larger than the E region wind.

The third branch shows coupling effects induced by gravity waves and travelling ionospheric disturbances (TIDs). A recent review of theoretical and experimental work on TIDs in the auroral zone has been written by Hunsucker (1982).

A changing magnetospheric electric field communicates to the ionosphere by a parallel electric field carried by field-aligned currents schematically indicated by the next branch. This process has been reviewed by Kan and Lee (1981). In the final branch, plasma waves propagate from the magnetosphere into the ionosphere during auroral substorms (see for example Kan et al. (1982) and references therein).

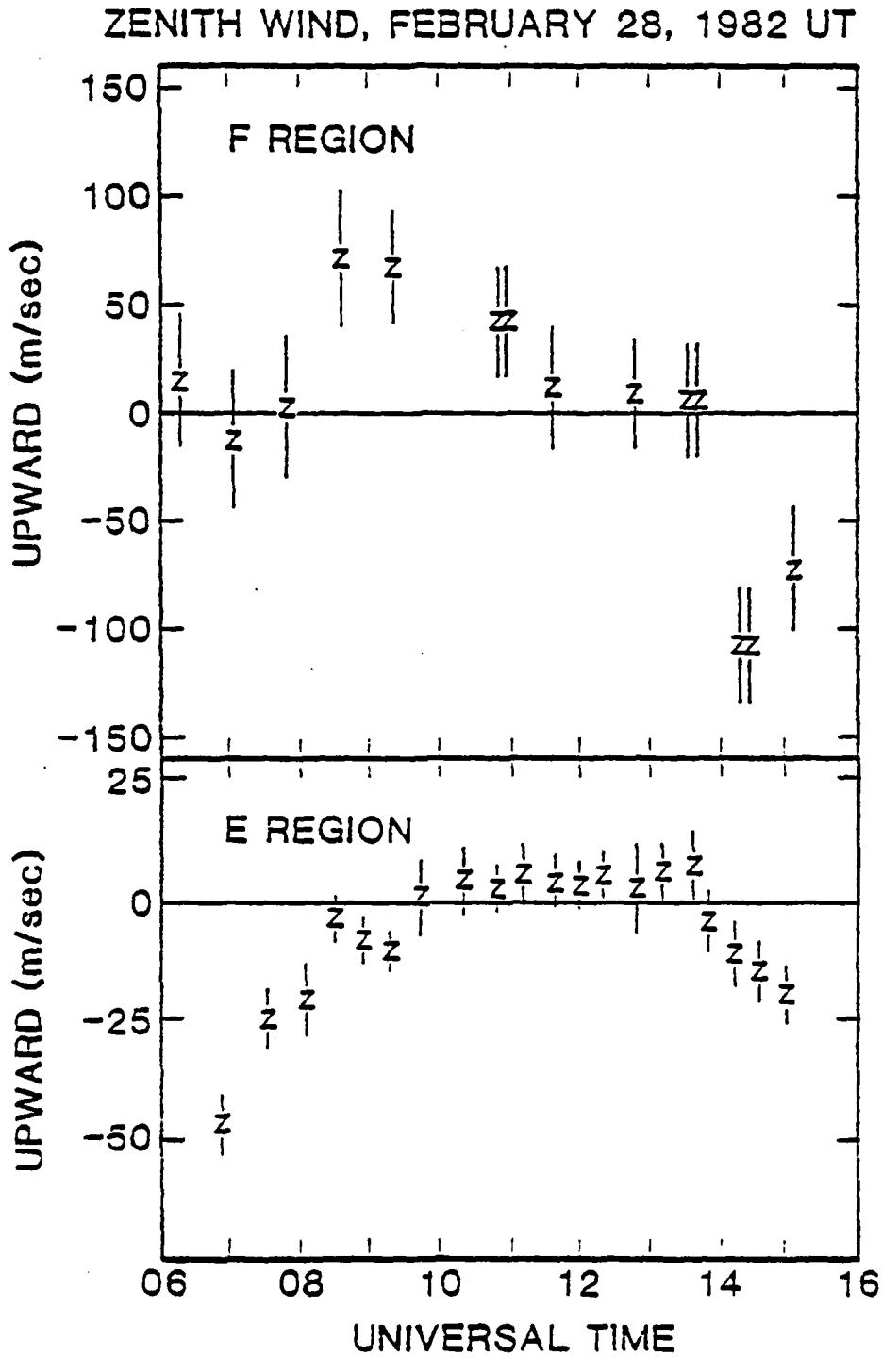

Figure 4.17 Vertical wind measurements in the E region from two Fabry-Perot interferometers at College on February 28, 1982UT. E region data courtesy of G. Hernandez.

Effects of the coupling forces between the magnetosphere, ionosphere and the neutral atmosphere are illustrated by wind and temperature data acquired during individual nights. It was found that the bulk motion of large scale auroral structures often correlates with the observed F region wind, exhibiting coupling between the E and F regions.

4.24 DECEMBER 20, 1982UT

Measurements of the thermospheric wind and temperature were obtained on December 20, 1982UT. This day was geomagnetically active with moderate previous day's solar flux. The cardinal point measurements were at 45° elevation angle. The evening meridional wind indicates that the station was farther north relative to the auroral oval than it was in the active wind average case. The equatorward Coriolis deflection in the polar cap is balanced by the poleward Coriolis effect in the auroral zone, unlike the active average case which has stronger poleward flow in the south. After 0:00MLT the meridional flow became equatorward, increasing to almost 400m/sec by 2:45MLT. At 2:50MLT a breakup occurred, with bulk motion to the east. The meridional wind then quickly decreased to about 150m/sec equatorward.

The zonal wind measurements were quite similar to the active average case, with slightly greater evening and morning magnitude (Figure 4.18b). Both components of the evening wind were westward. A breakup appeared in the station field-of-view from the southeast moving to the northwest at 20:15MLT, creating a gradient in the westward flow, followed by an eastward-moving breakup at 21:30MLT. The College magnetometer data show that the westward electrojet

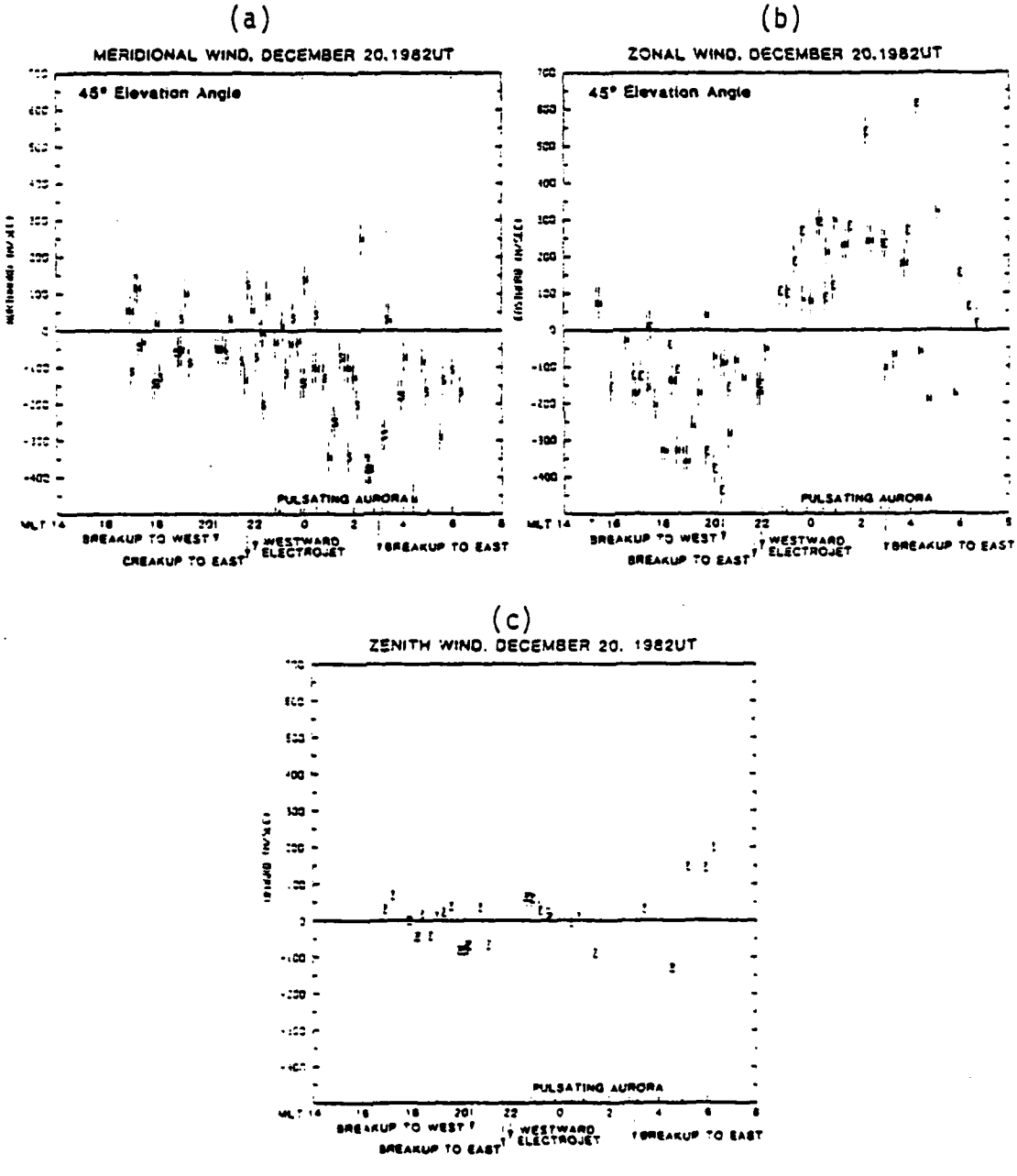

Figure 4.18 Wind measurements on December 20, 1982UT, a: meridional, b: zonal and c: zenith.

arrived at 22:00MLT (Figure 4.19). The zonal wind crossover time was about 22:50 MLT. The meridional wind crossed from poleward to equatorward about an hour later. The horizontal magnetic disturbance vectors were quite large, about 700γ, with correspondingly large westward and eastward neutral velocities.

In the morning the wind measured to the west varied considerably in the diffuse pulsating aurora. However, the magnetometer chain data show the westward electrojet occurring over Fort Smith, Canada after 2:00MLT, when the east and west velocities became unequal. The eastward velocity measured east of the station remained enhanced while the current system was in the east. The wind measured to the west decreased and turned westward at 2:45MLT, after an eastward traveling surge was observed to the west of College. The wind to the west flowed westward for the remainder of the night, except at 4:00 and 5:30MLT. The zonal wind to the west was then strongly (>200m/sec) eastward. The zonal temperature was about 950°K, as opposed to about 1200°K during the period after the surge, when the zonal wind was westward (Figure 4.20b).

This change in wind direction could be interpreted as the wind to the west of College responding to a westward ion drag momentum source, while in the east the wind is being driven by eastward ion drag. A change in the interplanetary magnetic field B_y component from negative to positive (for negative B_z) could shift the Harang discontinuity from the dusk to dawn side of the auroral oval. The station would then pass through the discontinuity a second time. However, this does not explain the change in neutral temperature observed in the west. The change in the direction of the wind may

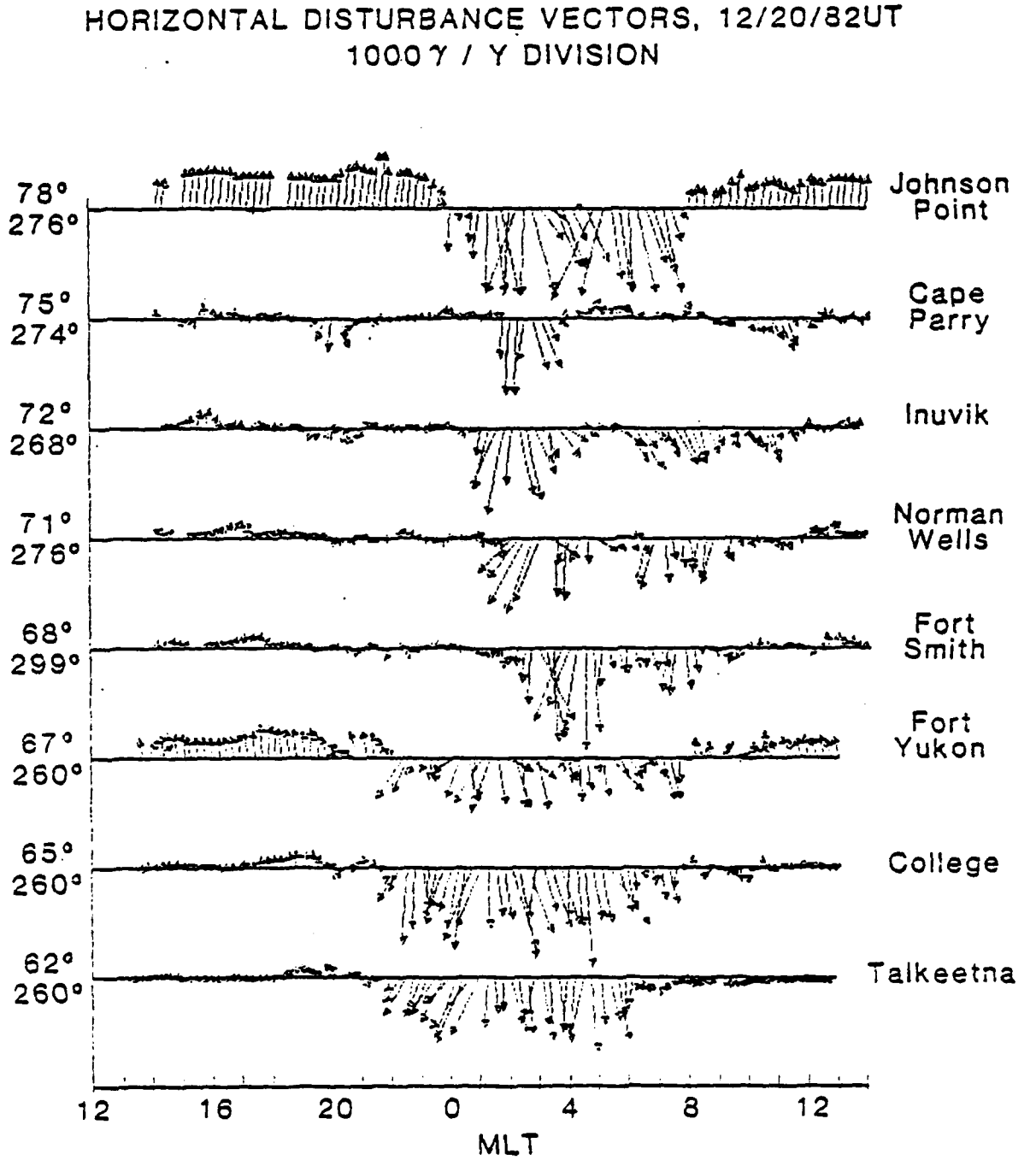

Figure 4.19 Horizontal magnetic disturbance vectors for local IMS stations on December 20, 1982UT. The distance between station zero lines corresponds to 1000γ.

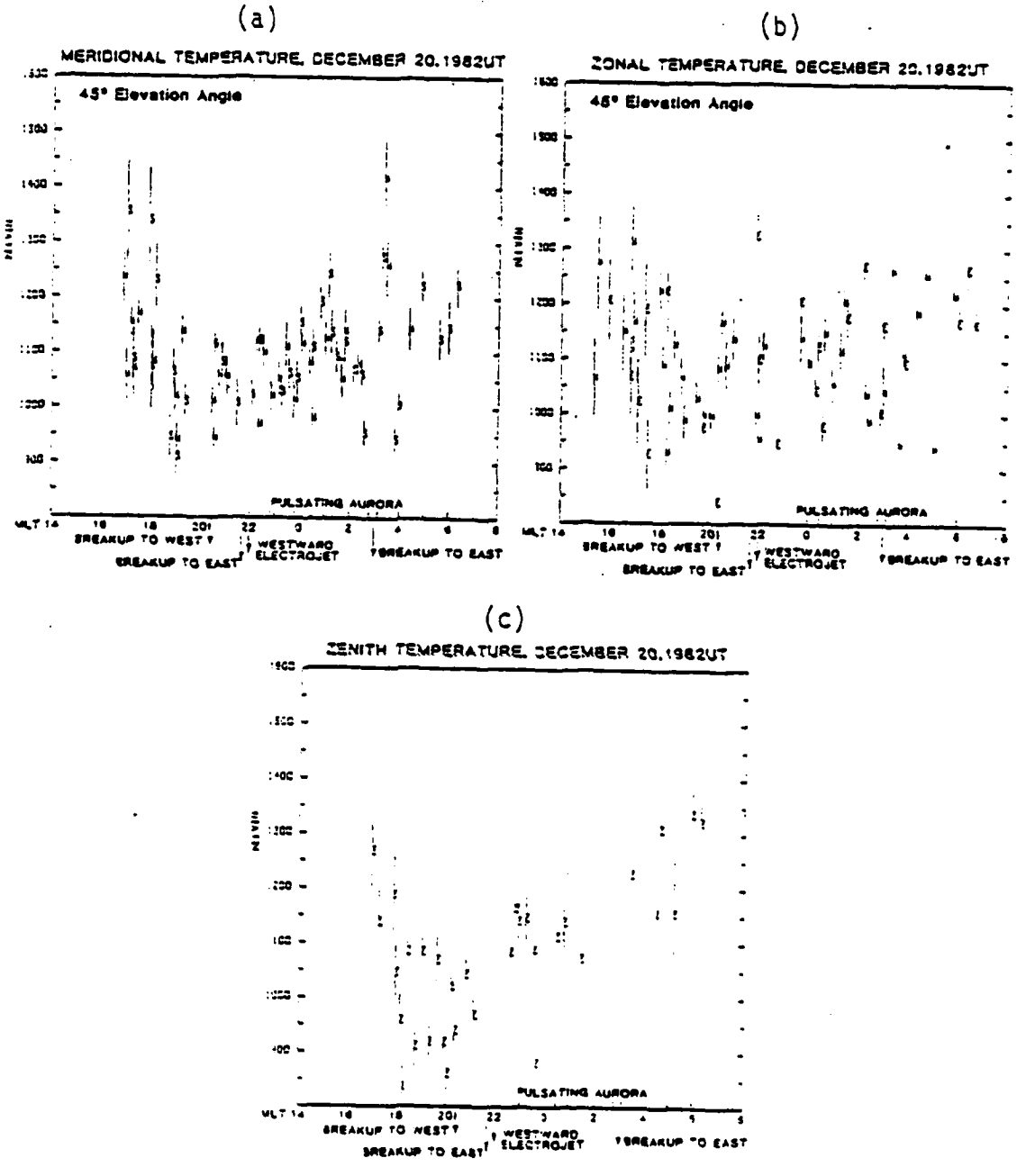

Figure 4.20 Temperature measurements on December 20, 1982UT, a: meridional, b: zonal and c: zenith.

have been due to wind shear in the F region. If the difference in temperature was due to the 6300A emission originating from a lower altitude at the lower temperature, the wind profile would have varied with height. The vertical wind observed during this period of pulsating aurora was much larger than any measured for other times of the night, consistent with the occurrence of wind shear.

The zenith wind was larger than in the active average case (Figure 4.18c). After the 20:05MLT breakup, the wind was downward for about forty-five minutes, turning upward for a short period after the 21:30MLT breakup. Following 4:00MLT, when pulsating aurora occurred and both the meridional and zonal wind components were highly variable, the zenith wind is less than about 75m/sec. A large downward wind followed by an upward wind was then observed.

The meridional and zonal temperature data are consistent with the average results for moderate solar flux and high Ap. The temperature decreases in the early evening, while the intensities of 6300A, 4278A, and 4861A, as measured by a tilting-filter meridian scanning photometer at Poker Flat, were at airglow emission levels (i.e., less than 200R of green line).

The zenith temperature measurements oscillated between 825°K and 1075°K after 17:30MLT, before the initial breakup at 20:00MLT (Figure 4.20c). After the 21:30 MLT breakup, the temperature increased. Another breakup occurred at 2:50MLT, and the temperature again rose, this time to about 1350°K.

To investigate if the zenith temperature variations were due to a change in the emission height profile or whether they were due to actual heating, the ratio of the 6300A to 4278A luminosity was

examined (Figure 4.21). In the evening airglow, the ratio was largest, since 4278A was nearly absent. As the auroral activity increased after 20:00MLT, the ratio decreased to between .4 and 1. Consequently, the emission height profile would have been broader after 19:30MLT, resulting in a lower measured temperature. Since the ratio data suggest that the emission height profile did not vary substantially after 19:30MLT, the elevated temperatures measured after the breakups were likely due to atmospheric heating.

4.25. DECEMBER 21, 1982UT

Measurements were made on the next night, December 21, 1982UT, during moderate global geomagnetic activity. The wind measurements are shown in Figure 4.22, at both 20° and 45° elevation angle. The meridional measurements at 45° resemble the active average; however, the evening poleward flow was quite large (≈200m/sec). The flow in the north turned from poleward to equatorward after the first breakup at 19:10MLT. To the south, the flow lagged the north in crossover time, but also decreased poleward after this breakup. When the second breakup occurred at 21:45MLT, the meridional wind viewed to the north at 45° decreased to near 0m/sec, while the wind seen in the south at 45° turned briefly poleward. After the 0:00MLT breakup, both north and south components at 45° decrease in equatorward velocity, with the wind in the north becoming poleward by morning.

The component in the south at 20° remained essentially zero after the first breakup until 4:00MLT. Apparently, there was a flow boundary that blocked the equatorward wind from the dayside. Neither the temperature in this region nor the intensities were

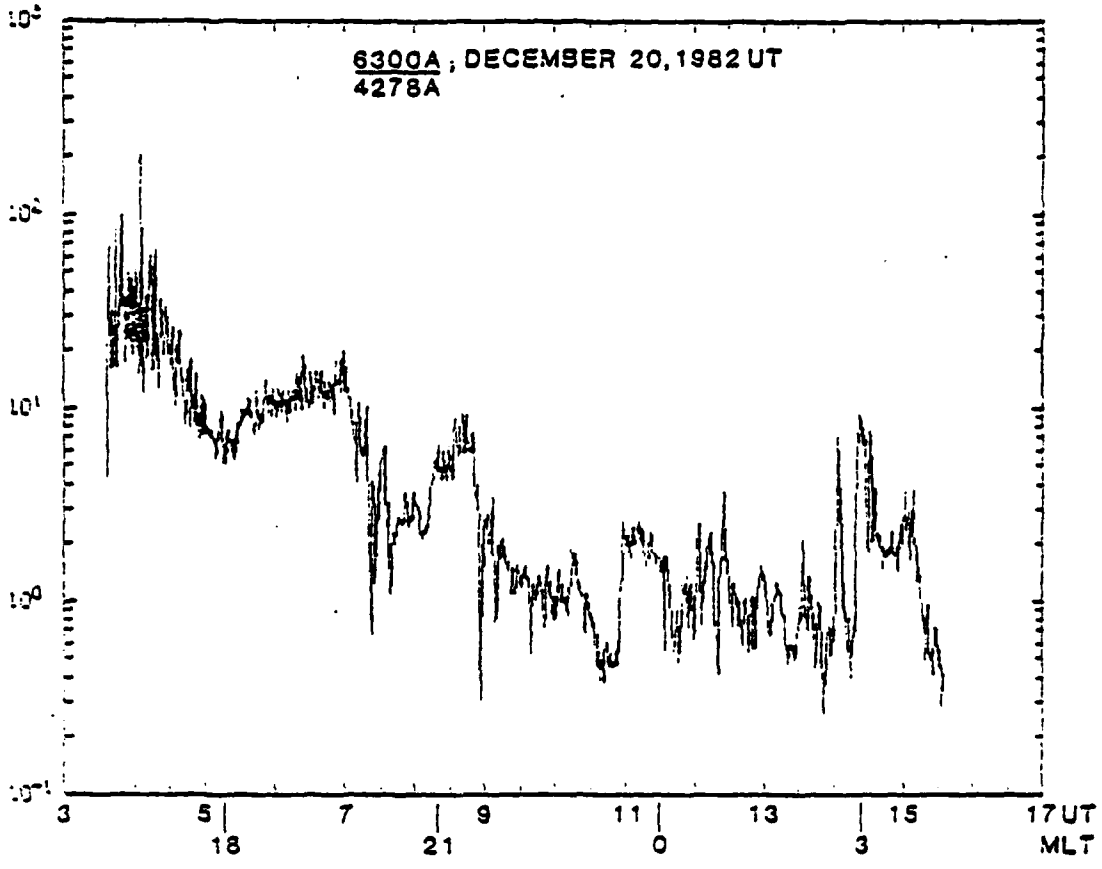

Figure 4.21 The ratio of 6300A to 4278A emission rates in the College magnetic zenith calculated from intensity measurements obtained with a tilting-filter meridian scanning photometer on December 20, 1982UT.

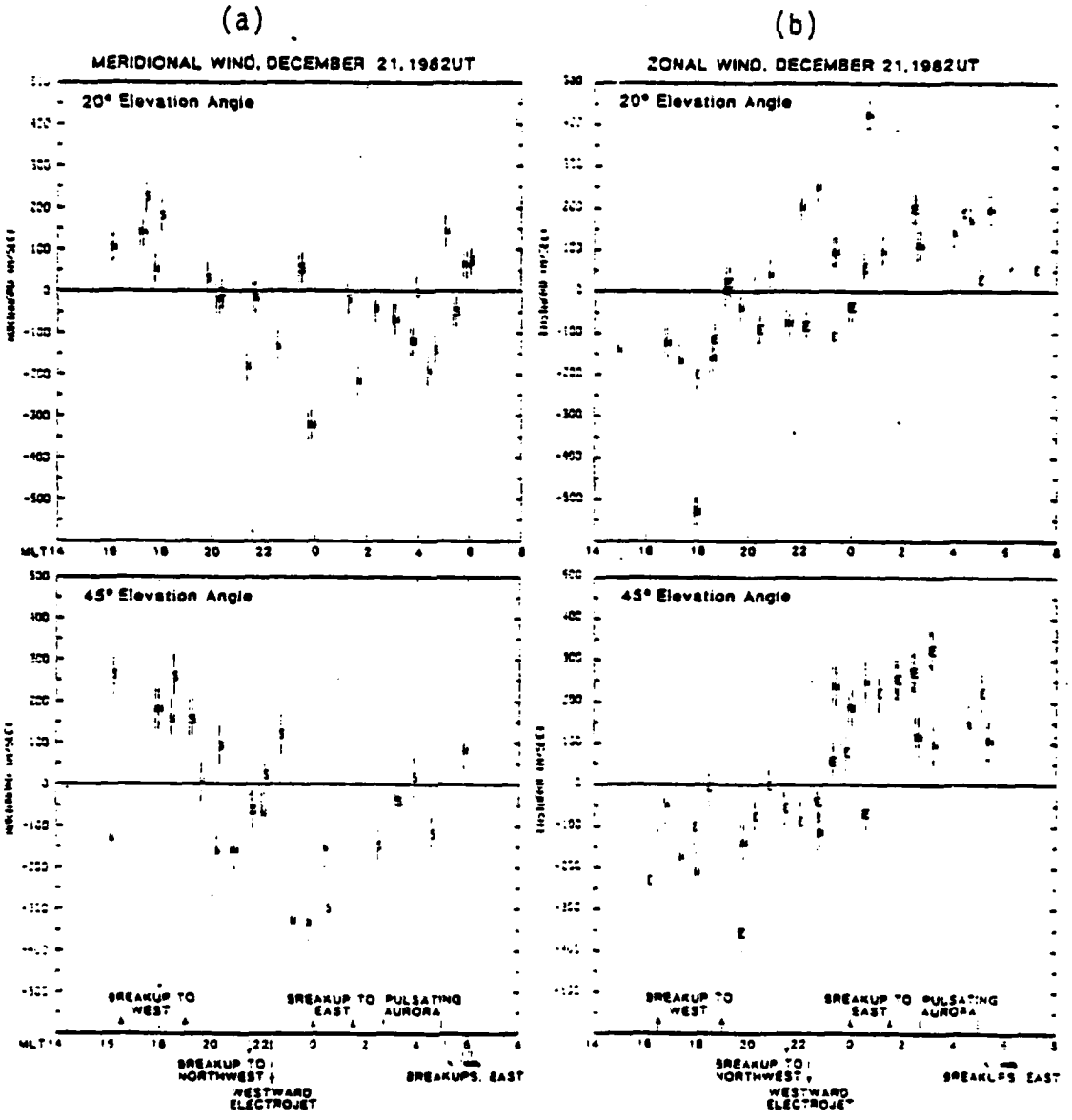

Figure 4.22 Wind measurements on December 21, 1982UT, a: meridional, b: zonal and c: zenith.

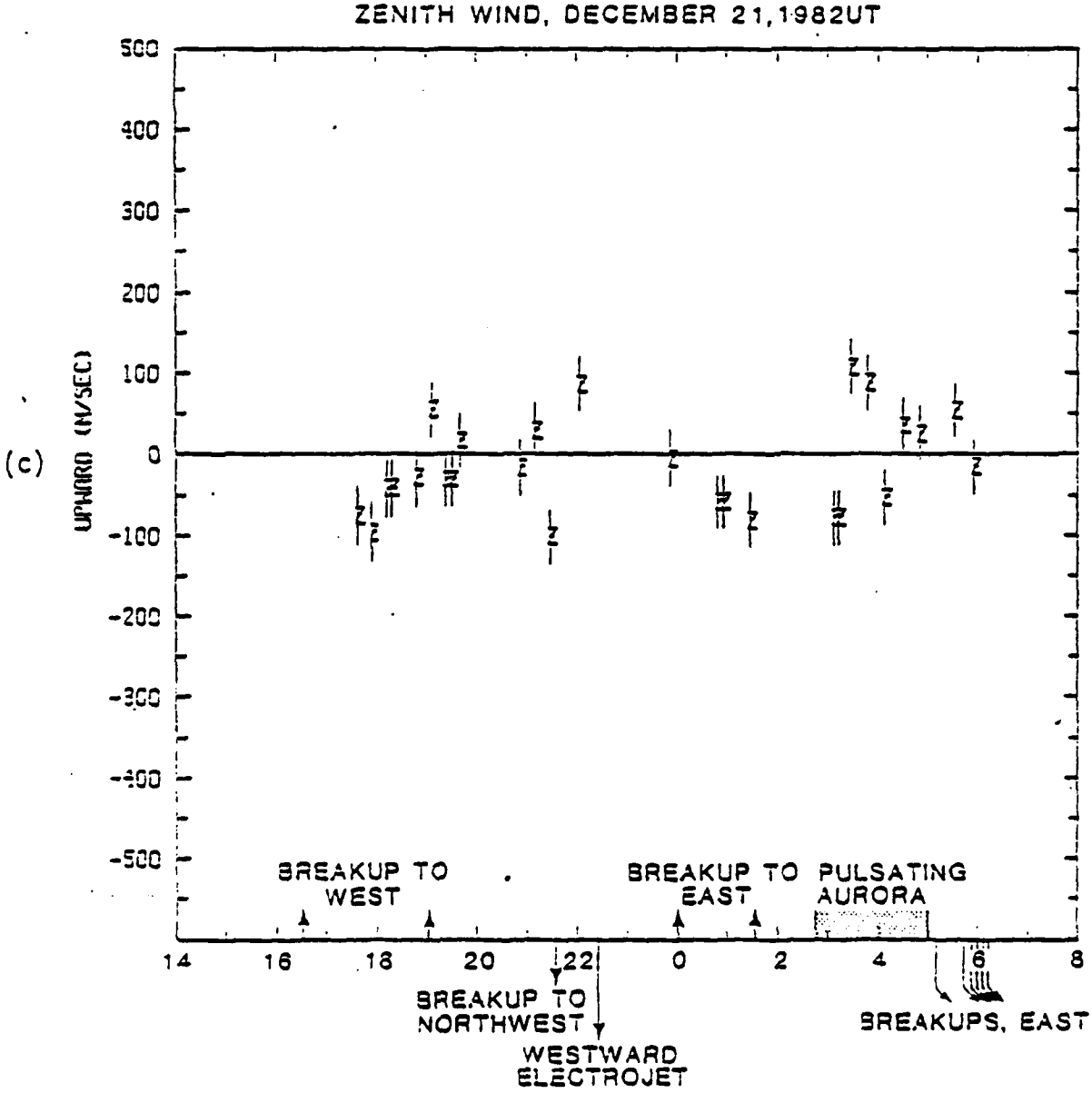

Figure 4.22 (Con't)

significantly different from the meridional measurements in the north and south at 45°.

The zonal wind components were similar to the moderate average in the evening, and to the active average in the morning (Figure 4.22). The horizontal disturbance vectors show that the westward electrojet appeared at College by 22:15MLT, about an hour after Fort Smith (Figure 4.23). An auroral breakup passed over the station moving to the northwest at 21:45MLT. The west-viewed component at 20° crossed zero and became eastward at this time. The wind component viewed in the east did not turn eastward until 0:20MLT. This crossover of wind in the east was preceded at 0:00MLT by a breakup with eastward bulk motion. Note that the northwest breakup at 21:55MLT affected the zonal components in the west at 20° but not the east at 20°.

The zonal wind was more uniform at 45°. Here both wind components crossed zero at 23:15MLT, about an hour after the westward electrojet was observed at College. The stronger morning eastward flow in the zonal component was probably due to the enhanced electrojet and morning auroral activity providing large conductivities and electron densities. This stronger eastward wind in the morning was different from the averages. After 5:00MLT there were multiple, intense breakups quickly traveling from the west to east horizons, consistent with the strong eastward velocities.

In the evening there was a downward 100m/sec wind around 18:00MLT. After the 0:00MLT breakup, the zenith wind again developed a downward component. The zenith wind shifted upward during the morning pulsating aurora, similar to the behavior on December 20, 1982UT.

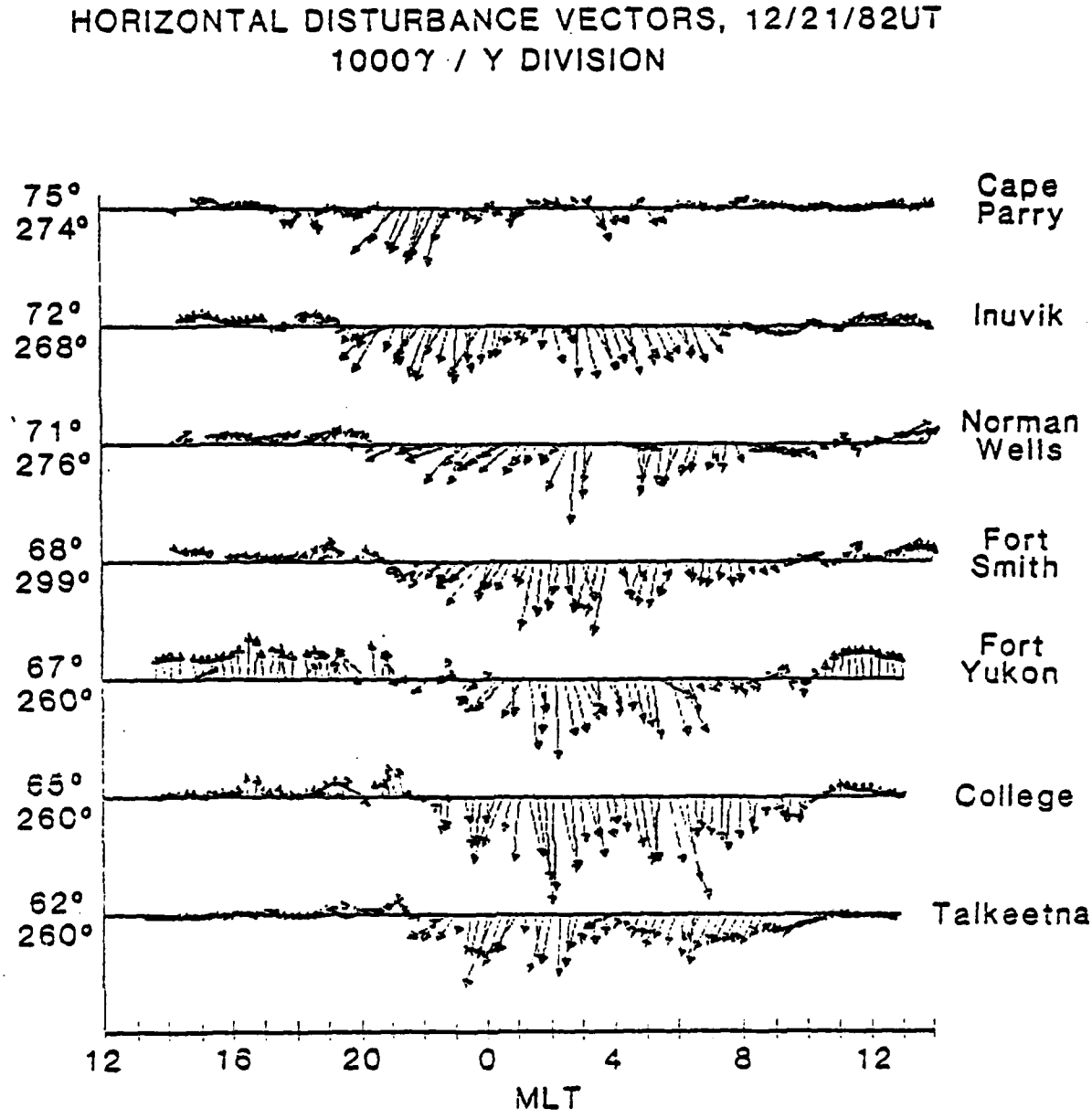

Figure 4.23 Horizontal magnetic disturbance vectors for December 21, 1982UT.

The temperature measurements are displayed in Figure 4.24. The temperature decreased from about 1000°K in the evening to about 850°K by 2:00MLT. These temperatures are lower than the average of about 1000°K for the moderate solar flux, moderate Ap case, suggesting that not much auroral heating occurred. The measurements in the north at 20° elevation angle and the zonal measurements at 45° showed morning temperatures to be slightly higher than the evening temperatures. However, the pronounced heating as indicated on the previous day was not repeated.

The zenith temperature from 19:00 to 22:00MLT varied similarly to the zenith temperature oscillations on the previous day, December 20, 1982UT. After 0:50MLT the zenith temperature remained between 750 and 800°K, lower than the cardinal point measurements. The temperature then increased to 1150°K at 3:00MLT, monotonically decreasing to 950°K by 5:00MLT before the multiple eastward surges. The final two measurements during the surge passage again show high temperatures.

The ratio 6300A/4278A calculated from the Poker Flat meridian scanning photometer measurements varied between .2 and 2 (Figure 4.25). The ratio is smaller through most of the night than it was on December 20, 1982UT, implying a harder average particle input spectrum. The emission height profile should remain nearly constant during the time of nearly constant 6300A/4278A. However, there was no significant local heating evident. The variations in temperature were similar to the NCAR TGCM results for a 60kV polar cap potential (Roble et al., 1982). This model result showed a temperature decrease from the evening to midnight of about 75°K.

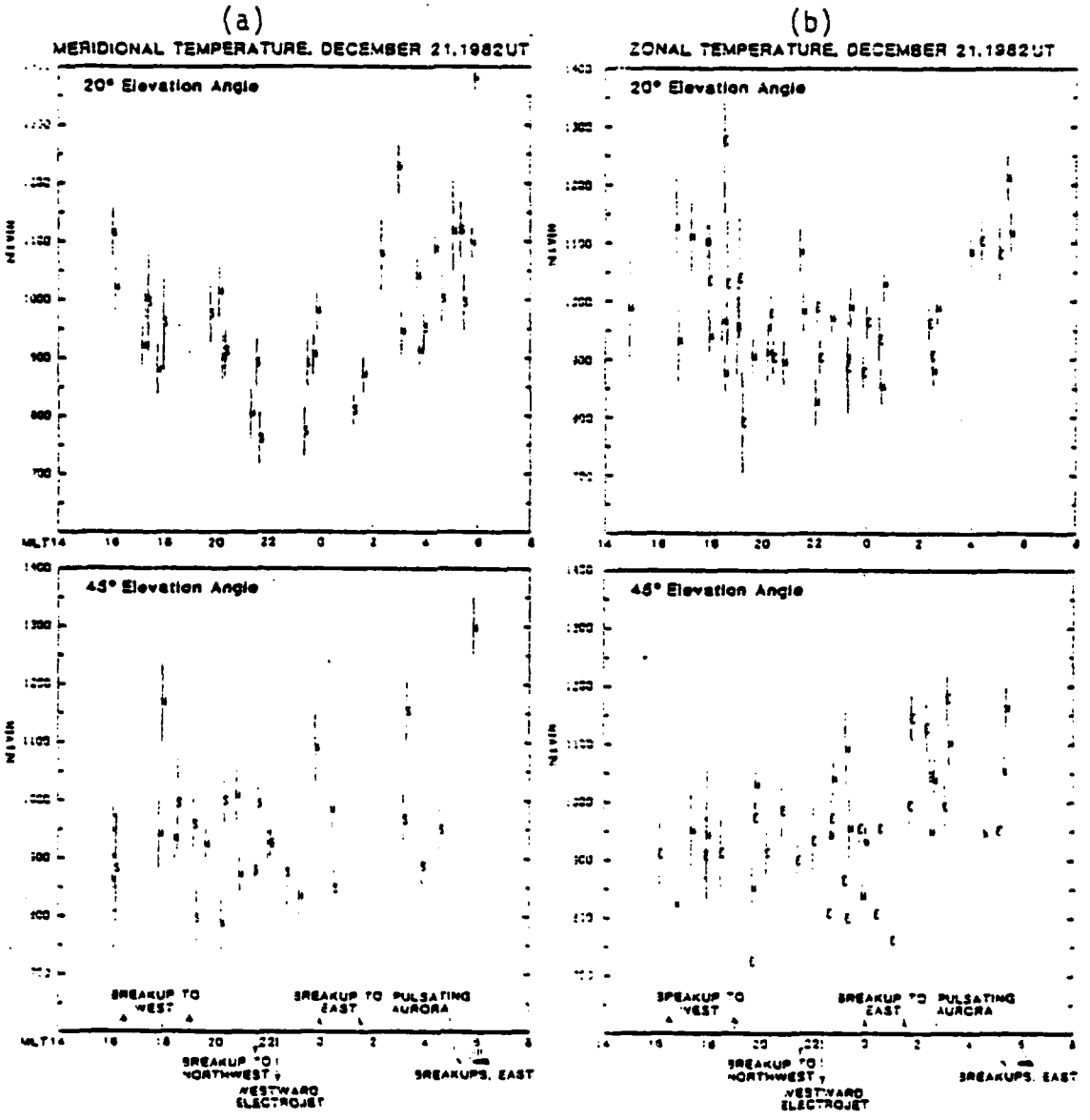

Figure 4.24 Temperature measurements for December 21, 1982UT, a: meridional, b: zonal and c: zenith.

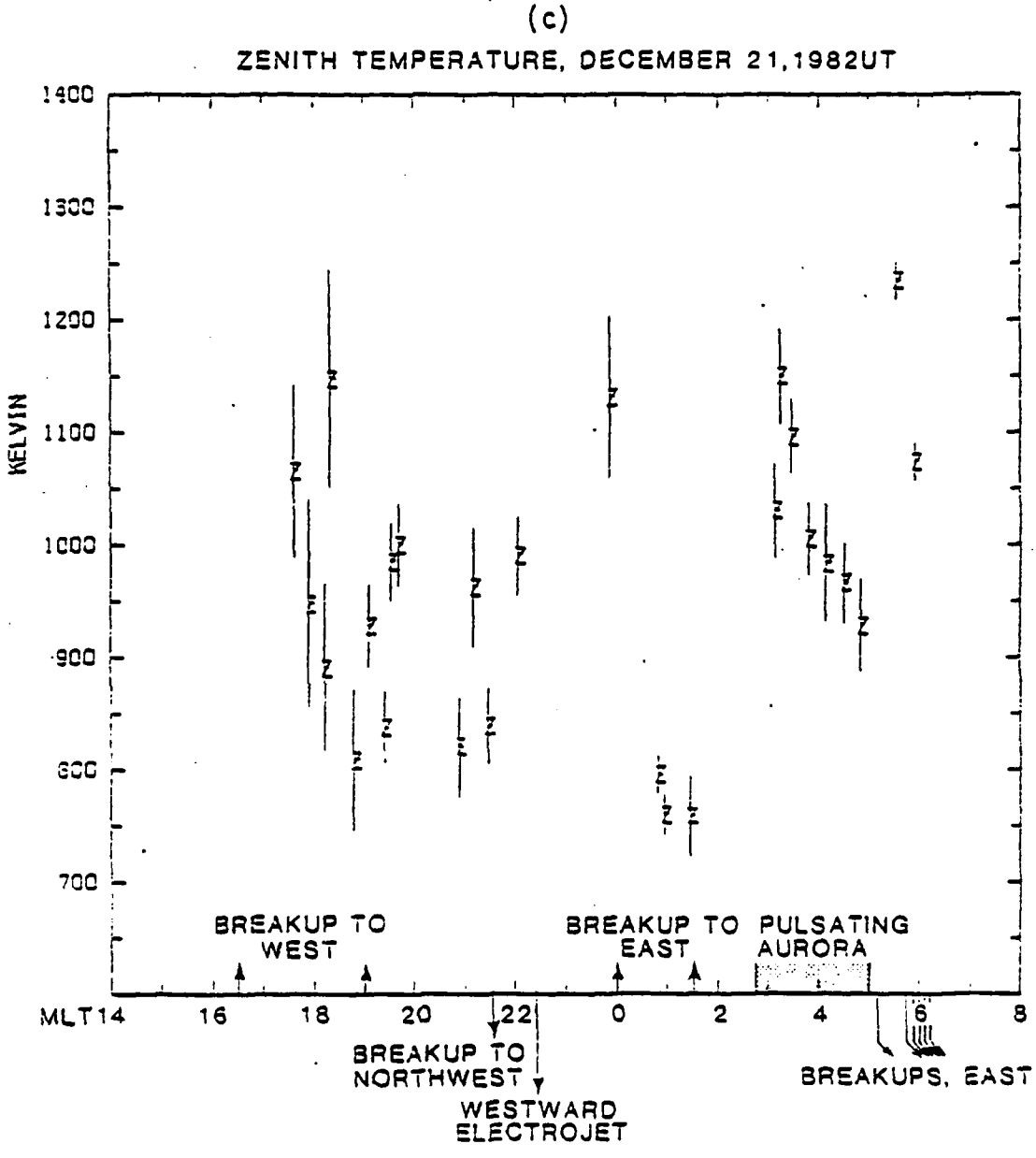

Figure 4.24 (Con't)

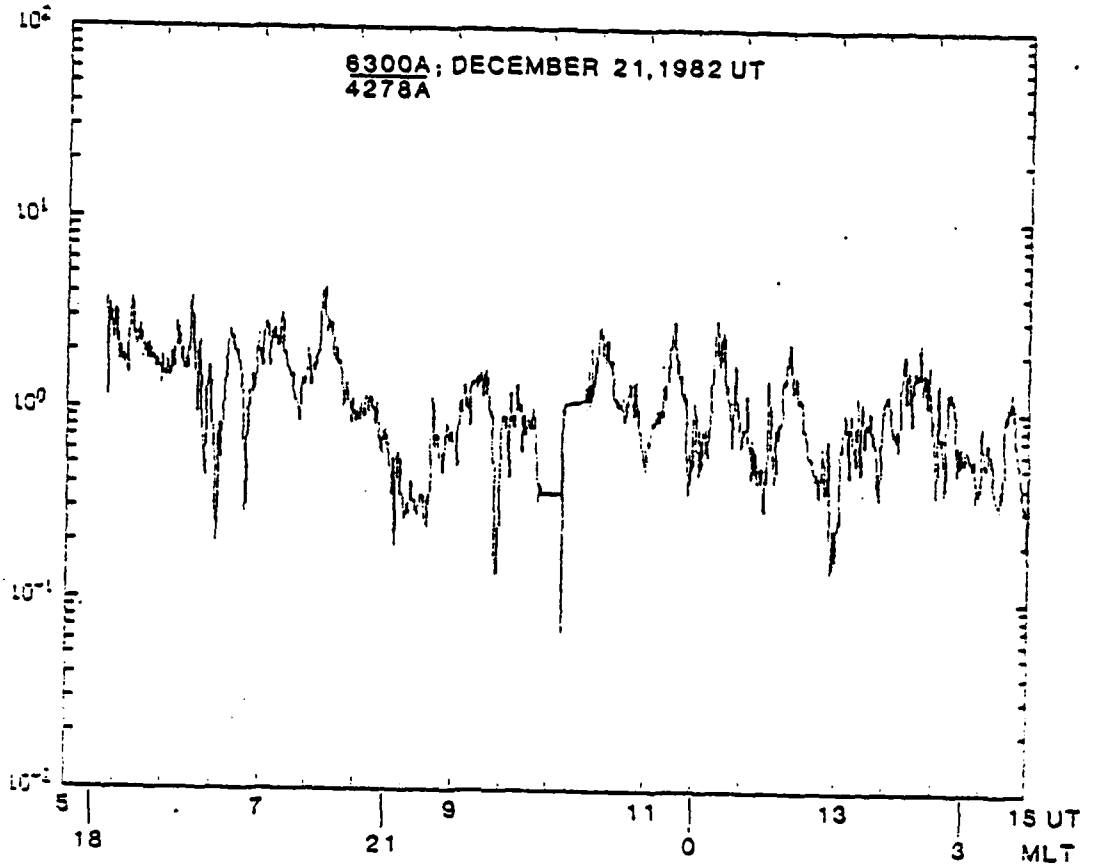

Figure 4.25 The ratio 6300A/4278A on December 21, 1982UT.

The temperature then increased to the evening level by dawn. Though the wind at 45° elevation angle was similar to the wind on December 20, 1982UT, global dynamics may be acting to transport local heating away from College. The temperature measurements in the morning after the 5:00MLT surges show an increase in the temperature. As the measurements ended at dawn, aurora was still visible overhead.

4.26. DECEMBER 22, 1982UT.

The meridional wind measured on December 22, 1982UT at 20° and at 45° elevation angle in the south and at 45° elevation angle shows the station in the poleward auroral zone evening flow (Figure 4.26). At 20° elevation angle, the meridional wind measured to the north became strongly equatorward after an intense westward traveling surge at 16:00MLT (which had visible type-A rays). The evening meridional wind was consistent with the polar cap-auroral zone boundary located between 45° and 20° elevation angle to the north of College. A stable convergence persisted between 18:00 and 20:00MLT in the meridional wind. The zonal component to the east was larger than to the west, but the flow was westward. Consistent with the existence of a convergence is a downward vertical wind of over 100 m/sec through much of the convergence period. The zenith decreased to near zero as the horizontal flow became more uniform (Figure 12c).

During a breakup and associated westward electrojet at 21:10MLT, the meridional wind vanished. Measured to the north the meridional wind then became equatorward while to the south it remained near zero. The equatorward flow decreased around the time of the eastward-moving breakup.

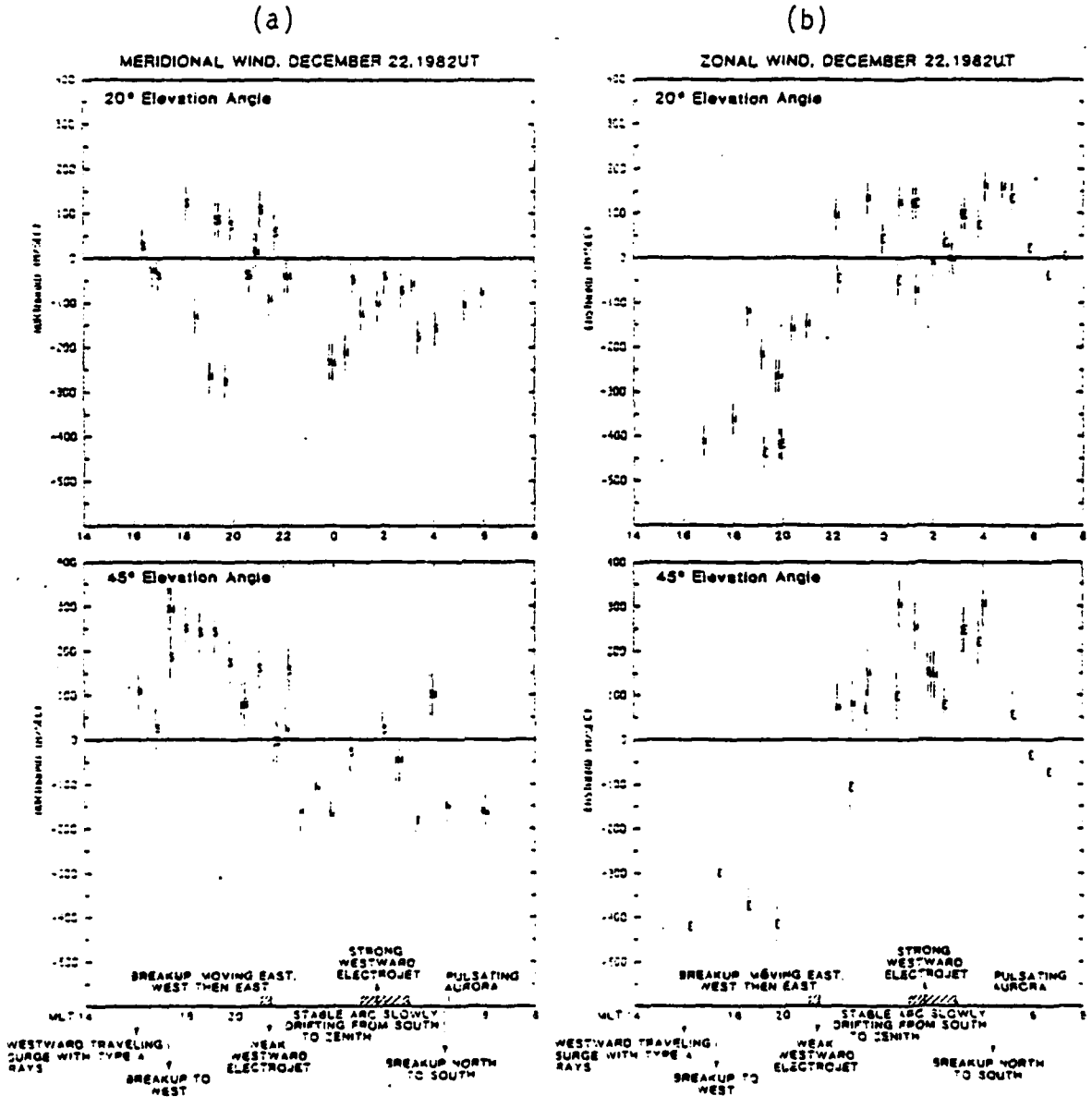

Figure 4.26 Wind measurements on December 22, 1982UT, a: meridional, b: zonal and c: zenith.

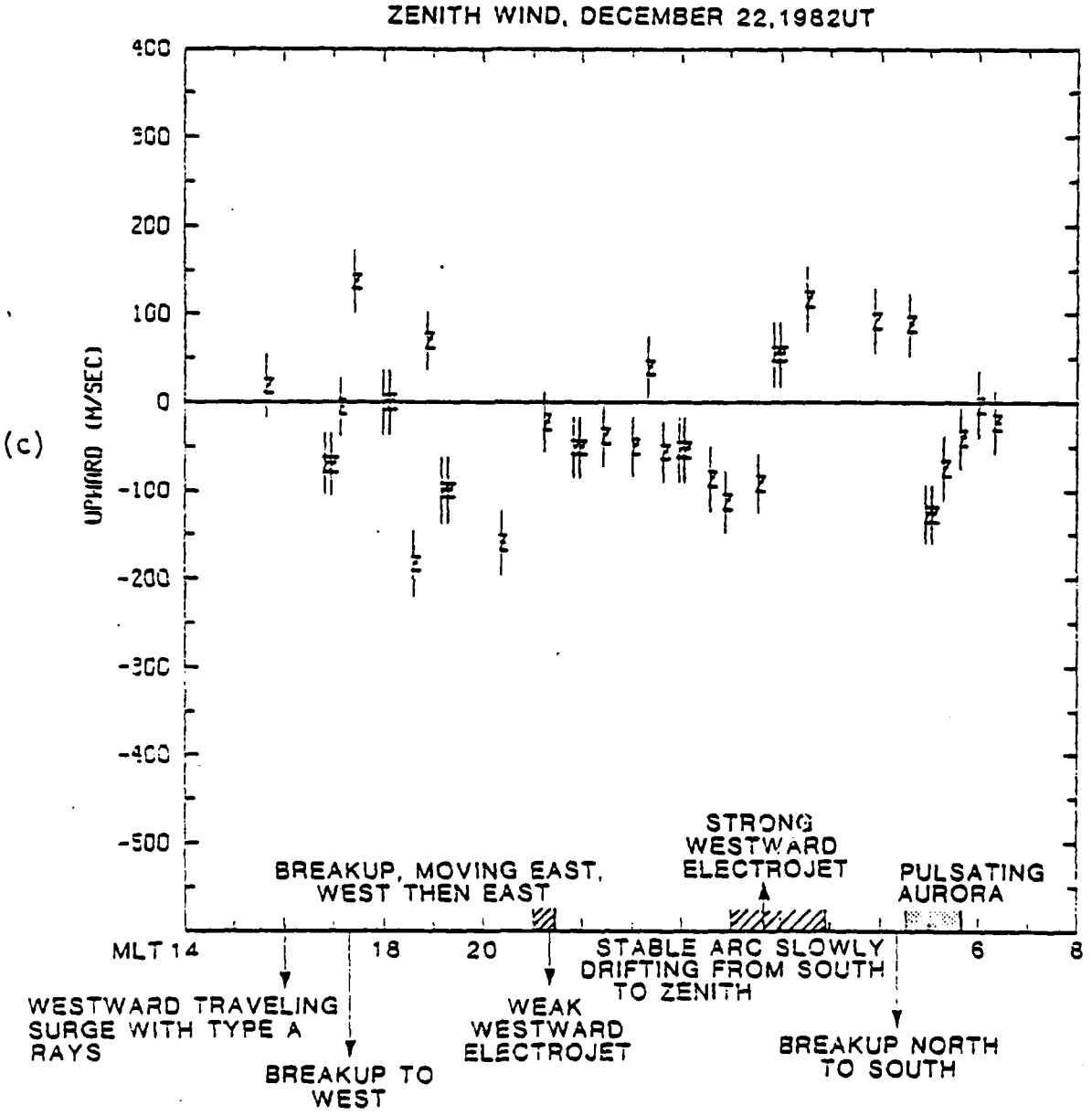

Figure 4.26 (Con't)

The zonal wind was typical of the active average (Figure 4.26b). The magnetic data indicated an extremely intense eastward electrojet at College through 19:00MLT. At the peak of this electrojet at 16:00MLT, an intense westward traveling surge occurred, with zonal wind westward velocities of over 500m/sec. A small westward electrojet developed over College at 21:45MLT. The wind measurements to the west then lead those to the east in crossing over from westward to eastward. The westward electrojet first appeared at 21:15MLT at College, about the time the westward component of the wind decreased to zero. The zonal components at 45° crossed zero first at 23:10MLT; the east component at 20° crossed about 50 minutes later. In the morning the westward electrojet arrived at Fort Smith about 4:45MLT, and about two hours later a second negative bay commenced at College.

After 1:00MLT, a stable arc developed at about 45° in the south and slowly drifted towards the zenith until about 2:15MLT. During this time, the wind measured in the west at 20° decreased to zero, while the component to the east began to increase. Just after 3:00MLT an eastward-traveling breakup occurred across the station and the component to the west increased eastward. The eastward component in the east decreased to zero after 5:00MLT as the geomagnetic activity subsided at College.

The zenith wind was downward through much of the evening meridional convergence (Figure 4.26). After 21:15MLT, when the eastward ion flow became established, the zenith wind remained constant and downward. As the stable morning arc moved towards the zenith after

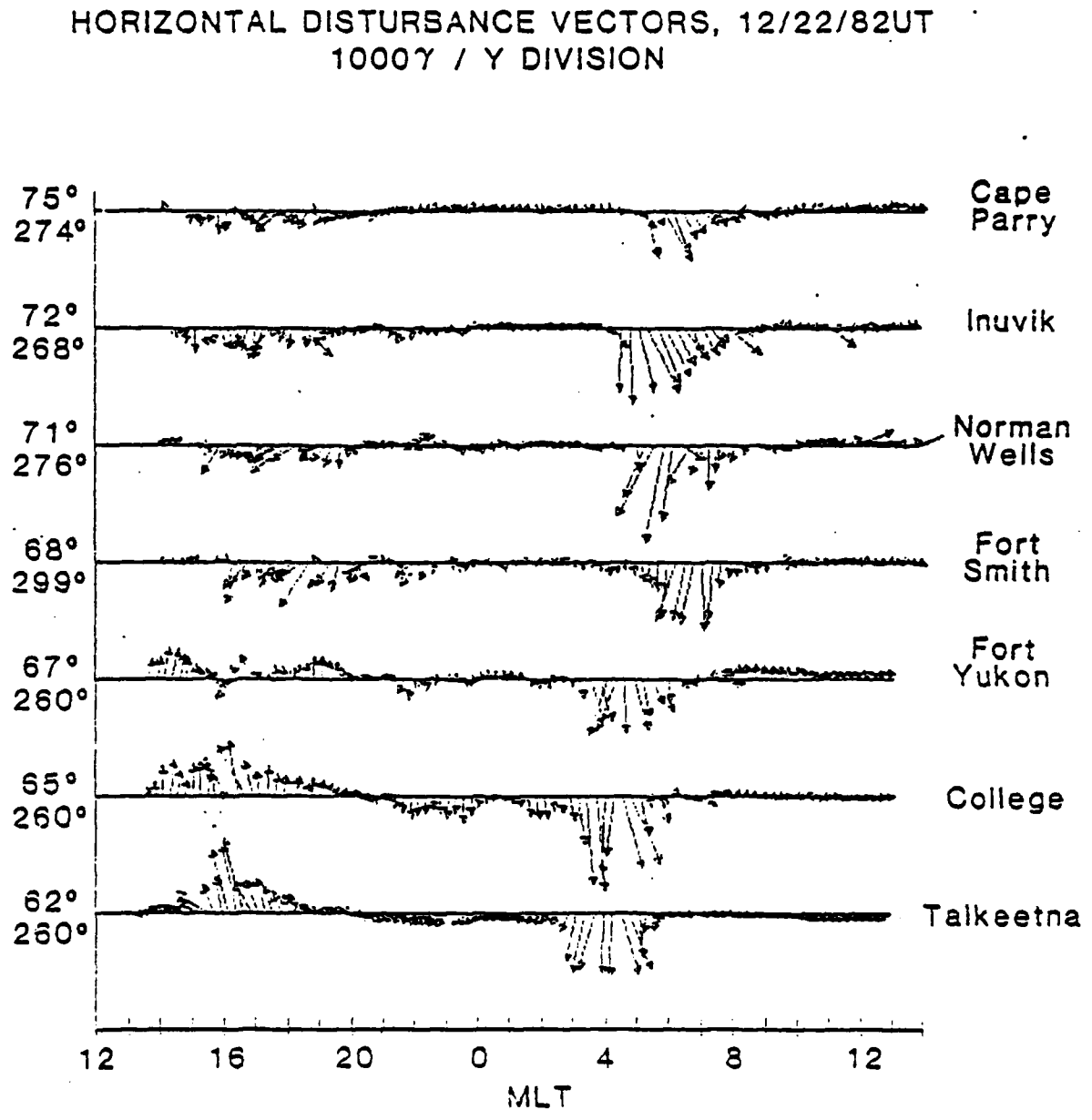

Figure 4.27 Horizontal magnetic disturbance vectors for December 22, 1982UT.

1:00MLT, the wind changed from downward to upward with high (100m/sec) velocities. During the pulsating aurora following the 4:15MLT breakup, it again became downward, decreasing to zero as the activity ended in the morning.

The temperature was similar to the moderate geomagnetic activity, moderate solar flux average, though the early evening temperature was enhanced in the westward traveling surge (Figure 4.28). The temperature decreased as the night progressed, returning to about the same level in the morning. The temperature measured in the south, a region of pulsating aurora through much of the morning, was lower than in the north. The lower temperature may be a consequence of the 6300A emission originating from a lower effective altitude region caused by harder particle flux energies in the pulsating aurora.

4.27. FEBRUARY 6, 1983UT

One additional active night to be discussed is February 6, 1983UT. Measurements on this night were made at 45° elevation angle. The meridional wind is shown in Figure 4.29a. Several breakups were observed prior to the start of measurements at 20:00MLT. After observations began at 22:00MLT, two westward surges passed over the station between 23:00 and 23:30MLT. The first eastward-surging breakup occurred at 2:00MLT, quickly followed by several additional eastward surges within the next twenty minutes. The equatorward meridional flow in the north then began to decrease. The component to the south followed about two hours later.

The magnetic data in Figure 4.30 indicate the presence of the westward electrojet over College at about 23:00MLT. The zonal wind

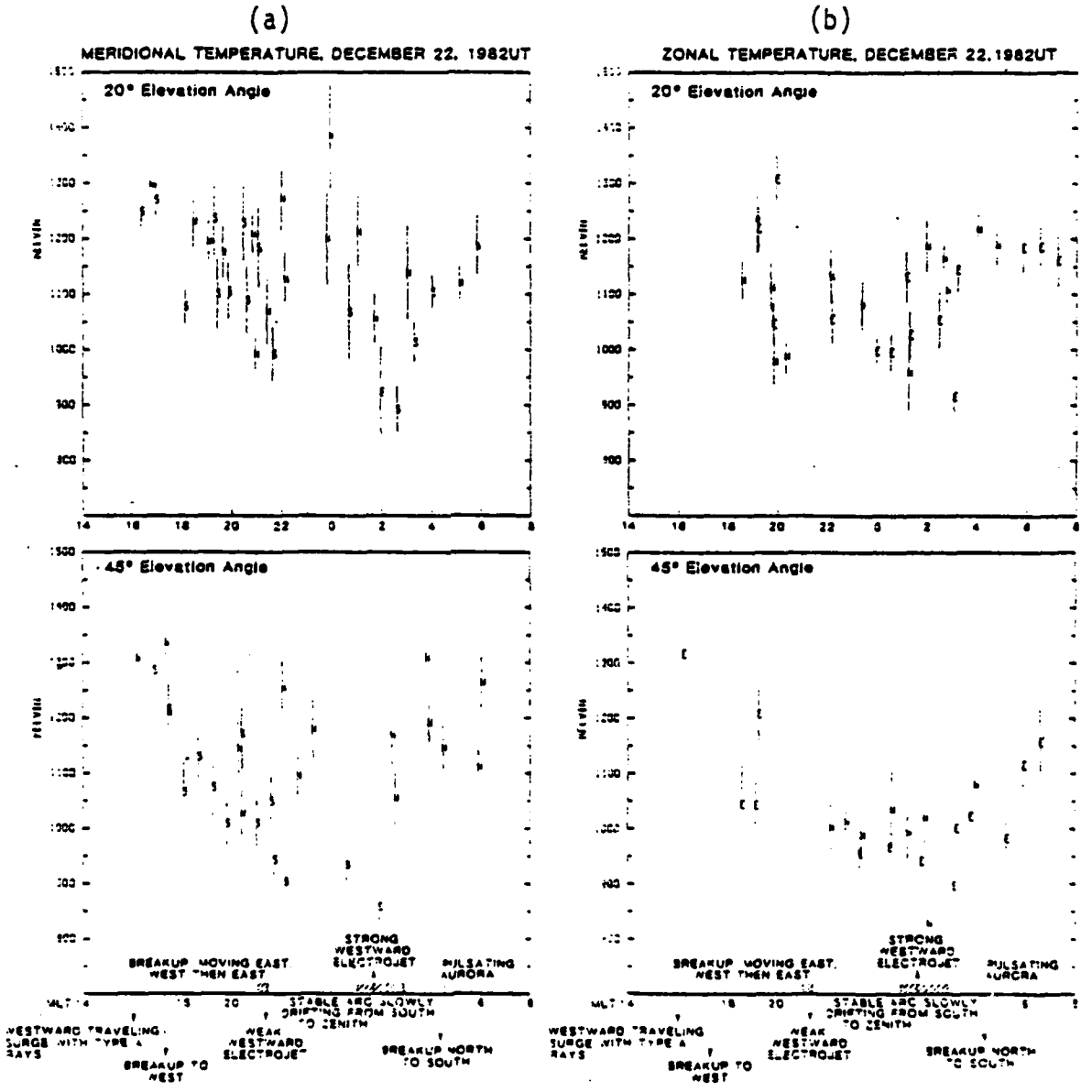

Figure 4.28 Temperature measurements on December 22, 1982UT, a: meridional, b: zonal and c: zenith.

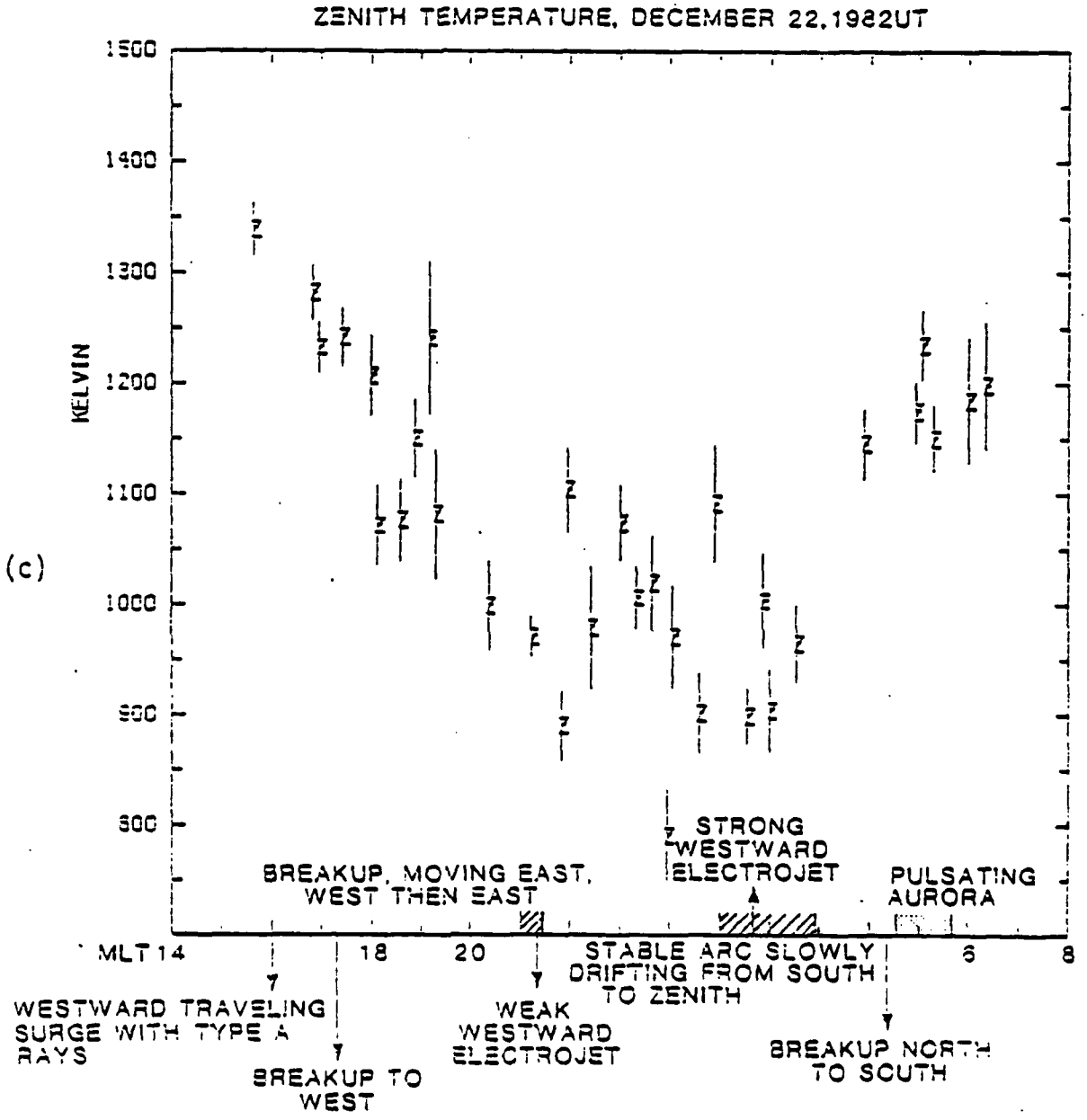

Figure 4.28 (Con't)

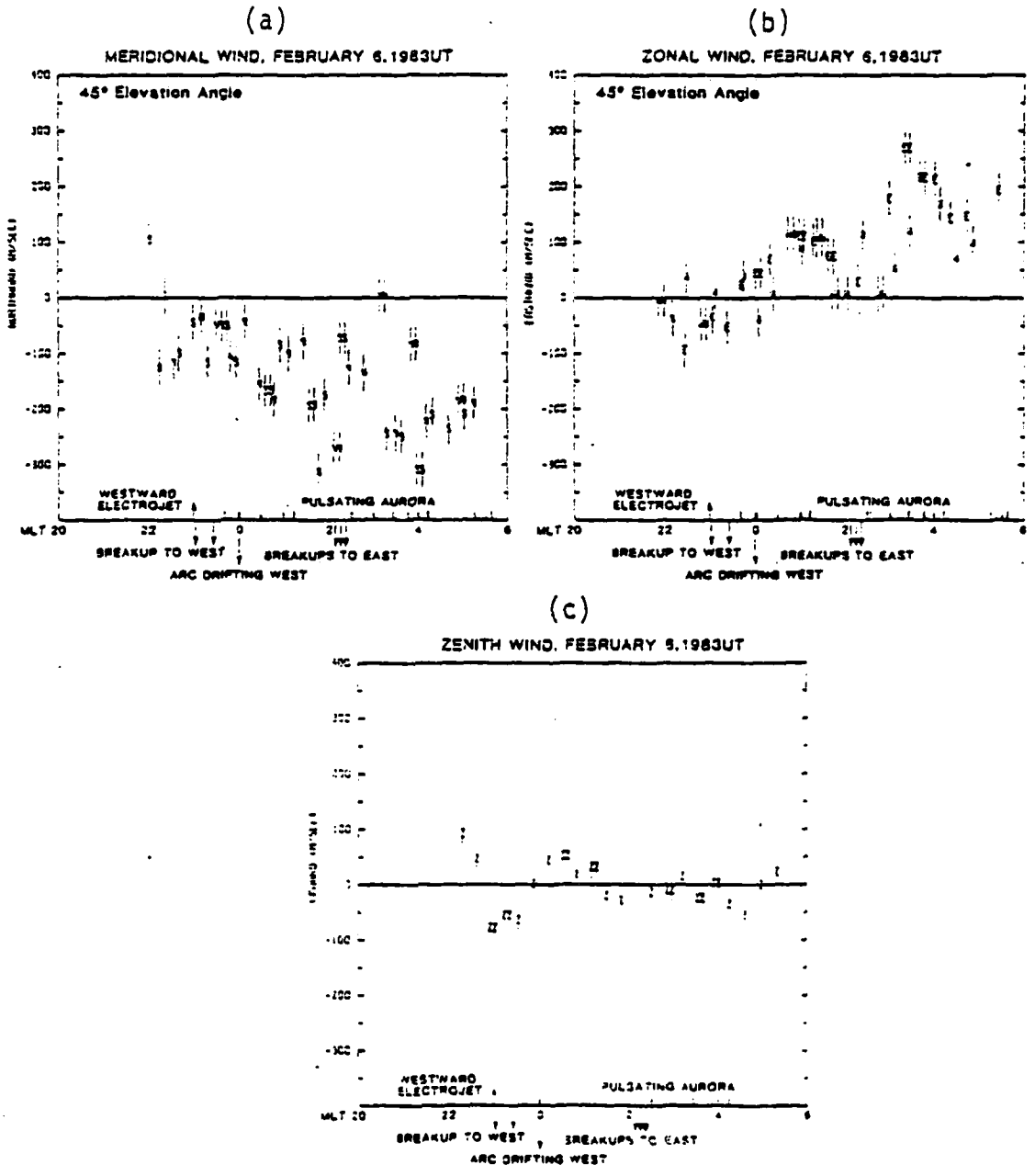

Figure 4.29 Wind measurements on February 6, 1983UT, a: meridional, b: zonal and c: zenith.

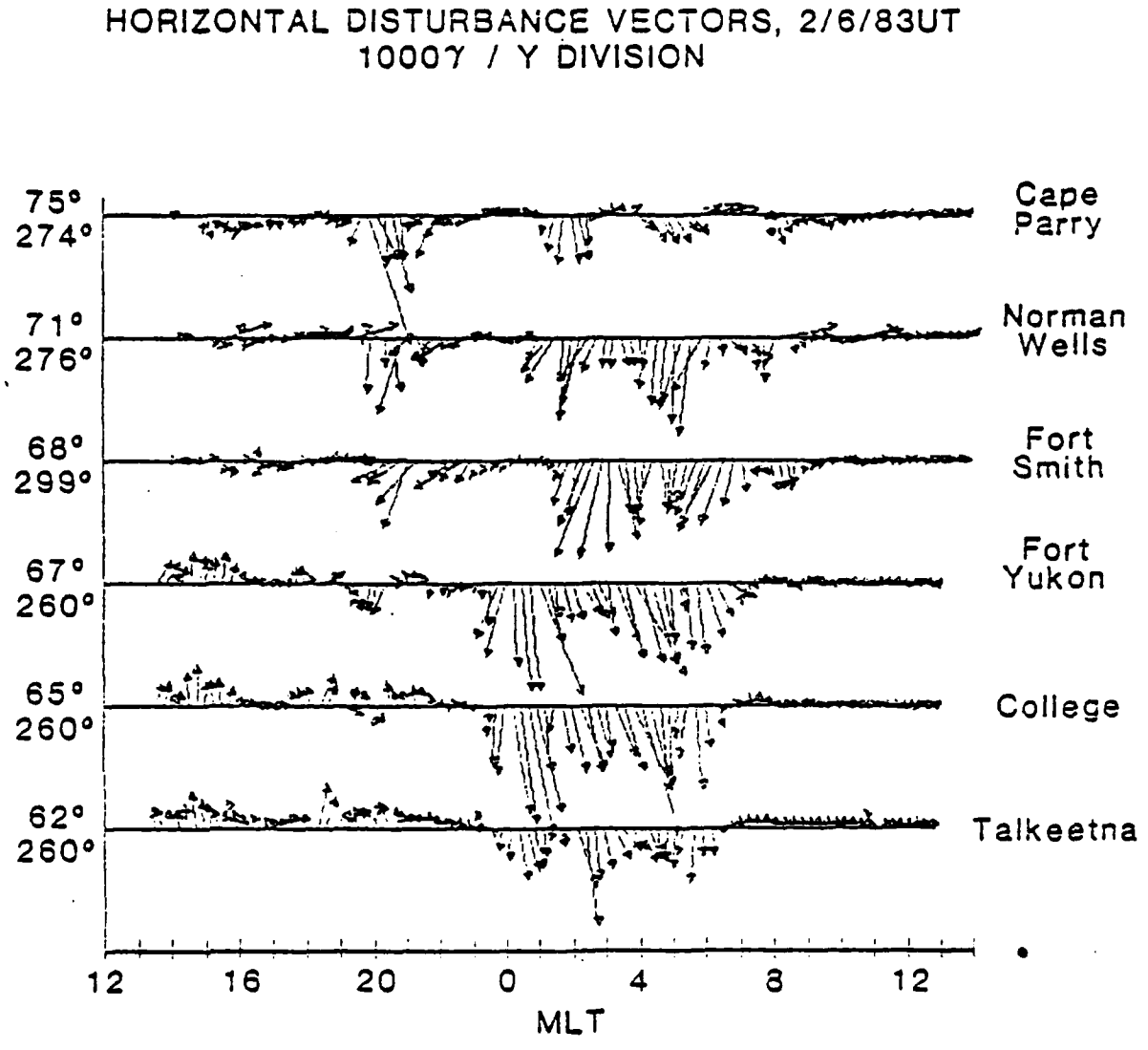

Figure 4.30 Horizontal magnetic disturbance vectors for February 6, 1983UT.

component followed the electrojet eastward in the east by about magnetic midnight (Figure 4.29b). The wind, viewed to the west, did not become fully eastward until 0:45MLT. A series of breakups with eastward motion occurred after 2:00MLT, coincident with the negative bay at Fort Smith. The zonal wind became small, then increased quickly in the eastward direction looking to the east, while the west remained near zero for another hour. The local substorm caused a large difference in the wind observed to the east and west.

The zenith wind was downward at about 75m/sec during the westward breakups at 23:00 and 23:25MLT (Figure 4.29c). It turned upward during the pulsating aurora between 23:45 and 1:15MLT. It then decreased to zero for the remainder of the night.

The temperatures are consistent with the moderate solar flux, moderate geomagnetic activity average (Figure 4.31). The temperature increased about 150°K in the zenith as an arc embedded in the pulsating aurora moved westward at 1:00MLT. About 45 minutes later, the west and the north showed a similar rise in temperature during an eastward-traveling breakup. The temperature in all directions exhibited an approximately 100°K increase, due at least in part to magnetospheric-ionospheric heating.

4.28. NOVEMBER 19, 1982UT

This was a moderate solar flux case with quiet global geomagnetic conditions. The meridional wind at 20° was similar to the quiet condition average (Figure 4.32a). The large poleward surge in the south after 20:00MLT was coincident with observations of low intensity pulsating aurora made by T. Hallinan with an intensified

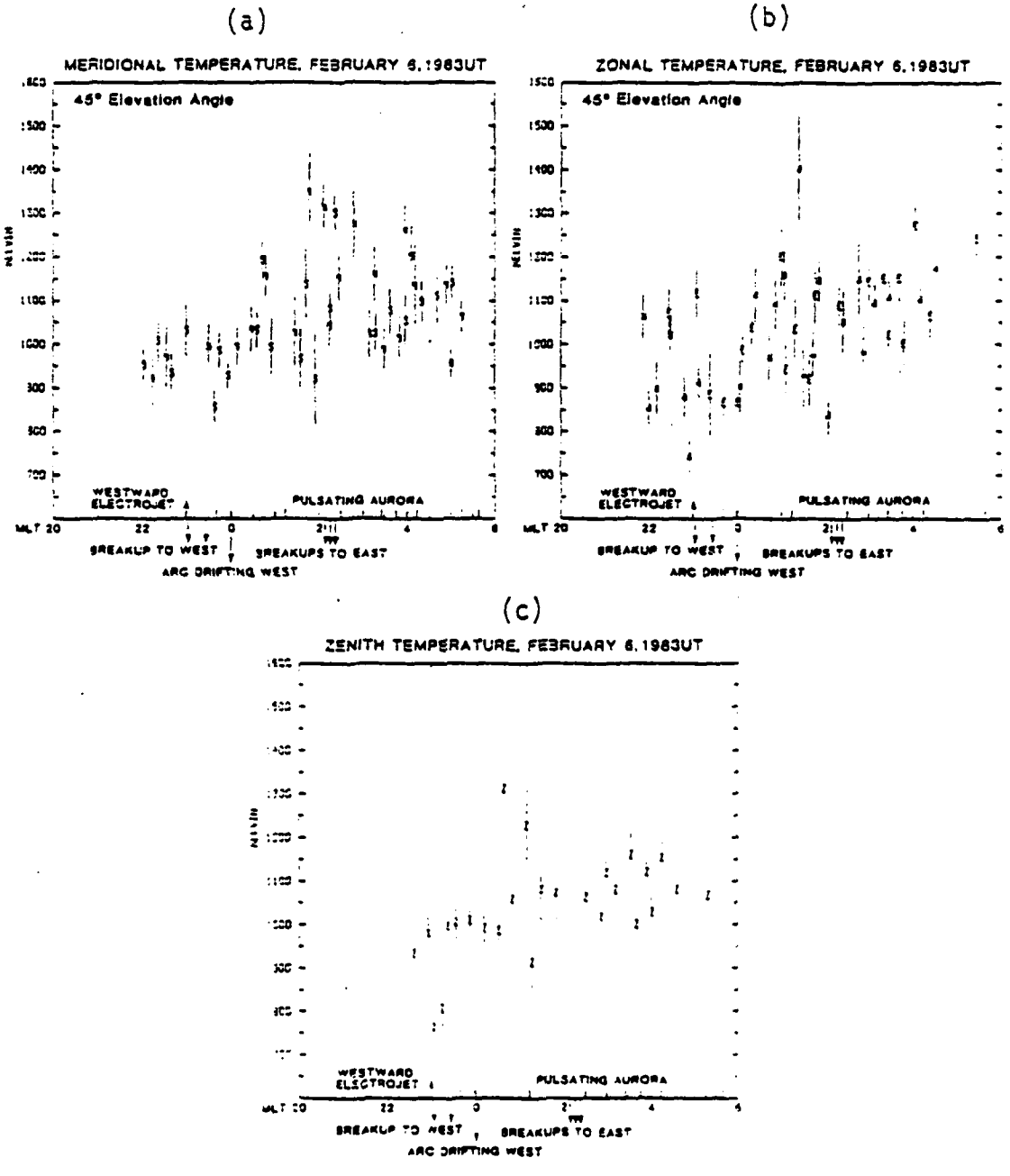

Figure 4.31 Temperature measurements on February 6, 1983UT, a: meridional, b: zonal and c: zenith.

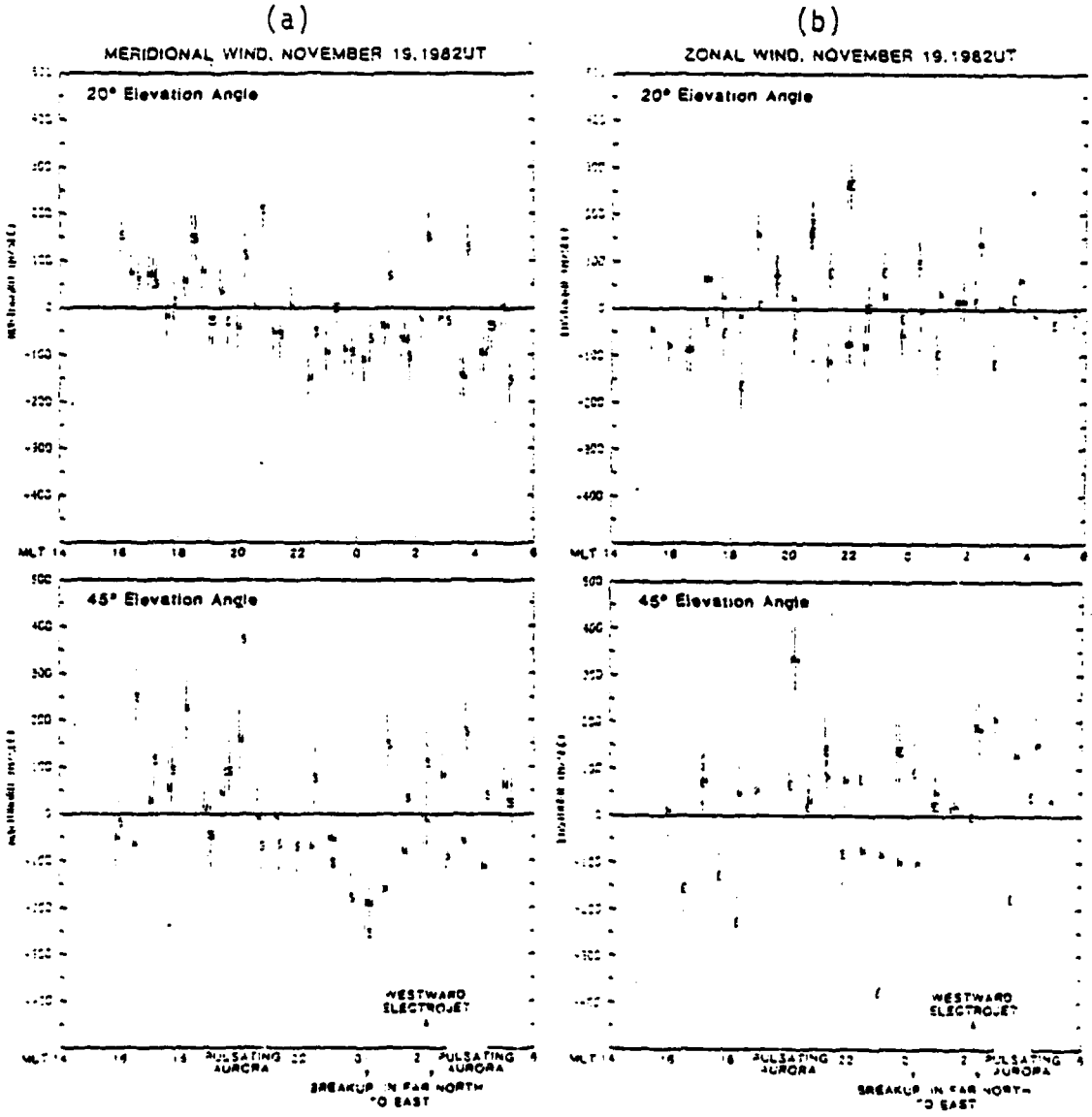

Figure 4.32 Wind measurements on November 19, 1982UT, a: meridional, b: zonal and c: zenith, d: zenith intensity normalized to the night's maximum of 1.11kR.

(c)

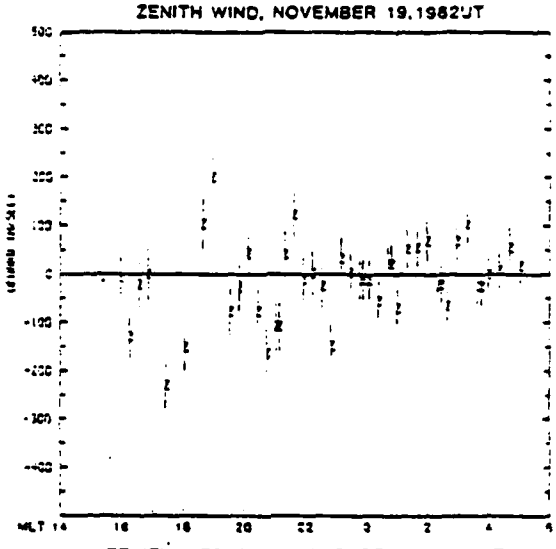

(d)

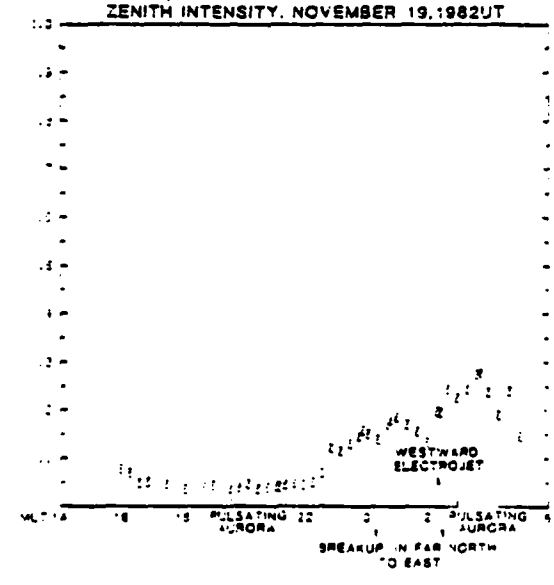

Figure 4.32 (Con't)

image orthicon television camera operating at the Geophysical Institute. The pulsations were subvisual, and may have occurred before 19:45MLT. After an eastward auroral surge occurred on the northern horizon at 0:30MLT, the meridional wind component to the south at 20° oscillated between poleward and equatorward. The component to the north at 20° remained equatorward and was generally less than 100m/sec.

The meridional wind components at 45° appear more like the moderate geomagnetic average, though there was little visible aurora (Figure 4.32a). Before and during the observed pulsations in the aurora, the wind in the north and south was poleward, varying between 0 and 250m/sec. The change to the south appeared to precede that in the north by about one hour. After 23:00MLT, the wind became strongly equatorward for about an hour, then the northern arcs surged eastward and the winds decreased in strength, as was observed during eastward breakups on the active nights. The morning wind varied around zero.

The horizontal disturbance vectors showed little geomagnetic activity (Figure 4.33). An unusual zonal wind pattern was observed, relative to the averages (Figure 4.32b). The zonal wind at 20° was generally small. The westward electrojet appeared over College at 2:00MLT. The component to the west was eastward at this time, while the east-viewed wind was unchanged. The zonal wind at 45° showed considerable scatter about zero. After the westward electrojet appeared at College at 2:00MLT, the flow in the west became eastward and behaved as on an average night. The local presence of the electrojet orders the "steady-state" flow. The lack of struc-

AD-A150 114 HIGH TIME RESOLUTION THERMOSPHERIC TEMPERATURE AND WIND 2/2
STUDIES IN THE ARCTIC(U) ALASKA UNIV FAIRBANKS
GEOPHYSICAL INST G G SIVJEE 30 SEP 84 4
UNCLASSIFIED AFOSR-TR-84-1255 AFOSR-80-0240 F/G 4/1 NL

END
FILMED
DTIC

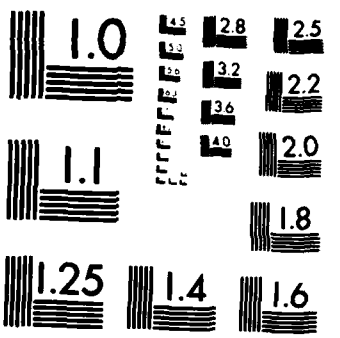

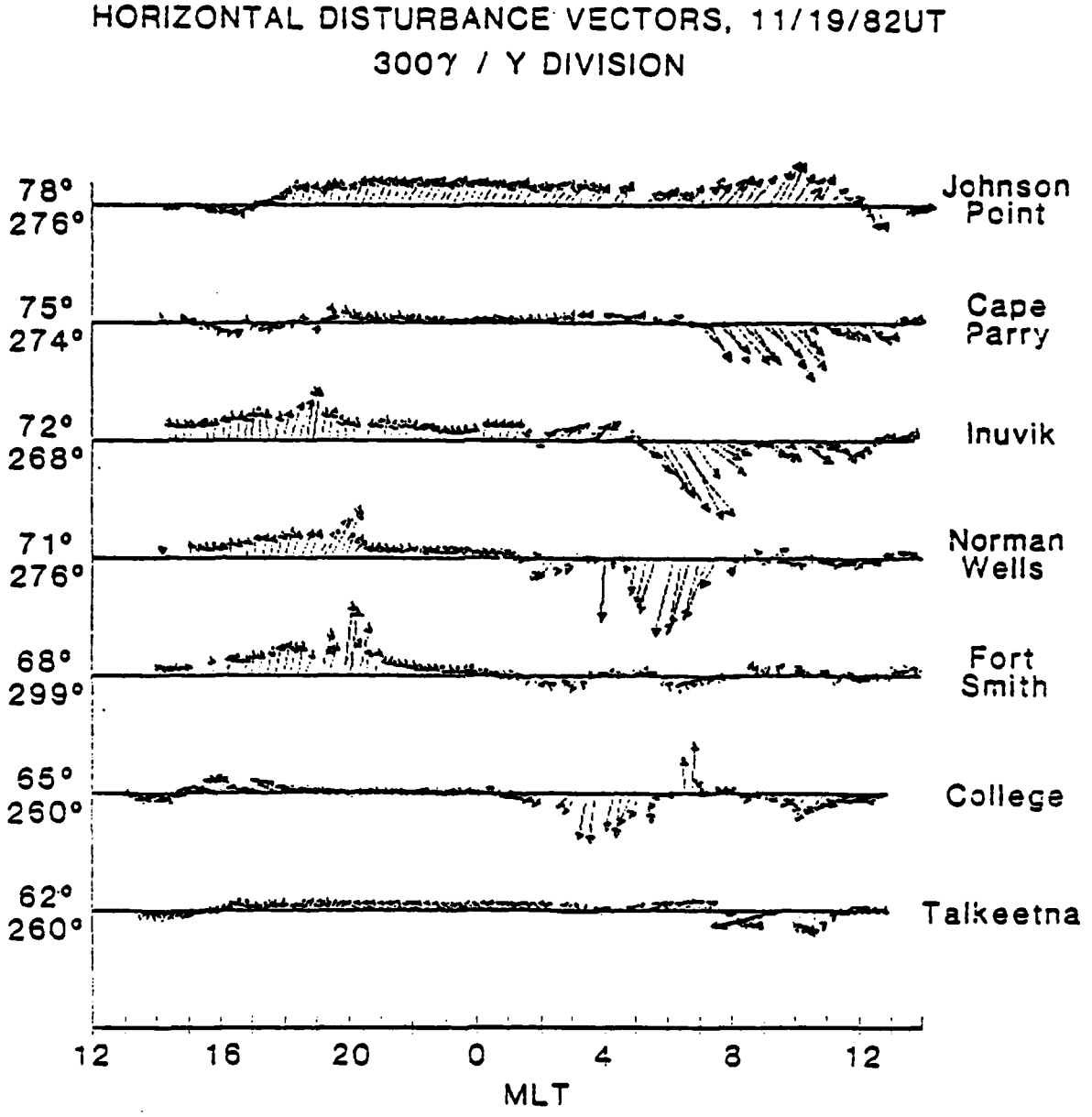

Figure 4.33 Horizontal magnetic disturbance vectors for November 19, 1982UT. The distance between station zero lines corresponds to 300γ.

turing of the zonal wind in the east is due to the arrival of the westward electrojet (i.e., eastward drifting ions) at a later local time, since the magnetic disturbance to the east observed at Fort Smith did not begin until after measurements had ceased at College.

The zenith wind had extremely large oscillations (≈200m/sec) before and during the observed pulsations (Figure 4.39c). These decreased near 23:45MLT as the intensity of 6300A increased in the zenith (Figure 4.32d). The zenith wind remained near zero until the auroral activity increased after 1:45MLT. Pulsations were again encountered after 3:00MLT, but the zenith wind soon decreased to zero.

This night is an example of the atmosphere deviating from the steady-state. Deviation is due to the absence of normal auroral activity over the station. The zonal measurements show large scatter because the low electron densities and small electric fields that probably existed could not order the wind. The station then appeared to shift farther south relative to the oval, to the transition zone between high and mid-latitude flow. The unusual presence of the early evening pulsating aurora also seemed to affect the dynamics by introducing large variations in the wind, particularly in the zenith.

4.29 GENERAL CHARACTERISTICS OF THE SELECTED INDIVIDUAL NIGHTS

A detailed examination of these nights reveals some consistent trends. Deviations from the average wind and temperature behavior described earlier due to auroral substorms are commonly observed. While global thermospheric dynamic models reasonably fit

the average data, individual substorm behavior has not been accurately represented, despite attempts to include particle precipitation in the codes. The local dynamic behavior is highly responsive to auroral activity.

The meridional wind has an increasing equatorward flow in the evening following westward breakups. The meridional wind velocity increases equatorward until eastward auroral bulk motion begins around magnetic midnight. The meridional wind then decreases but often remains equatorward. Due to the spatial separation between the north and south measurements, the flow to the north can become equatorward earlier than in the south, with a time lag of one to two hours.

The zonal wind shows the importance of ion drag as the major momentum source. However, the mesoscale variations of the zonal wind are governed by local substorms and the position and intensity of the electrojets. The evening westward wind velocity is related to the magnitude of the horizontal magnetic disturbance vectors. The time period of westward neutral flow is coincident with bulk motion of auroral forms to the west. When the auroral motion becomes eastward and the westward electrojet arrives over College, the westward zonal wind becomes eastward, with time lags varying from minutes to a few hours. This change in direction must certainly be related to increased ion velocities due to an increasing ionospheric electric field and electron density enhancements from particle precipitation generating a large ion drag momentum source. Whether the wind viewed to the west or east will change direction first depends on the location of the substorm onset. If the onset

is west (east) of College, the wind viewed to the west (east) will usually respond first. Examples presented at 20° and 45° elevation angles clearly demonstrate this principle. Measurements on November 19, 1982UT, a night with little magnetic activity or aurora, supports the contention that ion drag orders the zonal wind.

The zenith wind shows large deviations from zero during auroral activity. Fluctuations in the zenith wind between downward and upward occur frequently during pulsating aurora. The zenith wind could be the neutral atmospheric response to rapid changes in the input of magnetospheric energy. The discrete and diffuse aurora mark the boundary between regions of plasmas originating from different parts of the magnetosphere (Akasofu, 1977). The response of the ionosphere due to this transition could produce a boundary region where vertical flow is generated from changes in the current system and the energy and flux of the precipitating particles. Thus, the power transmitted from the magnetosphere to the ionosphere can generate a distrubance which drives a zenith wind, as predicted by the model of Richmond and Matsushita (1975). Large zenith winds are not predicted by current three-dimensional global models. Additionally, large zenith winds imply the existence of circulation cells in order to conserve mass in the thermosphere. This of course presumes that the assumption of zero wind using the weighted average of the zenith measurements is valid.

Another possible source of vertical wind is atmospheric gravity waves generated by auroral disturbances. Internal gravity waves can support a large vertical phase component (Hines, 1960, 1964). Without dissipation, vertical velocities on the order of typical

horizontal velocities could occur. However, important dissipative effects such as molecular viscosity and thermal conduction remove many of the possible wave propagation modes. Gravity waves can also transport energy from the E region to the F region. For example, at 220km, if the horizontal wind speed is 250m/sec, the vertical wind speed 50m/sec and the density $1.5 \times 10^{-13} g/cm^3$, then an energy flux of about .25ergs cm^{-2} sec^{-1} could reach the F region (Hines, 1965). This energy flux is one to two orders of magnitude less than the energy flux deposited by a typical auroral substorm, but at times it could be significant.

Temperature measurements on individual nights from College show variations that are often larger than can be explained by a change in emission height profile caused by variations in the incident particle energy. Many nights show heating from auroral substorms. This conclusion is supported by 6300A/4278A measurements in the zenith. The ratio measurements also show that the large decreases in temperature during breakups are probably the result of a broadening of the emission height profile to lower altitudes. Temperature increases between the evening and morning are less pronounced on certain nights. This may occur when the large scale thermospheric wind system alters the local temperature structure, as predicted by global circulation models.

The ability of the current global models to successfully represent individual nights from even a single station is limited by the input parameters. The convection pattern, composition, ionosphere and particle precipitation all use average results, which smooth local effects. The large grid cell size of the models also aver-

ages out small scale structures. Consequently, though the agreement with the average data in this study is quite good, local effects are not predicted. To better model the individual nights, a varying convection pattern which can self-consistently alter the ionosphere is needed, along with a finer grid mesh. This is limited by a lack of time-dependent convection models and computer resources. Efforts to couple global thermospheric and ionospheric models are now underway. At this point, the large local variations observed from College cannot be accurately represented on an individual night by a three-dimensional time-dependent model. Though an attempt has been made to study global substorm effects, the grid spacing employed is too large for comparison with data from a single station (Fuller-Rowell & Rees, 1981).

4.295. DISCUSSION OF INDIVIDUAL NIGHTS

The presence of the auroral oval defines the steady-state of the thermosphere over College during solar maximum. On a night with no aurora overhead at College, November 19, 1982UT, the absence of the steady-state auroral zone forces caused large deviations from the average wind behavior. Based on the results of the forty-four nights studied, when the auroral oval contracts well poleward of College, the thermosphere begins to relax to a mid-latitude flow. This relaxation ends when the auroral oval arrives over College, accompanied by enhanced magnetospheric convection and increased particle precipitation.

A detailed study of selected individual nights demonstrated the coupling between the E and F regions. This is manifested by the relation between the bulk motion of auroral forms and the

direction of the thermospheric wind. In the evening, westward motion occurs in the optical aurora and in the zonal wind. Eastward bulk motion of the aurora in the morning corresponds to decreasing equatorward meridional wind and ultimately to an eastward zonal wind.

Temperatures on individual nights usually decrease in the early evening, before auroral activity begins. On some nights, rapid oscillations in the temperature are observed at this time. As the auroral oval arrives overhead, the temperature often increases. However, during some evenings, the temperature decreases during periods of auroral particle precipitation. This is probably due to the 6300A emission height profile extending to lower altitudes. Thus, the observed temperature may decrease or remain unchanged while heating occurs. With decreasing precipitation, the emission height profile may move to higher altitudes, but the global circulation can act to carry some of the local heating away from the region of the auroral oval.

5.0 FUTURE PLANS

The data obtained in 1984 with the piezoelectric scanning interferometer has been partially reduced and upon completion will be compared with previous results. Because of its much higher time resolution, detailed studies associated with geomagnetic changes and individual auroral events can be more fully investigated. These studies are planned in addition to those associated with existing models of thermospheric dynamics.

A number of scientific articles are in progress and should be submitted for publication in the next six months. We anticipate the continued operation of the piezoelectric scanning system modified to monitor two atmospheric emissions simultaneously. Initially these will be the 630 n meter OI and 732 n meter OII emissions in order to study the neutral and ion dynamics simultaneously. Other combinations will be the 630 n meter OI and 557.7 n meter OI emissions to look at upper and lower thermospheric dynamics at the same time, and the 557.7 n meter OI and the 731.6 n meter OH emissions to study the lower thermosphere and mesosphere dynamics at the same time. We anticipate one of the main thrusts of the experimental program in the future will be the investigation of the use of molecular emissions to study the dynamics of the upper atmosphere.

6. PERSONNEL ASSOCIATED WITH THIS PROGRAM

The principal investigator at the start of this project was Dr. G. J. Romick. Senior research personnel were Drs. G. G. Sivjee, T. Hallinan and G. Hernandez. Junior research personnel were R. Sica (Ph.D. graduate student) and J. Baldridge (programmer). With the retirement of Dr. Romick, Dr. G. G. Sivjee became the principal

investigator in 1983. Dr. Romick as Senior Research Consultant still remained as an active member of the Senior Research personnel. After the decision to discontinue the use of the imaging systems in 1983, Dr. Hallinan decreased his activity in the Senior Research personnel group. R. Sica submitted his Ph.D. dissertation (see references) and obtained his degree in the fall of 1984. J. Baldridge developed a number of sophisticated software programs that allow digital processing of T. V. images and the conversion of intensity variations into digital time series information.

REFERENCES

Akasofu, S.-I, Polar and Magnetospheric Substorms, Springer-Verlag, New York, 1968.

Akasofu, S.-I., Physics of Magnetospheric Substorms, D. Reidel, Boston, 1977.

Akasofu, S.-I., B.-H. Ahn and G. J. Romick, A study of the polar current systems using the IMS meridian chains of magnetometers, 1. Alaska Meridian Chain, Space Sci. Rev., 36, 337, 1983.

Banks, P. M., Observations of Joule and particle heating in the auroral zone, J. Atmos. Terr. Phys., 39, 179, 1977.

Bevington, P., Data Reduction and Error Analysis for the Physical Sciences, McGraw-Hill, New York, 1969.

Bloomfield, P., Fourier Analysis of Time Series: An Introduction, John Wiley and Sons, New York, 1976.

Bostrøm, R., Electrodynamics of the ionosphere, in Cosmical Geophysics, edited by A. Egeland, Ø. Holter and A. Omholt, Universitetsforlaget, Oslo, 181, 1973.

Cole, K. D., Eccentric dipole coordinates, Aust. J. Phys., 16, 423, 1963.

Edwards, H. D., J. F. Bedinger and E. R. Manring, Emission from a sodium cloud artificially produced by means of a rocket, in The Airglow and the Aurorae, edited by E. B. Armstrong and A. Dalgarno, Pergamon Press, New York, 1956.

Fedder, J. A. and P. M. Banks, Convection electric fields and polar thermospheric winds, J. Geophys. Res., 77, 2328, 1972.

Fuller-Rowell, T. J. and D. Rees, A three-dimensional time-dependent simulation of the global dynamical response of the thermosphere to a geomagnetic substorm, J. Atmos. Terr. Phys., 43, 701, 1981.

Hallinan, T. J., G. Hernandez, G. J. Romick, G. G. Sivjee and R. Sica, Lower thermosphere neutral winds and temperatures in the auroral zone, EOS, 63, 392, 1982.

Heelis, R. A., J. K. Lowell, and R. W. Spiro, A model of high-latitude ionospheric convection patterns, J. Geophys. Res., 87, 6339, 1982.

Heppner, J. P. and M. L. Miller, Thermospheric winds at high latitudes from chemical release observations, J. Geophys. Res., 87, 1633, 1982.

Hernandez, G. and O. A. Mills, Feedback stabilized Fabry-Perot interferometer, Appl. Opt., 12, 126, 1973.

Hernandez, G., Mid-latitude thermospheric neutral kinetic temperatures, 1. Solar, geomagnetic, and long term effects, J. Geophys. Res., 87, 1623, 1982a.

Hernandez, G., R. Sica, G. J. Romick, V. B. Wickwar, R. T. Tsunoda, Lower thermosphere dynamics in the auroral region near Fairbanks, Alaska, IAGA, Hamburg, Germany, August, 1983.

Hernandez, G., J. L. Smith, R. G. Roble, T. L. Killeen, R. Sica and G. J. Romick, Auroral zone thermospheric winds near solar minimum, EOS, 65, 250, 1984.

Hernandez, G., R. J. Sica, and G. J. Romick, An equal noise spectroscopic measurement, Appl. Opt., 23, 915, 1984.

Hernandez, G., R. Sica and G. J. Romick, Equal noise spectrometry measurements, Appl. Opt., 23, 915, 1984.

Hernandez, G. and J. L. Smith, Mesospheric wind determinations and the $P_1(2)_{c,d}$ lines of the $X^2\pi$ OH (8-3) Band", Geophys. Res. Lett., 11, 532, 1984.

Hines, C. O., Internal atmospheric gravity waves at ionospheric heights, Can. J. Phys., 38, 1441, 1960.

Hines, C. O., Correction to 'Internal atmospheric gravity waves at ionospheric heights', Can. J. Phys., 42, 1424, 1964.

Hines, C. O., Dynamical heating of the upper atmosphere, J. Geophys. Res., 70, 177, 1965.

Hughes, T. J. and G. Rostoker, A comprehensive model current system for high-latitude magnetic activity - 1. The steady state system, Geophys. J. R. Astr. Soc., 58, 525, 1979.

Hunsucker, R. D., Atmospheric gravity waves generated in the high-latitude ionosphere: A review, Rev. Geophys. Space Phys., 20, 293, 1982.

Iijima, T. and T. A. Potemra, The amplitude distribution of field-aligned currents at northern high-latitudes observed by Triad, J. Geophys. Res., 81, 2165, 1976.

Kan, J. K. and L. C. Lee, Formation of auroral arcs and inverted V precipitation: An overview, in Physics of Auroral Arc Formation, edited by S.-I. Akasofu and J. R. Kan, Geophysical Monograph 25, AGU, Washington, D.C., 1981.

Kan, J. R., D. U. Longenecker and J. V. Olson, A transient response model of Pi 2 pulsations, J. Geophys. Res., 87, 7483, 1982.

Kennealy, J. P., F. P. Del Greco, G. E. Caledonia and B. D. Green, Nitric oxide chemiexcitation occurring in the reaction between metastable nitrogen atoms and oxygen molecules, J. Chem. Phys., 69, 1574, 1978.

Killeen, T. L. and R. G. Roble, An analysis of the high-latitude thermospheric wind pattern calculated by a thermospheric general circulation model, 1. Momentum forcing, J. Geophys. Res., in press, 1983.

Link, R., J. C. McConnell, and G. G. Shepherd, A self-consistent evaluation of the rate constants for the production of the OI6300A airglow, Planet. Space Sci., 29, 589, 1981.

Mayaud, P. N., Derivation, Meaning, and Use of Geomagnetic Indices, Geophysical Monograph 22, AGU, Washington, D.C., 1980.

Parratt, L., Probability and Experimental Errors in Science, Wiley, New York, 1961.

Richmond, A. D. and S. Matsushita, Thermospheric response to a magnetic substorm, J. Geophys. Res., 80, 2839, 1974.

Roble, R. G. and M. H. Rees, Time-dependent studies of the aurora: Effects of particle precipitation on the dynamic morphology of ionospheric and atmospheric properties, Planet. Space Sci., 25, 991, 1977.

Roble, R. G. , R. E. Dickinson, and E. C. Ridley, Global circulation and temperature structure of the thermosphere with high-latitude plasma convection, J. Geophys. Res., 87, 1599, 1982.

Roble, R. G., Global dynamic models of the Earth's thermosphere and ionosphere, ESA Journal, 7, 405, 1983.

Romick, G. J., The detection and study of the visible spectrum of the aurora and airglow, SPIE, 91, 63, 1976.

Romick, G. J., T. J. Hallinan, G. G. Sivjee and G. Hernandez, High time resolution intensified images of λ6300A Fabry-Perot fringes applied to auroral thermospheric studies, IAGA Bulletin, 45, 291, 1981.

Romick, G. J., G. G. Sivjee, R. C. Roble and G. Hernandez, Upper thermosphere neutral winds and temperatures in the auroral zone derived from [OI] 630 nm emission, EOS, 63, 392, 1982.

Rusch, D. W., J. C. Gerard and W. E. Sharp, The reaction of $N(^2D)$ with O_2 as a source of $O(^1D)$ atoms in aurorae, Geophys. Res. Lett., 5, 1043, 1978.

Sica, R., M. H. Rees, G. J. Romick, G. G. Sijee, G. Hernandez and G. R. Swenson, Thermospheric wind measurements in the auroral zone, EOS, 63, 392, 1982.

Sica, R., M. H. Rees, G. J. Romick, G. Hernandez and R. T. Tsunoda, An experimental picture of the high latitude E and F Regions, EOS, 63, 1051, 1982.

Sica, R. J., Auroral zone thermospheric dynamics using Fabry-Perot interferometric measurements of the OI 15867K emission, Ph.D. thesis, Univ. of Alaska, Fairbanks, 1984.

Smith, J. L., G. Hernandez, V. B. Wickwar and R. T. Tsunoda, Winds and temperatures in the lower thermosphere in the auroral region, EOS, 63, 274, 1983.

Sojka, J. J., W. J. Raitt and R. W. Schunk, Effect of displaced geomagnetic and geographic poles on high-latitude plasma convection and ionospheric depletions, J. Geophys. Res., 84, 5943, 1979.

Torr, M. R., D. G. Torr and H. E. Hinteregger, Solar flux variability in the Schumann-Runge continuum as a function of solar cycle 21, J. Geophys. Res., 85, 6063, 1980.

Wallis, D. D., Geomagnetic influences on thermospheric winds observed in the auroral zone, Ph.D. thesis, Univ. of Alaska, College, 1974.

Wallis, D. D., and E. E. Budzinski, Empirical models of height integrated conductivities, J. Geophys. Res., 86, 125, 1981.

Wickwar, V. B., W. Kofman, M. Rees, R. Sica, G. J. Romick, G. Hernandez and S. Mende, Examination of a type red aurora with radar, optics and theoretical modeling, XXI URSI General Assembly, Florence, Italy, 28 August-5 September, 1984.

END

FILMED

2-85

DTIC